BILINGUAL PUBLISHING CO.
Pioneer of Global Academics Since 1984

Journal of Geographical Research

Volume 5 • Issue 3 • July 2022
ISSN 2630-5070(Online)

BILINGUAL
PUBLISHING CO.
Pioneer of Global Academics Since 1984

Volume 5 Issue 3 • July 2022 • ISSN 2630-5070 (Online)

Journal of Geographical Research

BILINGUAL PUBLISHING CO.
Pioneer of Global Academics Since 1984

BILINGUAL PUBLISHING CO.
Pioneer of Global Academics Since 1984

Volume 5 | Issue 3 | July 2022 | Page1-62
Journal of Geographical Research

Contents

Articles

BILINGUAL PUBLISHING CO.
Pioneer of Global Academics Since 1984

Journal of Geographical Research
https://ojs.bilpublishing.com/index.php/jgr

ARTICLE

Spatial-temporal Evolution and Its Influencing Factors of Tourism Eco-efficiency in China

Chengpeng Lu[1,2*] Tianyang Ma[2] Zhiliang Liu[2]

1. Institute of County Economic Development & Rural Revitalization Strategy, Lanzhou University, Lanzhou, 730000, China
2. School of Economics, Lanzhou University, Lanzhou, 730000, China

ARTICLE INFO

Article history
Received: 04 May 2022
Revised: 25 May 2022
Accepted: 31 May 2022
Published Online: 20 June 2022

Keywords:
Tourism eco-efficiency
Spatial pattern
Influencing factors
Spatial analysis
China

ABSTRACT

Eco-efficiency is an invaluable indicator for the measurement of the relationship between production activities and environmental depletion. This study measures the tourism eco-efficiency of 30 provinces in China from 2005 to 2020 based on the super-efficiency SBM model, and explores its spatial-temporal evolution characteristics using the kernel density function, standard deviation ellipse, and center of gravity model. Then, the influencing factors of the tourism eco-efficiency in China are analyzed by Tobit regression model. The results show that the tourism eco-efficiency of China is generally fluctuating upwards, but has not yet reached the maximum production possibility frontier. The kernel density curve shows a unimodal-bimodal-unimodal pattern, while the inter-provincial differences have been decreasing and becoming more balanced. The center of gravity of tourism eco-efficiency is located at the junction of Henan and Hubei province and generally moves to the south (slightly to the southwest). Meanwhile, it is revealed that the level of economic development and the tourism eco-efficiency has a significant inverted U-shaped relationship. The level of economic openness, traffic conditions, and tourism eco-efficiency is positively correlated. The environmental regulations and industrial structure have a negative but limited impact on tourism eco-efficiency. Finally, recommendations and suggestions for policy formulation to promote quality and sustainable development of the tourism industry are put forward, such as increasing investment in ecological protection and governance in tourism development, improving capacity-building in allocating green and low-carbon technologies and resources, strengthening tourism infrastructure construction, and enhancing environmental governance systems and mechanisms.

*Corresponding Author:
Chengpeng Lu,
Institute of County Economic Development & Rural Revitalization Strategy, Lanzhou University, Lanzhou, 730000, China; School of Economics, Lanzhou University, Lanzhou, 730000, China;
Email: lcp@lzu.edu.cn

DOI: https://doi.org/10.30564/jgr.v5i3.4688

1. Introduction

After more than 40 years of unremitting efforts, China's tourism development has achieved world-renowned achievements. However, the increasing pressure on the tourism environment from increasingly frequent tourism activities has caused various problems associated with tourism resources and environment [1], such as the destruction of tourism resources and the degradation of environmental quality in tourist destinations [2], mainly manifested as water pollution, air quality decline, and local ecological environment damage [3]. Therefore, how to improve the efficiency of tourism resource utilization and environmental protection, reduce resource input and pollutant emissions, and achieve high-quality and sustainable development of the tourism industry are the challenges [4].

Eco-efficiency was proposed by German scholars Schaltegger and Stum [5] as an important indicator of resource and environmental efficiency, which can be used to explore the resource consumption and environmental effect of tourism in the process of creating tourism revenue, and measure a level of coordination between economic development and environmental protection. Ideally, the added value of the tourism economy is maximized, resource consumption and environmental pollution are minimized [6]. Existent studies about tourism eco-efficiency mainly focused on the definition of tourism eco-efficiency [7,8], quantitative measurement [9,10], influencing factors and mechanisms [11,12], and related recommendations [13,14]. Research methods mainly include Ecological Footprint [15], Life Cycle Assessment [16], Ecological Multiplier Measurement Model [17], and Data Envelopment Analysis (DEA) [18,19]. Most scholars used the radial angle DEA to calculate the directional distance function in their empirical studies to incorporate pollutant emissions into the efficiency evaluation framework [20-22]. Driven by the actual demand for China's tourism and inspired by international tourism research, the research on the tourism eco-efficiency in China has received increasing attention and achieved many results in recent years. On the one hand, research topics have been expanding, from a focus on tourist hotels [23] to various scopes such as the hotel industry [24], travel agencies [25], tourism transport [26], tourism resources [27], tourism environment [28], and overall tourism development efficiency studies [29-31]. On the other hand, research methods have been innovated, and the traditional efficiency measurement models used in the early stages have been gradually improved, such as the SORM-BCC super-efficiency model [32], DEA-MI model [33], and modified DEA model [29], Bootstrap-DEA model [34], and three-stage DEA model [35]. In short, the academic research on tourism eco-efficiency has achieved certain results, but from the perspective of geography, the research on the spatial-temporal evolution of tourism eco-efficiency by spatial analysis methods still needs to be explored in depth.

Based on the super-efficiency SBM model, this study constructs a comprehensive evaluation model to measure the tourism eco-efficiency of 30 provinces in China from 2005 to 2020 (excluding Tibet, Hong Kong, Macao, and Taiwan due to data availability), explores the spatial-temporal evolution characteristics with the kernel density function, the standard deviation ellipse, and the center of gravity model, and analyzes the influencing factors with the Tobit regression model. The purpose is to provide decision-making support to address resource efficiency issues and to realize the high-quality sustainable development of the tourism economy.

2. Methods and Data

2.1 Index System

The calculation of the tourism eco-efficiency requires comprehensive consideration of resource consumption, environmental cost, and economic output. Based on relevant literature [18,36-38], this study introduces two types of indicators, input and output, to construct a measurement index system (Table 1). The input indicators involve economic, resource, and environmental factors. Economic factors include labour force and capital investment. The labour force is measured by the total number of tourism employees, while the capital investment is measured by the number of star-rated hotels and the number of travel agencies. Resource factors include energy, water, and land resources. Considering the lack of statistical data, the consumption of land resources in tourism is measured by the weighted sum of the total number of A-level tourist attractions (i.e., one 1A destination weights 1, while one 5A destination weights 5), on the premise that the number of tourist destinations can reflect the input of land resources to some extent. Environmental factors include wastewater discharge, carbon emission, and solid waste disposal by the tourism industry. In terms of output, tourism revenue and the number of tourists are considered important indicators as they reflect the level of comprehensive development efficiency of the tourism industry. Note that this study does not consider the possible lagged effect of inputs on tourism efficiency.

2.2 Super-efficiency SBM Model

The super-efficiency SBM model was used to calculate

the tourism eco-efficiency. Firstly, the input and output indicators were integrated into four types of indicators, i.e., the economic input, the resource input, the environmental input, and the economic output. Then the entropy weight-TOPSIS method was adopted to process the indicators (assuming that there are *n* units to be evaluated, and each unit has m evaluation indicators).

Table 1. Evaluation index system of tourism eco-efficiency

Indicator type	Primary indicator	Secondary indicator (Unit)
Input indicators	Economic factors	Total number of tourism employees
		Number of star-rated hotels
		Number of travel agencies
	Resource factors	Tourism resource endowment
		Tourism energy consumption
		Tourism water consumption
	Environmental factors	Tourism wastewater discharge
		Tourism Carbon emission
		Tourism solid waste emissions
Output indicators	Economic outputs	Total tourism revenue
		Total number of tourists

The entropy method determines the weight ωj of indicator j, and then a weighting matrix is constructed:

$$R = (r_{ij})_{n\times m},\ r_{ij} = \omega_j \cdot x_{ij} \tag{1}$$

The optimal and the worst solution can be determined as follows:

$$S^+ = \max(r_{1j}, r_{2j}, \cdots, r_{mj}) \tag{2}$$

$$S^- = \min(r_{1j}, r_{2j}, \cdots, r_{mj}) \tag{3}$$

Then the Euclidean distance between the *i-th* evaluation unit and the optimal or the worst solution is calculated:

$$D_i^+ = \sqrt{\sum_{i=1}^{m}(S^+ - r_{ij})^2},\ D_i^- = \sqrt{\sum_{i=1}^{m}(S^- - r_{ij})^2} \tag{4}$$

A comprehensive evaluation index can be calculated as follows:

$$C_i = \frac{D_i^-}{D_i^- + D_i^+} \tag{5}$$

If the production system has *n* decision-making units (DMU), and each unit includes four vectors, i.e., economic cost input, resource cost input, environmental cost input, and economic output, the efficiency analysis framework can be formed as follows:

$$T = (x^m, x^r, x^e, y^d) \tag{6}$$

where, $x^m \in R_+^{a\times n}$, $x^r \in R_+^{b\times n}$, $x^e \in R_+^{c\times n}$ and $y^d \in R_+^{J\times n}$ are data matrixes of economic cost input, resource cost input, environmental cost input, and economic output, respectively, and *a, b, c,* and *f* represent the number of input and output factors, respectively.

The production possibility frontier under variable returns to scale and weak disposability can be defined as:

$$P = \{(x^m, x^r, x^e, y^d | x^m \geq \lambda X^m, x^r \geq \lambda X^r, x^e \geq \lambda X^e, y^d \leq \lambda Y^d, \lambda \geq 0\} \tag{7}$$

The super-efficiency SBM model with variable returns to scale is:

$$Min\rho = \frac{1+\frac{1}{m}\sum_{i=1}^{m} s_i^-/x_{ik}}{1-\frac{1}{q}\sum_{r=1}^{q} s_r^+/y_{rk}} \tag{8}$$

$$\sum_{j=1,j\neq k}^{n} \lambda_j x_j - s_i^- \leq x_{ik} \tag{9}$$

$$\sum_{j=1,j\neq k}^{n} \lambda_j y_j - s_r^+ \geq y_{rk} \tag{10}$$

$$1 - \frac{1}{a}\sum_{r=1}^{s} s_r^+/y_{rk} > 0 \tag{11}$$

$$\lambda,\ s^-,\ s^+ \geq 0 \tag{12}$$

$$\sum_{j=1,j\neq k}^{n} \lambda_j = 1 \quad j = 1,2,\cdots,n(j \neq k) \tag{13}$$

where, x and y represent input and output variables, respectively, m and q represent the number of input and output variables, respectively, s- and s+ represent slack variables of input and output, respectively, and λ is a weight vector. Based on the above linear programming, the inefficiency value of resource for Province *I* in period *t* is calculated. The efficiency loss of resource input (*IEr*), environmental input (*IEe*), and economic output (*IEy*) can be decomposed as follows:

$$IE_r = \frac{1}{b}\sum_{i=1}^{b} \frac{s_i^{r-}}{x_{ik}^r} \tag{14}$$

$$IE_e = \frac{1}{c}\sum_{i=1}^{c} \frac{s_j^{e-}}{x_{ik}^e} \tag{15}$$

$$IE_y = \frac{1}{f}\sum_{r=1}^{f} \frac{s_r^+}{y_{rk}^d} \tag{16}$$

This study set the decision goal as $g = (-x^m, -x^r, -x^e, +y^d)$. It means that this study aims to achieve optimal production conditions by reducing the economic input, resource consumption, and environmental cost while gradually increasing the economic output. Assume that the actual observation value of the decision-making unit *DMU0* is *(M, R, E, D),* where *M, R, E, and D* represent economic input, resource consumption, environmental cost, and economic output, respectively. When *DMU0* reaches the best production possibility frontier, its observed value is *(M*, R*, E*, D*)*. Then the terms of $IE_R = (R - R^*)/R$, $IE_E = (E - E^*)/E$, $IE_D = (D^* - D)/D$ are defined to represent the inefficiency of resource input, the inefficiency of environmental in-

put, and the inefficiency of economic output, respectively.

$$E_e = \frac{E^*/D^*}{E/D} = \frac{1-(E-E^*)/E}{1+(D^*-D)/D} = \frac{1-IE_E}{1+IE_D} \quad (17)$$

2.3 Kernel Density Estimation (KDE)

KDE is a non-parametric estimation method to estimate the probability density of random variables. Assume that *x1, x2…xn* are independent and identically distributed sample points, and the probability density function is *f(x)*, then the probability density estimation equation of the random variable at point *x* is:

$$\bar{f}(x) = \frac{1}{Nh}\sum_{i=1}^{n} K\left[\frac{X_i - x}{h}\right] \quad (18)$$

where, *K(*)* is the kernel function, *N* is the number of sample observations, and *h* is a bandwidth that affects the smoothness and deviation of the density curve.

2.4 Standard Deviation Ellipse (SDE) and the Center of Gravity Model (CGM)

SDE quantitatively describes the centrality, directionality, spread ability, and other characteristics of the spatial distribution of elements from a global and spatial perspective. It reveals the spatial distribution and temporal evolution of geographic elements [39]. *CGM* solves the problem of spatial changes in regional attributes by depicting the concentrated and discrete trends of regional attributes and their time-varying offset trajectories. The calculation equations are as follows:

$$\bar{x} = \frac{\sum_{i=1}^{n} M_i X_i}{\sum_{i=1}^{n} M_i} \quad (19)$$

$$\bar{y} = \frac{\sum_{i=1}^{n} M_i Y_i}{\sum_{i=1}^{n} M_i} \quad (20)$$

where, *(Xi, Yi)* is the center coordinate of the *i-th* region, and *Mi* is an attribute value of the tourism eco-efficiency.

2.5 Tobit Regression Model

In order to investigate the influencing factors of tourism eco-efficiency, a Tobit regression model was constructed by taking the influencing factors as explanatory variables and the efficiency value as an explained variable. The model can be expressed as follows:

$$Y = \begin{cases} Y^* = \alpha + \beta X + \varepsilon, \ Y^* > 0 \\ 0, \ Y^* \le 0 \end{cases} \quad (21)$$

where, *Y* is a truncated dependent variable vector, *X* is an independent variable vector, β is an intercept term vector, α is a regression parameter vector, and ε is a disturbance term, $\varepsilon \sim N(0, \sigma 2)$. Since the dependent variable is discretely distributed, the parameters of the Tobit regression model would be biased and inconsistent if estimated by Ordinary Least Square (*OLS*), so Maximum likelihood (*ML*) is used to estimate the parameters of the model.

2.6 Data Sources

Data were collected from the 2006-2021 China Statistical Yearbooks, China Tourism Yearbooks, China Energy Yearbooks, regional statistical yearbooks, and statistical bulletins. Some indicators were obtained from the official website of the Ministry of Culture and Tourism of the People's Republic of China (*https://mct.gov.cn/*).

3. Results

3.1 Spatial-temporal Evolution Characteristics

DEA-Solver Pro 8.0 software was used to calculate the tourism eco-efficiency of 30 provinces in China. Based on related research results [36], this study divides China into high-efficiency regions ($\rho \ge 1$), relatively high-efficiency regions ($0.8 \le \rho < 1$), medium-efficiency regions ($0.6 \le \rho < 0.8$), and low-efficiency regions ($\rho \le 0.6$) according to different levels of tourism eco-efficiency.

From Figure 1, the overall tourism eco-efficiency shows a fluctuating upward trend. The average efficiency index has increased from 0.602 in 2005 to 0.809 in 2020, indicating that the tourism eco-efficiency in China has increased from the medium-efficiency level to the relatively high-efficiency level, but has not yet reached the maximum production possibility frontier. This is mainly due to that the Chinese government clearly put forward the concept of green development in the 13th Five-Year Plan, and governments at all levels lay their emphases on how to take the lead in realizing the green development of tourism. This concept not only considers the regional tourism economic growth, but also pays attention to the environmental impact, and enhances the green evaluation of tourism by governments at all levels from the perspective of government governance, which is conducive to governments at all levels to formulate corresponding policies to guide the green development of tourism, thereby improving the tourism ecological efficiency. The average tourism eco-efficiency index in the eastern region was 0.872, which was significantly higher than those in the central and western regions. The tourism eco-efficiency level in the central region was higher than that in the western region, having been continuously increasing since 2015 and reached the maximum of 0.733 in 2020. However, there was still a large gap compared with the eastern region. Although the tourism eco-efficiency in the western region had been continuously improved, the overall level was still not high.

From Figure 2, the overall spatial pattern of tourism eco-efficiency of China is high in the southeast and low in the northwest. The reason is that most of the southeast regions are tourism hot spots or highly developed regions with unique advantages in tourism ecological efficiency and tourism green innovation, which have realized the coupling and coordinated development of the two. The northwest region lays more emphases on tourism economic benefits but pays less attention to the green ecological development of Tourism, and also lacks financial investment. Specifically, Tianjin and Guangdong are high-efficiency regions; Beijing, Shandong, Zhejiang, and Ningxia are relatively high-efficiency regions; and Anhui, Jiangsu, Heilongjiang, Shanghai, Hunan, Hainan, Fujian, Henan, Hubei, and Jilin are medium-efficiency regions. In 2010, significant improvements were observed in all provinces. Beijing, Liaoning, Jiangsu, Shanghai, and Hainan had evolved into high-efficiency regions. Henan, Chongqing, and Heilongjiang had stepped into the relatively high-efficiency category. Sichuan and Shaanxi had progressed to the medium-efficiency level. In 2020, high-efficiency regions were generally distributed in southern China with a C-shaped distribution pattern, surrounded by relatively high-efficiency and medium-efficiency regions. The spatial agglomeration was obvious, mainly the high-efficiency agglomeration in the south and the low-efficiency agglomeration in the north.

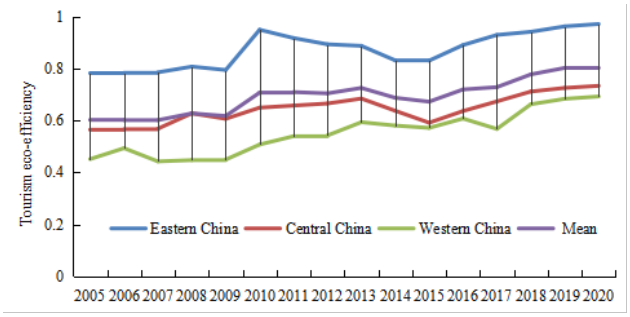

Figure 1. Trend of tourism eco-efficiency of China from 2005 to 2020

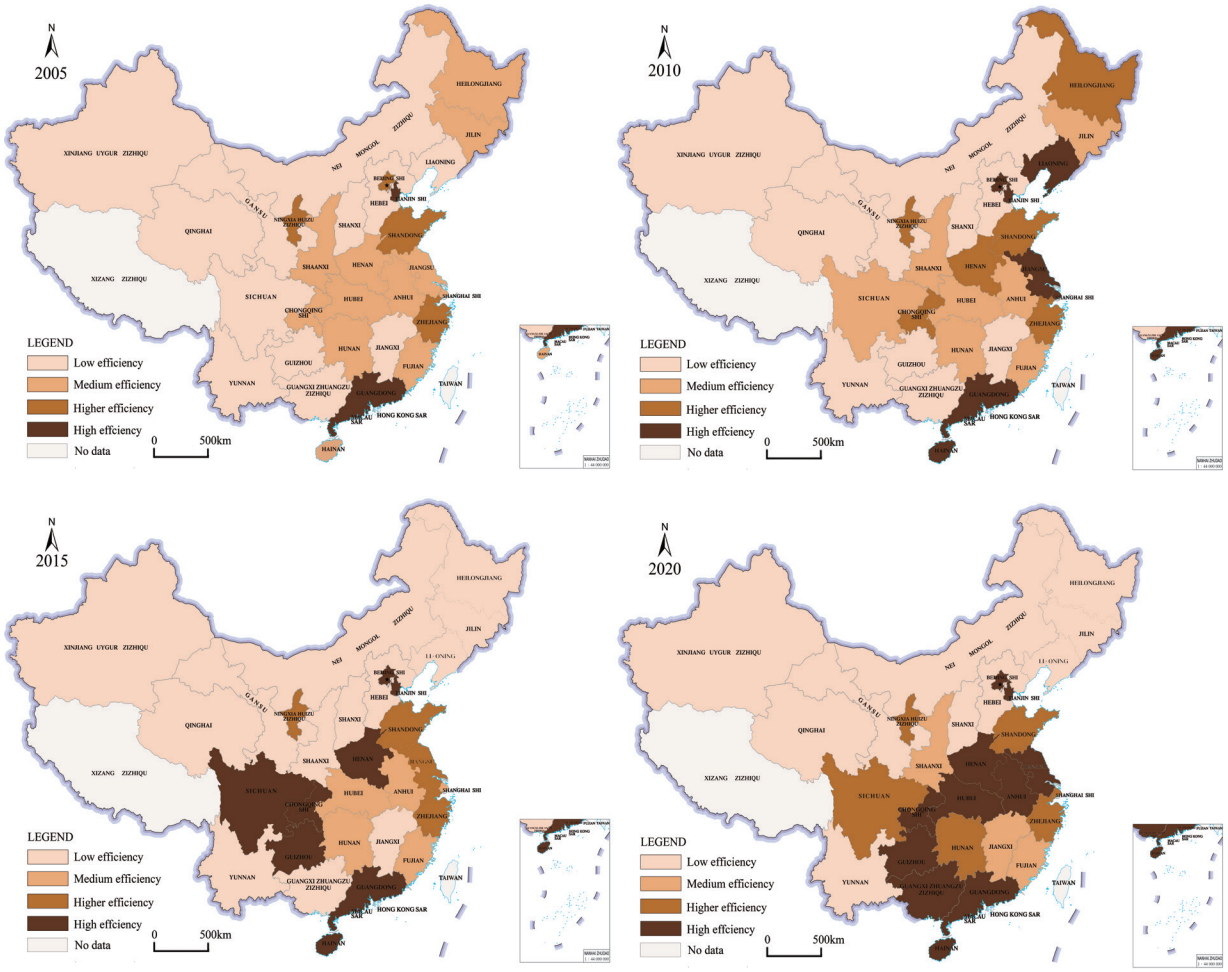

Figure 2. Spatial pattern of tourism eco-efficiency of China in 2005, 2010, 2015 and 2020

3.2 Analysis of Kernel Density Curve and Evolution of the Center of Gravity

From Figure 3, the Kernel density curves of tourism eco-efficiency from 2005 to 2020 show a unimodal-bimodal-unimodal evolution pattern, but with a trailing tail. In 2005, the tourism eco-efficiency corresponding to the highest value was maintained at a low level of about 0.5, and the curve had a right tail, indicating that the development in different provinces was remarkably imbalanced and the low-efficiency regions accounted for a relatively large proportion. In 2010, the highest efficiency value of the first wave was around 0.5, and the peak value of the second wave was around 0.9, indicating the existence of polarization and the significant difference between provinces. In 2015, the curve was weakened, with lower peaks and wider waves, indicating less inter-provincial variations. In 2020, the peak value further shifted to the right, the peak was higher, and the width became wider, indicating that the curve gradually transformed into a normal distribution. When the corresponding peak efficiency value increased to about 1.0, the diffusion effect in the eastern region and the late-development advantage in the western region with lower efficiency initially worked, which indicated that the tourism eco-efficiency was significantly improved, and the difference between provinces gradually became smaller.

The center of gravity of tourism eco-efficiency in China was at the junction of Henan and Hubei provinces, indicating that the tourism eco-efficiency in the eastern region was higher than that in the western region. From Figure 4, in 2005-2010, the center of gravity of the tourism eco-efficiency mainly shifted to the east from Pingdingshan City to Luohe City in Henan Province by a total of 52.842 kilometres; in 2011-2017, the center of gravity mainly shifted to the southwest by 231.14 kilometres, and came to Suizhou City, Hubei Province in 2017; in 2018-2020, the center of gravity moved northwards by 12.184 kilometres to the junction of Xiangyang City and Suizhou City in Hubei Province. Overall, the center of gravity of environmental efficiency moved to the southwest, from Henan to Hubei province, which indicated that the tourism eco-efficiency in the southern and western regions was improved faster than that in the northern and eastern regions.

3.3 Analysis of Standard Deviation Ellipse

Form Table 2, the length of the minor axis of SDE dropped from 788.72 km in 2005 to 762.29 km in 2020, indicating that the tourism eco-efficiency has been polarized in the direction of the minor axis. The changes in the length of the minor axis can be divided into two stages: from 2005 to 2013, the length continuously decreased from 976.91 km to 774.77 km, indicating that the tourism eco-efficiency at this stage was continuously polarizing; after 2013, the length remained stable and fluctuated at around 780 km, indicating that there was no significant change in the agglomeration of tourism eco-efficiency. Overall, the area of the eclipse showed a fluctuating decreasing trend. The shape index of the tourism eco-efficiency SDE decreased from 0.84 to 0.64 from 2005 to 2013. From 2013 to 2020, this shape index increased from 0.64 to 0.70, which suggested that the tourism eco-efficiency in all directions has become more and more balanced.

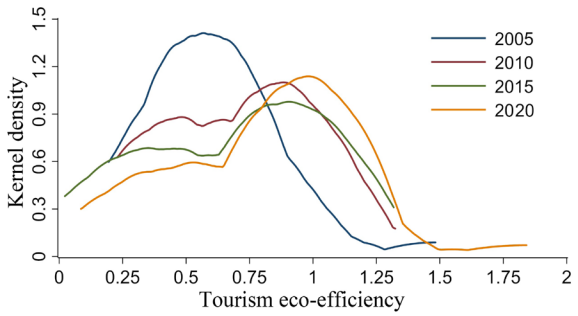

Figure 3. Trend of the kernel density curve of tourism resource efficiency of China

From the perspective of azimuth rotation, the azimuth angle of the tourism eco-efficiency SDE exhibited an M-shaped change. From 2005 to 2011, it increased from 22.671° to 25.866°. When rotating clockwise, it gradually approached the northeast-southwest direction, indicating a rapid improvement in the tourism eco-efficiency in the direction of "south-by-southeast" to "north-by-northwest". During 2011-2012, the azimuth angle decreased to 23.999°, and the standard deviation ellipse rotated 1.877° counter-clockwise from northeast to southwest. During 2012-2014, the azimuth angle increased to 25.781°. After 2014, the fluctuation of the azimuth angle eased, and the azimuth angle dropped to 23.514° in 2020. Overall, the azimuth angle fluctuated greatly during the study period, but there was little change in 2020 compared to 2005, with only a slight increase of 0.843°, which indicated that in general, the tourism eco-efficiency evolved in a north-northeast to south-southwest pattern, with no significant change in the overall trend.

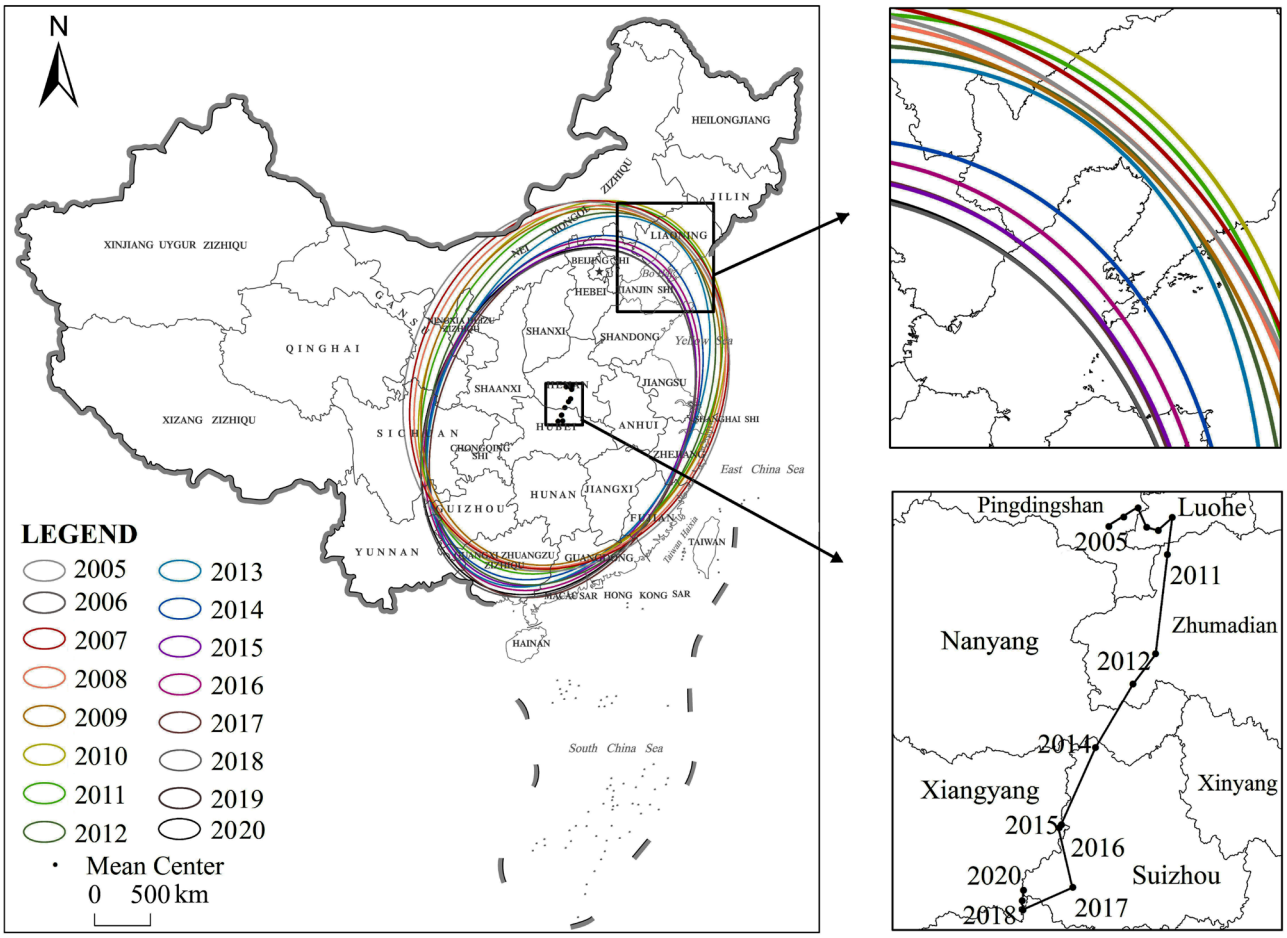

Figure 4. Shift of standard deviation ellipse and the center of gravity of tourism eco-efficiency

Table 2. Results of standard deviation ellipse parameters of the tourism eco-efficiency in China

Year	Major semi-axis(km)	Minor semi-axis(km)	Shape index	Area (km^2)	Azimuth An(°)
2005	1167.64	976.91	0.84	358.34	22.67
2006	1170.32	962.56	0.83	356.27	23.08
2007	1171.65	943.70	0.81	347.34	23.53
2008	1154.95	918.37	0.80	333.20	24.08
2009	1138.89	879.03	0.77	314.49	23.80
2010	1196.85	882.17	0.74	331.68	25.77
2011	1198.09	855.28	0.71	321.9	25.87
2012	1205.57	820.13	0.68	310.60	24.00
2013	1214.60	774.77	0.64	295.62	25.59
2014	1120.10	777.73	0.69	273.66	25.78
2015	1102.75	766.46	0.7	265.5	23.93
2016	1133.06	786.68	0.69	280.01	23.71
2017	1133.20	766.71	0.68	272.94	21.23
2018	1126.47	781.64	0.69	276.60	23.90
2019	1120.36	783.52	0.69	276.36	23.72
2020	1118.30	785.75	0.70	276.04	23.51

3.4 Influencing Factors of the Tourism Eco-efficiency in China

Referring to relevant literature [40-42], combined data availability, variables including economic development level, environmental regulation, economic openness, industrial structure, traffic condition, and locality were selected to establish a panel Tobit regression model to analyze the influencing factors of the tourism eco-efficiency in China.

$$Y_{it} = \alpha_0 + \beta_1 \ln ED_{it} + \beta_2 (\ln ED_{it})^2 + \beta_3 ER_{it} + \beta_4 OW_{it} + \beta_5 IS_{it} + \beta_6 IA_{it} + \beta_7 (IA_{it})^2 + \beta_8 TC_{it} + \beta_9 L_{1it} + \beta_{10} L_{2it} + \varepsilon_{it} \quad (22)$$

where, Y is tourism eco-efficiency, and ED is economic development level, measured by per capita GDP. In order to minimize the impact of heteroscedasticity, ED was processed by logarithm, and a quadratic term was introduced to verify the EKC theory. ER is environmental regulation, measured by the proportion of environmental governance investment in GDP, OW is economic openness level, measured by the proportion of FDI in GDP, IS is indus-

trial structure, measured by the proportion of tertiary industries, and *IA* is industrial agglomeration, measured by tourist location entropy. Because industrial agglomeration and resource efficiency are not linearly related, a quadratic term was introduced. *TC* is traffic condition, measured by highway density, *L* is locality, with *L1=1* as the eastern region and *L2=1* as the central region, $\alpha 0$ is a constant term, βn is a regression coefficient of variable *n*, and εit is an error term.

The Random Effect Panel Tobit Regression Model was used to analyze the influencing factors. From Table 3, all first-order coefficients of the logarithm of economic development level are positive, while all the quadratic coefficients are negative, which indicates that the tourism eco-efficiency has evolved in an inverted U-shaped curve, i.e., first rising and then declining. Currently, the efficiency in most provinces was on the rise, in line with the Environmental Kuznets Curve [43]. There is an U-shaped relationship between the tourism eco-efficiency and the level of industrial agglomeration. Once the industrial agglomeration reaches a certain level, the industrial specialization and scale effect will promote the accumulation of tourism elements and the overflow of technological innovation, which will then produce agglomeration and radiation effects that can improve the tourism eco-efficiency [44]. Simultaneously, positive environmental externalities have emerged, the scale effect of environmental governance has gradually increased, the marginal cost of pollution control for enterprises in agglomeration regions has been reduced, and the tourism eco-efficiency has been effectively improved [45]. Environmental regulations have a significantly negative impact on tourism eco-efficiency. In this regard, it provides evidence in support of both the "compliance cost theory" and the "innovation compensation theory" [46]. It is also verified that the command-control environmental governance model characterized by environmental governance investment can reduce the ecological effect of investment in the absence of incentive mechanisms in environmental governance [47]. The economic openness coefficients are significantly positive, indicating that the increasing openness is conducive to the improvement of efficiency. The industrial structure coefficients are all significantly negative with small absolute values, indicating that environmental governance for tertiary industries is more difficult compared to other industries because they generate more types of and more broadly distributed pollution [48]. The traffic condition coefficients are significantly positive, indicating that the improvement of traffic conditions can directly reduce transportation and travel costs. In the eastern region, the coefficients are not significant, while in the central region, they are all negative but at different significance levels, which indicates that locality has a negative impact on tourism eco-efficiency in central provinces.

Table 3. Tobit regression analysis results of tourism eco-efficiency

Influencing factors	Explanatory variables	Coefficient	Standard error	Z-statistics
Economic development level	ln (*ED*)	1.352***	0.476	2.84
	$\ln^2$ (*ED*)	–0.061***	0.023	–2.59
Environmental regulations	*ER*	–0.055***	0.017	–3.3
Economic Openness	*OW*	0.189***	0.057	3.33
Industrial structure	*IS*	–0.006***	0.002	–2.9
Industrial agglomeration	*IA*	–0.435***	0.099	–4.39
	IA2	0.138***	0.033	4.18
Traffic condition	*TC*	0.595***	0.098	6.1
Locality	*L1*	–0.135	0.116	–1.17
	L2	–0.200*	0.12	–1.67
Constant	$\alpha 0$	–6.674***	2.434	–2.74

Note: ***, ** and * represent 1%, 5% and 10% significance levels, respectively.

4. Conclusions and Discussion

This study measured the tourism eco-efficiency of 30 provinces in China from 2005 to 2020 and analyzed its spatial-temporal characteristics as well as its influencing factors. The results showed that the tourism eco-efficiency in China generally fluctuated and raised, but has not yet reached the maximum production possibility frontier. Regarding the evolutionary trend, the Kernel density curve showed an unimodal-bimodal-unimodal pattern, while inter-provincial differences have been decreasing and becoming more balanced. The center of gravity of tourism eco-efficiency was located at the junction of Henan and Hubei provinces. The center of gravity of tourism eco-efficiency generally shifted to the south-southwest from Henan to Hubei province, indicating that the tourism eco-efficiency in southern and western regions improved faster than in northern and eastern regions. Based on the SDE analysis, both the major and minor axes showed a shrinking trend, and the area of the eclipse was continuously decreasing, indicating that the spatial agglomeration of tourism eco-efficiency became more and more significant. In terms of influencing factors, there was a significant inverted U-shaped relationship between economic

development level and tourism resources. Increasing the level of economic openness and the optimization of traffic conditions can help improve the tourism eco-efficiency. The industrial structure, environmental regulation, and locality had negative but limited effects on the tourism eco-efficiency.

Eco-efficiency is the core indicator to promote the high-quality development of tourism, reflecting the resource and environmental cost of creating a certain economic output in the process of tourism development, which can be used to measure whether tourism economic development is environmentally friendly [49]. The higher the eco-efficiency, the more coordinated the development of the tourism economy and the environment, and the higher the level of resource utilization. Therefore, the tourism eco-efficiency should be comprehensively evaluated and its influencing factors should be analyzed. In recent years, the rapid development of tourism economy in provinces has increased non-desired output and a large amount of inefficient output, leading to the tourism eco-efficiency in provinces being lower than that in southeast coastal areas. It is crucial to construct a reasonable evaluation model of tourism eco-efficiency, especially in the critical period of economic transformation. Based on the study and analysis of the spatial characteristics of China's tourism eco-efficiency and its influencing factors, this study objectively evaluated the differences in tourism eco-efficiency among provinces in China, which is helpful for policymakers to identify the main problems and take targeted measures [50], and is of great practical significance to promote the high-quality development of tourism. In addition, the findings of this study are consistent with the existing studies [51,52,53], and strengthens the spatial analysis of tourism eco-efficiency, which can provide scientific reference for tourism spatial governance and optimization. For the sustainable and coordinated development of tourism, it is also necessary to analyze the causes of tourism environmental problems, the modes of impact, and the caused results, hoping to provide services for the management and decision-making of tourism development [54]. Notably, the causes of environmental damage and degradation of environmental quality in tourism areas are multiple, and human economic behaviour is one of the most important factors [55].

In order to advance the tourism eco-efficiency to reach the maximum production possibility frontier, and narrow the gap between the eastern, central, and western regions, the following policy recommendations are proposed. First, the eastern region can give full play to its leading edge, further increase the investment in tourism ecological protection and governance, and improve the high-tech application and resource allocation capacities. The eastern region's exemplary and leading role can facilitate the tourism development in the central and western regions. Meanwhile, the central and western regions can exert the late-development advantage by fully tapping their potentials, actively learning from the eastern high-efficiency regions about tourism development concepts, technologies, and experiences, innovating green and low-carbon technologies, and promoting the ecotourism with the construction of ecological civilization as the mainline. Second, rationally introduce foreign direct investment (FDI), adhere to both quantity and quality, diversify tourism development, promote the upgrading of tourism consumption, and focus on introducing advanced environmental protection and innovative technologies in tourism development. Third, perfect the tourism infrastructure, improve traffic networks, enhance transport capacity, and promote the openness and collaboration of the intra- and inter-regional tourism industry. Fourth, improve the institutional arrangement for environmental governance, promote the transformation of environmental regulation from "regulating" to "governing", mobilize relevant tourism enterprises to actively participate in environmental governance, and enhance environmental protection awareness to facilitate the transformation of the tourism industry into a resource-saving and environment-friendly industry.

Conflict of Interest

There is no conflict of interest.

References

[1] Liu, Z., Lu, C., Mao, J., et al., 2021. Spatial–Temporal Heterogeneity and the Related Influencing Factors of Tourism Efficiency in China. Sustainability. 13, 5825.
DOI: https://doi.org/10.3390/su13115825

[2] Geng, Y., Miao, H., Jia, F., et al., 2019. The Visualized Analysis on the Research Cooperation Network of Tourism Research Based on Cite Space. Tourism Research. 11(05), 14-24.
DOI: https://doi.org/10.3969/j.issn.1674-5841.2019.05.002

[3] Ma, J., Miao, H., Wen, S., et al., 2020. Temporal and Spatial Pattern Evolution of Tourism Ecological Security in Gansu Province Based on P-S-R Model. Journal of Hunan University of Science & Technology (Natural Science Edition). 35(03), 118-124.
DOI: https://doi.org/10.13582/j.cnki.1672-9102.2020.03.017

[4] Guo, L., Li, C., Peng, H., et al., 2021. Tourism eco-efficiency at the provincial level in China in the context of energy conservation and emission reduc-

tion. Progress in Geography. 40(08), 1284-1297.
DOI: https://doi.org/10.18306/dlkxjz.2021.08.003

[5] Schaltegger, S., Sturm, A., 1990. Okologische rationalitatan-satzpunkte-zur ausgestalung von okologieorientierten management instrumenten. Die Untemehmung. (4), 273-290.

[6] Gossling, S., Petters, P., Gerin, J., 2005. The eco-efficiency of tourism. Ecological Economic. 54(4), 417-434.
DOI: https://doi.org/10.1016/j.ecolecon.2004.10.006

[7] Raymond, C., Booth, A., Louis, B., 2006. Eco-efficiency and SMES in Nova Scotia, Canada. Journal of Cleaner Production. 14(6-7), 542-540.
DOI: https://doi.org/10.1016/j.jclepro.2005.07.004

[8] Susanne, K., Ariane, W., Mattia, W., 2011. How Can Tourism Use Land More Efficiently? A Model-based Approach to Land-use Efficiency for Tourist Destination. Tourism Management. 32, 629-640.
DOI: https://doi.org/10.1016/j.tourman.2010.05.014

[9] Medina, L., Gomez, I., Marrero, S., 2012. Measuring efficiency of sun & beach tourism destinations. Annals of Tourism Research. 39(2), 1248-1251.
DOI: https://doi.org/10.1016/j.annals.2011.12.006

[10] Qiu, X., Fang, Y., Yang, X., 2017. Tourism eco-efficiency measurement, characteristics, and its influence factors in China. Sustainability. 9(9), 16-34.
DOI: https://doi.org/10.3390/su9091634

[11] Xu, Q., Cheng, H., 2021. Temporal and Spatial Characteristics and Influencing Factors of Coupling Coordination Between China's Tourism Eco-efficiency and Tourism Green Innovation Efficiency. Journal of Zhongzhou University. 38(02), 33-40.
DOI: https://doi.org/10.13783/j.cnki.cn41-1275/g4.2021.02.007

[12] Joe, K., Wolfgang, H., 2007. Stated Preferences of Tourists for Eco-efficient Destination Planning Options. Tourism Management. 28, 377-390.
DOI: https://doi.org/10.1016/j.tourman.2006.04.015

[13] Tang, R., 2021. Trade facilitation promoted the inbound tourism efficiency in Japan. Tourism Management Perspectives. 38, 100-105.
DOI: https://doi.org/10.1016/j.tmp.2021.100805

[14] Li, Z., 2013. The Use of an Efficiency Evaluation Method in the Tourism Service Industry Based on a Low-carbon Economy Perspective. Tourism Tribune. 28(10), 71-80.
DOI: https://doi.org/10.3969/j.issn.1002-5006.2013.010.009

[15] Yao, Z., Chen, T., Yin, S., et al., 2016. Regional Tourism Eco-Efficiency Model and an Empirical Research of Hainan Province. Scientia Geographica Sinica. 36(03), 417-423.
DOI: https://doi.org/10.13249/j.cnki.sgs.2016.03.013

[16] Zhong, Y., 2016. Carbon emission measurement and eco-efficiency evaluation of tourism industry. Tourism Tribune. 31(09), 11-12.
DOI: https://doi.org/10.3969/j.issn.1002-5006.2016.09.005

[17] Peng, H., Zhang, J., Han, Y., et al., 2017. Measurement and empirical analysis of eco-efficiency in tourism destinations based on a Slack-based Measure-Data Envelopment Analysis model. Acta Ecologica Sinica. 37(02), 628-638.
DOI: https://doi.org/10.5846/stxb201507311616

[18] Wang, Z., Zhao, S., 2019. Temporal and Spatial Dynamic Evolution and Influencing Factors of Tourism Efficiency in Hunan Province Based on DEA-Malmquist Model. Resources and Environment in the Yangtze Basin. 28(08), 1886-1897.
DOI: https://doi.org/10.11870/cjlyzyyhj201908012

[19] Chen, L., Wang, W., Wang, B., 2015. Economic Efficiency, Environmental Efficiency and Eco-efficiency of the So-called Two Vertical and Three Horizontal Urbanization Areas: Empirical Analysis Based on HDDF and Co-Plot Method. China Soft Science. (02), 96-109.

[20] Yang, H., Wu, Q., 2017. Study on the eco-efficiency of land use transformation in Jiangsu province from the perspective of carbon remission—Based on the mixed directional distance function. Journal of Natural Resources. 32(10), 1718-1730.
DOI: https://doi.org/10.11849/zrzyxb.20160906

[21] Lin, X., Guo, Y., Wang, D., 2019. Spatial Evolution and Influencing Factors of Industrial Resource and Environmental Efficiency in China. Scientia Geographica Sinica. 39(3), 377-386.
DOI: https://doi.org/10.13249/j.cnki.sgs.2019.03.003

[22] Liu, J., Ma, Y., 2017. The Perspective of Tourism Sustainable Development: A Review of Eco-efficiency of Tourism. Tourism Tribune. 32(09), 47-56.
DOI: https://doi.org/10.3969/j.issn.1002-5006.2017.09.010

[23] Peng, J., Chen, H., 2004. A Study on the Efficiency of Star-rated Hotels-A Case Study on the Relative Efficiency of Beijing, Shanghai and Guangzhou Province. Tourism Tribune. 19(2), 59-62.
DOI: https://doi.org/10.3969/j.issn.1002-5006.2004.02.018

[24] Sun, J., Zhang, J., Zhang, J., et al., 2012. Spatial Characteristics and Optimition Countermeasures of Chinese City Hotel Industry Efficiency. Economic Geography. 32(08), 155-159.
DOI: https://doi.org/10.15957/j.cnki.jjdl.2012.08.030

[25] Zhao, L., Duan, W., 2012. The measurement and analysis of total factor productivity of China's travel agency industry. Journal of Arid Land Resources and

Environment. 26(8), 180-183.
DOI: https://doi.org/10.13448/j.cnki.jalre.2012.08.013

[26] Ma, H., Liu, J., Gong, Z., 2019. Carbon Emission and Evolution Mechanism of Tourism Transportation in Shanxi Province. Economic Geography. (4), 223-231.
DOI: https://doi.org/10.15957/j.cnki.jjdl.2019.04.027

[27] Cao, F., Huang, Z., Wu, J., et al., 2012. The Relationship between Tourism Efficiency Measure and Location Accessibility of Chinese National Scenic Areas. Acta Geographica Sinica. 67(12), 1686-1697.

[28] Fang, Y., Huang, Z., Zhang, H., et al., 2013. The Asynchronous Phenomenon and Relative Efficiency of Tourism Resources in China Based on Panel Data for 31 Provinces from 2001 to 2009. Journal of Resources and Ecology. 38(10), 1754-1764.
DOI: https://doi.org/10.5814/j.issn.1674-764x.2014.03.011

[29] Fang, Y., Huang, Z., Li, D., et al., 2015. The Measurement of Chinese Provincial Tourism Developing Efficiency and Its Spatio-Temporal Evolution. Economic Geography. 35(8), 189-195.

[30] Hu, Y., Mei, L., Chen, Y., 2017. Spatial and Temporal Differentiation Analysis on the Efficiency of the Three Mainstays of Tourism Industry in China. Scientia Geographica Sinica. 37(3), 386-393.
DOI: https://doi.org/10.13249/j.cnki.sgs.2017.03.008

[31] Liu, Z., Lu, C., Mao, J., et al., 2021. Spatial–Temporal Heterogeneity and the Related Influencing Factors of Tourism Efficiency in China. Sustainability. 13, 5825.
DOI: https://doi.org/10.3390/su13115825

[32] Ji, S., Xi, Y., Li, F., 2011. Operational Efficiency and Convergence Trend of Chinese Hotel &Tourism Industry. Journal of Shanxi University of Finance and Economics. 33(11), 63-72.
DOI: https://doi.org/10.13781/j.cnki.1007-9556.2011.11.002

[33] Liang, M., Yi, T., Bin, L., 2013. Study on the Evolutional Model of Tourism Efficiency Based on DEA-MI. Tourism Tribune. 28(5), 53-62.
DOI: https://doi.org/10.3969/j.issn.1002-5006.2013.05.006

[34] Cao, F., Huang, Z., Xu, M., et al., 2015. Spatial-temporal pattern and influencing factors of tourism efficiency and the decomposition efficiency in Chinese scenic areas: Based on the Bootstrap-DEA method. Geographical Research. 34(12), 2395-2408.
DOI: https://doi.org/10.11821/dlyj201512016

[35] Wang, Y., Sun, C., Jiang, J., 2016. Research on Efficiency and Empirical of Cultural Tourism in Gansu Province Based on Three Stage Data Envelopment Analysis Model. Resource Development & Market. 32(1), 125-128.
DOI: https://doi.org/10.3969/j.issn.1005-8141.2016.01.028

[36] Wang, Z., Liu, Q., 2019. The spatio-temporal evolution of tourism eco-efficiency in the Yangtze River Economic Belt and its interactive response with tourism economy. Journal of Natural Resources. 34(09), 1945-1961.
DOI: https://doi.org/10.31497/zrzyxb.20190911

[37] Han, Y., Shi, Q., Feng, W., et al., 2019. Temporal spatial differences of tourism industry efficiency and the influencing factors in Shanxi province. Journal of Arid Land Resources and Environment. 33(07), 187-194.
DOI: https://doi.org/10.13448/j.cnki.jalre.2019.218

[38] Li, Z., Wang, D., 2020. Temporal and Spatial Differentiation of Tourism Economy-Ecological Efficiency and Its Influencing Factors in Wuling Mountain Area. Economic Geography. 40(06), 233-240.
DOI: https://doi.org/10.15957/j.cnki.jjdl.2020.06.025

[39] Wei, L., Zhang, Y., Li, Q., et al., 2020. Study on Spatial Variation of China's Territorial Ecological Space Based on Standard Deviation Ellipse. Ecological Economy. 36(07), 176-181.

[40] Deng, H., Lu, L., 2014. The Urban Tourism Efficiencies of Cities in Anhui Province Based on DEA Model. Journal of Natural Resources. 29(02), 313-323.
DOI: https://doi.org/10.11849/zrzyxb.2014.02.013

[41] Lu, Y., Yuan, P., 2017. Measurement and spatial econometrics analysis of provincial industrial ecological efficiency in China. Resources Science. 39(07), 1326-1337.
DOI: https://doi.org/10.18402/resci.2017.07.10

[42] Wu, Y., Song, Y., 2019. Spatio-temporal Pattern Evolution and Driving Factors of Tourism Efficiency in Northeast China. Areal Research and Development. 38(05), 85-90.
DOI: https://doi.org/10.3969/j.issn.1003-2363.2019.05.016

[43] Maddison, D., 2006. Environmental Kuznets Curves: a spatial econometric approach. Journal of Environmental Economics and Management. 51(2), 218-230.
DOI: https://doi.org/10.1016/j.jeem.2005.07.002

[44] Yang, R., 2015. Whether Industrial Agglomeration Can Reduce Environmental Pollution or Not. China Population, Resources and Environment. 25(02), 23-29.
DOI: https://doi.org/10.3969/j.issn.1002-2104.2015.02.004

[45] Yuan, Y., Xie, R., 2015. Empirical research on the relationship of industrial agglomeration, technological innovation and environmental pollution. Studies in Science of Science. 33(09), 1340-1347.
DOI: https://doi.org/10.16192/j.cnki.1003-2053.2015.09.007

[46] Li, S., Chu, S., Shen, C., 2014. Local government

competition, environmental regulation and regional eco-efficiency. The Journal of World. 37(04), 88-110.

[47] Ren, H., Yao, Y., 2016. Effects of Environmental Regulation on Eco-efficiency from the Perspective of Resource Dependence-Based on Super Efficiency SBM Model. Soft Science. 30(06), 35-38.
DOI: https://doi.org/10.13956/j.ss.1001-8409.2016.06.08

[48] Shen, P., Zhu, G., 2011. Resources and environmental problems in the development of tertiary industry in Jiangsu Province. China Population, Resources and Environment. 21(S1), 125-128.

[49] Hong, Z., Wang, L., Zhang, C., 2021. Influencing factors of regional tourism eco-efficiency under the background of green development in the western China. Acta Ecologica Sinica, 41(9), 3512-3524.
DOI: https://doi.org/10.5846/stxb202002140253

[50] Zhao, L., 2019. Assessing Eco-efficiency of China Tourism Industry with DEA Approach. Journal of Beijing University of Aeronautics and Astronautics (Social Sciences Edition). 32(1), 91-97.
DOI: https://doi.org/10.13766/j.bhsk.1008-2204.2016.0306

[51] Guo, L., Li, C., Peng, H., et al., 2021. Tourism eco-efficiency at the provincial level in China in the context of energy conservation and emission reduction. Progress in Geography. 40(08), 1284-1297.
DOI: https://doi.org/10.18306/dlkxjz.2021.08.003

[52] Lu, J., Liu, Z., Zhang, B., et al., 2020. Ecological Efficiency and Spatial Effects of Tourism Industry in China. Journal of Northeast Forestry University. 48(10), 49-54,60.
DOI: https://doi.org/10.3969/j.issn.1000-5382.2020.10.009

[53] Wang, F., Fang, Y., 2021. Eco-effciency Measurement and Evolution Mechanism of Tourism: A Case Study of Provincial Panel Data in Mainland China. Journal of Huaiyin Teachers College (Natural Sciences Edition), 20(04), 311-318.
DOI: https://doi.org/10.16119/j.cnki.issn1671-6876.2021.04.005

[54] Wang, S., Qiao, H., Feng, J., et al., 2020. The Spatio-Temporal Evolution of Tourism Eco-Efficiency in the Yellow River Basin and Its Interactive Response with Tourism Economy Development Level. Economic Geography. 40(5), 81-89.
DOI: https://doi.org/10.15957/j.cnki.jjdl.2020.05.009

[55] Li, Z., Wang, D., 2020. Temporal and Spatial Differentiation of Tourism Economy-Ecological Efficiency and Its Influencing Factors in Wuling Mountain Area. Economic Geography. 40(6), 233-240.
DOI: https://doi.org/10.15957/j.cnki.jjdl.2020.06.025

BILINGUAL PUBLISHING CO.
Pioneer of Global Academics Since 1984

Journal of Geographical Research
https://ojs.bilpublishing.com/index.php/jgr

ARTICLE

An Analysis of Urban Vacant Land on the Macau Peninsula

Ye Lin[1] Hanxi Li[2*]

1. Hengqin Branch, Guangdong Urban & Rural Planning and Design Institute CO., Ltd, Guangzhou, 510290, China
2. Institute of Shenzhen Urban Planning, Shenzhen Tianhua Urban Planning and Design Co., Ltd, Shenzhen, 518000, China

ARTICLE INFO

Article history
Received: 04 April 2022
Revised: 07 May 2022
Accepted: 12 May 2022
Published Online: 26 July 2022

Keywords:
Macau peninsula
Urban vacant land
Urban renewal

ABSTRACT

With the development and construction of the city, the urban development of the Macau Peninsula has entered an era of stock development against the background of the limited scale of urban land. With the shortage of land resources, the problem of unused land on the Macau Peninsula is coming to the fore. This paper mainly studies the problem of idle land in the Macau Peninsula, based on the urban development and particular historical background of the region, investigates and elaborates on its complex formation causes through the literature research method, and analyzes the spatial distribution characteristics of idle land in the current situation of the Macau Peninsula by using GIS technology. Based on the above research, suggestions are put forward to prevent and manage the urban vacant land problem in the future urban management and development of Macau.

1. Introduction

Macau is one of the two special administrative regions of the People's Republic of China. Including the Macau Peninsula and the outlying islands, the land area is 32.9 km^2, and the total population is 679,600 (as of the third quarter of 2020). Fifty-seven percent of the population of Macau resides on the peninsula, which is only 9.1 square kilometers in size [1]. With urban construction, industrial restructuring, population migration, and deficiencies in land management policies, a large amount of idle land has been created in the peninsula of Macau, which hurts the urban environment, social security, and residents' health.

In a narrow sense, idle land refers to land that cannot be developed according to the time conditions specified by the original approval unit after the landowner has legally acquired the right to use the land. In a broad sense, idle land also includes land that has been approved by the relevant authorities for conversion from other land types to built-up land but has not been constructed in time [2].

For the idle land in the city, the Macau government

*Corresponding Author:
Hanxi Li,
Institute of Shenzhen Urban Planning, Shenzhen Tianhua Urban Planning and Design Co., Ltd, Shenzhen, 518000, China;
Email: 2320158858@qq.com

DOI: https://doi.org/10.30564/jgr.v5i3.4595

only defines the idle units in the completed buildings, and there is no clear definition for the idle land in the city. However, the problem of idle land has become a problem that cannot be ignored in Macau's urban development. Idle land is not only a waste of resources but also has a severe impact on the healthy development of the city. On the one hand, it damages the image of the city. On the other hand, it fragments the ecological and social fabric of the city, which seriously affects land management system and economic and social development [3].

The problem of idle land in Macau has a long history, but relevant scholarly studies are non-existent. For example, the new Land Law passed in 2013 has improved the prevention of idle land. In 2020, the Macau Urban Master Plan (2020-2040) was drafted and after the public consultation, the Macao government started to transform some unused land in Macao. These initiatives demonstrate the urgent relevance of analyzing and studying idle land.

2. Causes and Effects of Urban Vacant Land in the Macau Peninsula

2.1 Lack of Land Management and Enforcement

Since 1987, Macau has granted more than 30 hectares of land every year in public auctions. In the 1960s, the rapid development of the Western economy led to the growth of Macau's tourism and export processing industries, and Macau's per capita income level rose sharply. In the late 1970s, thanks to the reform and opening-up policy of the mainland China, foreign capital poured into Macau, and large number of immigrants from the mainland China created a high level of supply and demand for Macau real estate.

In 1992, the Macau government received close to 3 billion yuan from land sales and property revenues. While urban construction was in full swing, corresponding construction management did not keep pace. The shortcomings of management began to emerge in 1993 when there was no more ready supply of land on the Macau Peninsula, most notably unused urban land [4]. Although the land law stipulates that land not completed within the deadline for construction will be reclaimed. However, the relevant agencies did not enforce management, resulting in some land developments that was not started as planned initially being left idle for a long time.

2.2 As a Result of the Land Reclamation Policy

To prevent real estate developers from hoarding land for profit, the new Land Law was passed by the Legislative Assembly of the Macau SAR in 2013 and has been in effect since March 2014. Since it came into effect, the Macau government has vacated, relocated, and rehabilitated many projects in Macau that were not built during the lease period. By 2020, about 700,000 square meters and more than 80 pieces of land have been reclaimed [5]. Most of the reclaimed land remains vacant. The government has fenced off the reclaimed land to prevent private encroachment, a move that has further reduced the utilization of the unused land.

The government reclaims this type of land because the planned construction is not completed within the lease period. However, due to imperfect laws and regulations, the rights and interests of the owners, developers and other nearby residents are not adequately protected after the land is resumed. The problem of entangled interests requires the resumed land to go through a rather long process of being left idle.

2.3 Urban Decay Due to Industrial and Population Shifts

Macau was once one of the most prosperous trading ports in the Far East, and the heyday of its entrepôt trade was from the late sixteenth century to the early seventeenth century. However, after the Opium War, Hong Kong quickly replaced Macau with the advantage of its natural harbor and other historical and economic reasons. In contrast, Macau's entrepot trade was drastically reduced in scale and scope due to the port's natural conditions, severe siltation, and especially the inconvenience of shipping from the era of sailing ships to the era of steam. The gaming and tourism industries overgrew in the middle of the twentieth century. They produced an one-of-a-kind phenomenon, which prompted the rapid shift of the city's population employment to the tertiary industry [6]. The original built environment has decayed due to population loss, and the land has been left unused.

A part from state-owned land and industrial land, most of the other land in Macau is private property. Smaller areas, such as residential land, that the property owners vacated, lead to inefficient land use, building decay, and environmental degradation resulting in land idleness.

Urban vacant land suffers from environmental decay quality, pollution, environmental problems, and a negative impact on the continuity of streets [5]. According to the "street eye", theory in Jane Jacobs's "The Death and Life of Great American Cities", when enough residents surround a street, pedestrians walking on the street will be under the surveillance of the residents on both sides of the street. This model creates a lower-cost surveillance environment, which leads to higher crime costs. However, due to fragmented unused urban land, a large amount of

unused land on the Macau Peninsula, especially in the Sha Lei Tou area, destroys the stability and continuity of the streets, resulting in unmonitored urban streets.

2.4 Investment Transfer from Reclamation Projects

Macau's long-standing method of acquiring land for urban construction through reclamation has likewise resulted in the formation of urban open spaces. According to statistics, the area reclaimed in Macau from 1912 to 2018 reached 235,000 km^2 [6]. Since 1993, Macau has relied on reclamation and the acquisition of old residential areas for redevelopment as the primary source of new land. From the investor's point of view, the land price on the Macau Peninsula is too high, and the urban environmental problems caused by high-density buildings are prominent. The acquisition of vacant land for investment is not very efficient. Therefore, it is often challenging to rebuild unused land on the Macau Peninsula under these circumstances. While environmental decay leads to empty urban land, which makes investment shifts and population migration increasingly evident, the idle land situated on the Macau Peninsula can easily fall into an undesirable cycle.

3. Status of Unused Land on the Macau Peninsula

3.1 Overview of Vacant Land in Macau

As of 2020, there are approximately 700 idle lands in Macau, with approximately 1.2 million square meters. Seven hundred thousand square meters have come from land reclaimed by the government since 2014 under the new land law. Approximately 62% of the idle land belongs to private ownership or long-term leases. Most of the vacant land in Macau is under 100 m^2, and is concentrated in the Sha Lei Tau area of the Macau Peninsula, which accounts for 55% of the total vacant land [6].

3.2 Types of Idle Land in the Macau Peninsula

According to the formation texture of idle land, it can be roughly divided into recycled land, abandoned land, and unused land. According to the original land use, abandoned land can be subdivided into industrial abandoned land and non-industrial abandoned land. Unused land is composed of long-term leased land and unused private land. According to Macau's current land law, land can be divided into private land and state-owned land. With the definition of unused land, the property rights of unused land in Macau belong to private land and state-owned private property. After a long period of urban development and land reclamation in Macau, the idle land in Macau has developed very distinctive physical characteristics with different property rights backgrounds. The characteristics of each type of idle land are shown in the following table (Table 1).

Since the new Land Law was implemented in 2014, the Macau government has reclaimed land that was not built according to the original plan and exceeded the lease term. Most of the government reclaimed land has been idle before reclaiming. The government has put fences around the reclaimed land after a simple cleanup of the environment and illegal occupation. Most of the government reclaimed land is significant. It retains remaining buildings or structures, with varying degrees of vegetation recovery over the time of inactivity. The degree of vegetation recovery is better due to less impact from human activities after the fence protection recovery.

Table 1. Types and Characteristics of Vacant Land in the Macau Peninsula

Type of idle land		Ownership	Characteristics
Reclaimed Land		State-owned	The site area is large, surrounded by a fence barrier, the land is exposed after site leveling. There are some leftover building structures. With the time after recycling, there are different degrees of vegetation recovery. The degree of vegetation recovery is good.
Abandoned Land	Industrial waste land	Private	The site is extensive, mainly hard-paved, with legacy industrial buildings or illegal occupation and pollution problems.
	Non-industrial waste land		The site area is small, mostly walled off, mainly hard paved, with legacy buildings or frames in the site, partly illegally occupied, with different degrees of vegetation recovery with the impact of abandonment time and human activities.
Unused land	Long-term land grant	State-owned	The site is regular in shape, with a large site area surrounded by a fence barrier, and the site is dominated by level grass.
		Private	The site's shape is irregular. Those with a slightly larger site area are used mainly by residents as parking lots or warehouses on their initiative, with hard paved surfaces dominating the site. Sites with small areas mostly have a small amount of garbage piled up. With idle time there is part of vegetation restoration.

Due to the transfer of population and industry, some privately owned land is abandoned. The industrial abandoned land, represented by the Inner Harbor Terminal, has a large site area, retains the original industrial buildings, and has illegal occupation has pollution problems. Most of the non-industrial abandoned sites were once used for residential or commercial purposes and were abandoned due to the relocation or bankruptcy of the property owner, most of them have been abandoned for a long time, and the buildings are seriously damaged or demolished.

Due to problems such as geographical location, land price, and construction cost, some land in the Macau Peninsula has been left unused for a long time. Long-term unused land belonging to the government is larger in size, surrounded by fences and blocked by human activities, and less affected by human activities, and the site is mainly a flat lawn. Long-term unused land belonging to the private sector is irregular in shape. Those with a slightly larger site area are used mainly by nearby residents as parking lots or warehouses on their initiative, with complex paved areas dominating the site. Smaller sites are primarily in the form of building gaps, with walls blocking them, a small number of garbage piles, and with idle time some vegetation restoration.

3.3 Distribution of Idle Land on the Macau Peninsula

According to the meaning of idle land, the authors used GIS technology to make an essential identification of idle land in the Macau Peninsula and then adjusted the location and boundary through field research. Following the above steps, we obtained the spatial distribution of 121 unused land parcels on the Macau Peninsula (e.g. Figure 1). The spatial distribution of the obtained current idle land was then further classified according to different types of idle land (e.g. Figure 2).

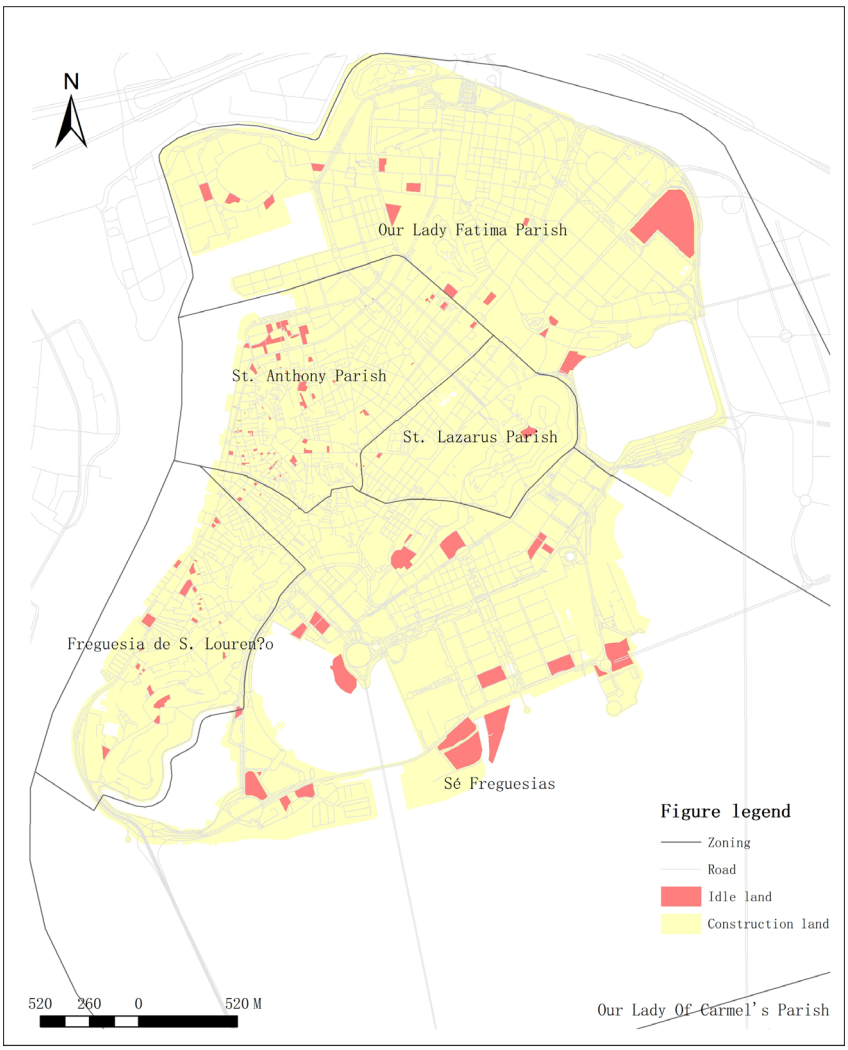

Figure 1. Distribution of idle land on the Macau Peninsula

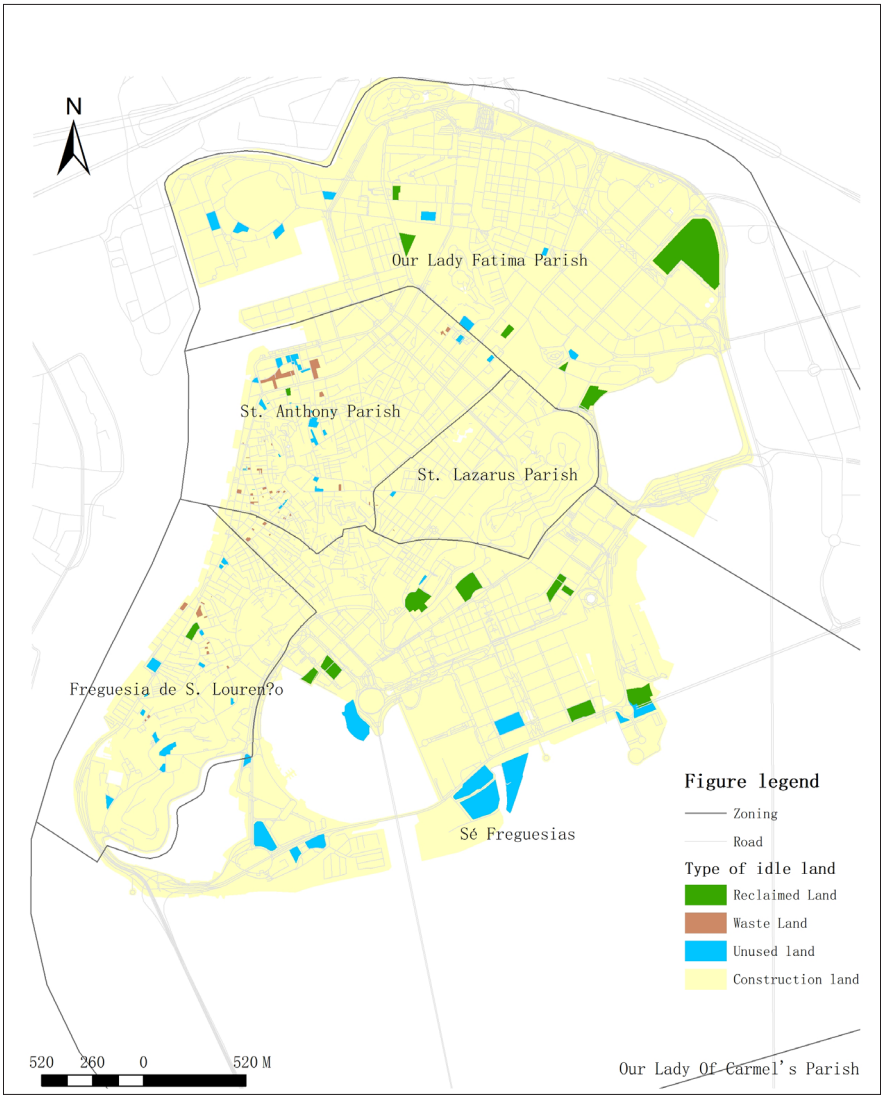

Figure 2. Distribution of different types of vacant land on the Macau Peninsula

According to the distribution map of unused land on the Macau Peninsula, St. Anthony's Parish has the largest number of unused land with 53 parcels, accounting for 43.8% of the total unused land and 18.7% of the total unused land. Freguesia de S. Lourenço and Sé Freguesias have the same amount of unused land, accounting for 19.8% and 21.4% of the total unused land. 19.8% and 21.4%, respectively. However, Figure 1 shows that Sé Freguesias has a larger area of idle land, accounting for 42% of the total idle land. In comparison, Freguesia de S. Lourenço has a smaller area of idle land, accounting for 12.6% of the total idle land. Our Lady Fatima Parish has 11.5% of the total idle land and 11.5% of the total idle land. 11.5% of the total idle land and 26% of the total idle land area; St. Lazarus Parish has the least idle land, accounting for 3.3% of the total idle land and 0.3% of the total idle land area (Table 2).

Table 2. The number and area of idle in different administrative regions

Administrative Zoning	Number of idle parcels	Area (m^2)
Our Lady Fatima Parish	14	41847
St. Anthony Parish	53	30123
Freguesia de S. Lourenço	24	20333
Sé Freguesias	26	67647
St. Lazarus Parish	4	626
Total	121	160648

The distribution of vacant land on the Macau Peninsula (e.g. Figure 2) shows that vacant land is the most numerous, accounting for 48% of the total number of unused land. Furthermore, it is the most widely distributed, with scattered distribution in all five districts, with St. Anthony Parish having the most significant distribution. Vancant land accounts for 38% of the total unused land, mainly in St. Anthony Parish and Freguesia de S. Lourenço; recycling accounts for 13% of the total number of unused land, mainly in Our Lady Fatima Parish and Sé Freguesias (Table 3).

Table 3. Number and area of different types of idle land

Type of idle land	Quantity	Area (m^2)
Recycle Land	16	55865
Waste Land	46	18014
Unused land	59	86769
Total	121	160648

Our Lady Fatima Parish is located in the northernmost part of Macau, with a predominantly residential and industrial site type. It is also the second most densely populated parish in Macau. Our Lady Fatima Parish has 42.9% of the total amount of reclaimed land in its area. And the area of unused land is the largest, accounting for 42.9% of the total, they are all located within the main residential areas. The amount of unused land is the highest, 57.1% of the total amount of unused land in its area, and the most significant area, 52.4% of the total area of unused land in its area.

St. Anthony Parish is located in the western part of the Macau Peninsula and is the most densely populated parish in Macau. St. Anthony Parish has 1.9% of the total amount of reclaimed land in its area and 3% of the total area of unused land in its area; the most significant amount of abandoned land, 66% of the total amount of unused land in its area, and the most significant area, 51% of the total area of unused land in its area; and 32.1% of the total amount of unused land in its area and 47% of the total area of unused land in its area. The number of unused land accounts for 32.1% of the total unused land in the region and 47% of the total unused land in the region. The municipality may consider mitigating the population pressure in the area by rationalizing the use of land.

Freguesia de S. Lourenço is located in the southwestern part of the Macau Peninsula. The headquarters of the Macau SAR Government (formerly the Macau Governor's Office) and some government departments are located in this parish. The eastern part of the parish is located in the area around the Mid-Levels of Sai Van, the most prestigious residential area in Macau. Freguesia de S. Lourenço has 4.2% of the total number of reclaimed land and 16.4% of the total area of unused land in the region; 45.8% of the total number of unused land and 15.9% of the total area of unused land in the region; and the enormous amount of unused land, 50% of the total number of unused land and the largest area of the total area of unused land in the region. The most significant number of unused land, accounting for 50% of the total number of unused land in its area, and the most prominent area, accounting for 67.7% of the region's total area of unused land. These unused lands have a negative impact on the spatial quality of the area.

Freguesia da Sé is located in the southeastern part of the Macau Peninsula, the largest parish in the area and the commercial center of the Macau Peninsula. The area's unused land is characterized by its large size, which diminishes the quality of the commercial space and may be detrimental to business vitality. Sé Freguesias has 30.8% of the total amount of reclaimed land and 46.8% of the total area of unused land in its region; 15.4% of the total amount of abandoned land and 1.4% of the total area of unused land in its region; the immense amount of unused land, 53.8% of the total amount of unused land in its region, and the most significant area, 67.7% of the total area of unused land in its region. The most significant number of unused land, accounting for 53.8% of the total unused land in the region, and the most significant area, accounting for 67.8% of the total unused land in the region.

Located in the middle of the Macau Peninsula, the smallest of the five parishes on the peninsula, the area has many old Portuguese buildings. And the unused land in the area hinders the continuity between these Portuguese buildings. St. Lazarus Parish has 50% of the total amount of abandoned land in its area and 10.3% of the total area of unused land. The most considerable amount of unused land is 50% of the total amount of unused land in its area and 89.7% of the total area of unused land in its area (Table 4).

Table 4. Number and area of each idle land type in different administrative regions

Administrative Zoning	Type of idle land	Quantity	Area (m²)
Our Lady Fatima Parish	Recycle Land	6	19929
	Waste Land	0	0
	Unused land	8	21918
	Total	14	41847
St. Anthony Parish	Recycle Land	1	904
	Waste Land	35	15350
	Unused land	17	13869
	Total	53	30123
Freguesia de S. Lourenço	Recycle Land	1	3342
	Waste Land	11	3231
	Unused land	12	13760
	Total	24	20333
Sé Freguesias	Recycle Land	8	31690
	Waste Land	4	939
	Unused land	14	35018
	Total	26	67647
St. Lazarus Parish	Recycle Land	0	0
	Waste Land	2	72
	Unused land	2	626
	Total	4	698

4. Utilization of Vacant Land in Macau Peninsula

4.1 Government Rehabilitation Measures

Macau's urban development did not consider the impact of development policies on the city's vacant land until the unprecedented growth of tourism after the handover when the damage to the cityscape caused by unused land began to be noticed. In 2002, the Macau SAR government renovated the unused land located in a tourist hotspot with temporary greening [8]. The residents well received this project, but the related evaluation system was not established. After implementing the new Land Law in 2014, a series of social impacts caused by the government's land resumption brought the use of unused land back into the public eye. To "optimize the use of unused land and expand leisure and recreational space for the public", the Municipal Department of Macau has started to convert some unused land in Macau into leisure and recreational parks and temporary community services.

4.2 Informal Use by Residents

The long-term idleness of the land has also led to many everyday uses, with residents mainly using the unused land for parking, stacking debris, or farming. On larger plots of unused land, informal warehouses are built to store equipment and building materials and are even managed by "security guards". This spontaneous use of unused land by residents is considered a "disorderly space" in the city due to the lack of management and guidance, inefficient use, and filthy environment, which hurts the order and environment of the city and poses a threat to the physical and mental health of the city residents [9].

After implementing the new Land Law of the Macao SAR in 2014, the reclaimed land was fenced off, and all unpermitted people and activities were prohibited. Informal activities in some of the unused land were restricted. However, there is no regulation or restriction on informal activities for the unused land that has not been reclaimed. Due to the shortage of parking spaces and the inadequate supply of community services on the Macau Peninsula, unused urban land instead provides a solution. Although the public often has a negative attitude towards it, its existence cannot be denied.

5. Utilization of Vacant Land in Macau Peninsula

5.1 Reflections on the Status of Unused Land in the Macau Peninsula

The urban idle land problem faced by the Macau Peninsula today is also manifested to varying degrees in the urban centers of the territory. The causes of the formation of idle land in the Macau Peninsula are somewhat unique due to its political and historical background. However, the characteristics and current use of idle land have similarities with other cities worldwide. Fortunately, the Macau government is aware of the impact of unused urban land and has developed prevention and utilization plans. However, due to the inherent complexity of urban idle land, fragmented and unregulated utilization is challenging to implement uniformly [10]. It is impossible to address the problem at its root. As a result, the problem of unused land on the Macau Peninsula and other urban problems arising from unused land has not been effectively solved so far. Some lessons can be learned from the causes and remedies of unused land in the Macau peninsula.

On the one hand, the problem of unused land in the city involves many factors, and it often takes a long time and is challenging to solve. Therefore, the best way to solve such problems is to prevent them before they arise and avoid creating large amounts of unused land. This requires urban planning managers to have a good understanding of urban idle land and to take responsibility for its preven-

tion. On the other hand, the stable maintenance of urban vitality is also an essential factor influencing the creation of idle land in cities. The stable existence of residents is the key. The reasonable development of urban industries guarantees residents to live and work in peace and happiness, ensuring the stability of human resources in cities to create lasting and sustainable urban development momentum.

5.2 Suggestions for the Prevention and Utilization of Idle Land on the Macau Peninsula

5.2.1. Improve Relevant Policies and Systems to Protect the Interests of All Parties

With the government as the leader, relevant policies are formulated and improved to prevent the generation of idle urban land, protect the interests of all parties, and encourage and guide the rebuilding of recovered land. Although the new Land Law of 2013 mentions the prevention of urban idle land and penalizes or recalls approved construction projects that have not been started for a long time. However, after the penalty or recall, there is no regulation to support protecting the rights and interests of the relevant stakeholders, especially citizens. On the other hand, the conflict between the relevant stakeholders leaves the land in an inefficient mode between idleness and redevelopment. This situation can be based on the mature experience of "transitional spaces" in foreign countries, such as the 2004 Vienna strategic plan to use unused land to build short-term public activity spaces to address the lack of public space in the inner city. Moreover, in 2016, the Philadelphia Water Department included unused land as part of the city's stormwater management strategy to reduce total sewer overflows by filtering and storing stormwater through green infrastructure [11].

5.2.2 Adopting Flexible Financing Models to Accelerate the Reuse of Idle Land

Due to the property rights situation of Macao land, idle land faces complex property rights problems in reuse, especially the private property rights of idle land, which is the central aspect that hinders its re-construction.

It is suggested that the pace of construction should be accelerated by drawing on mature foreign construction investment models—for example, the U.S. Land Bank's "Land Transfer Program" for idle land use. Neighborhood homeowners purchase vacant land at a lower price without taking ownership, providing a formal opportunity for the rational use of vacant land. The transfer of vacant land also resolved vacant land tax arrears [11]. Most of the vacant land within the Macau Peninsula is small, the investment threshold is not high, and the governance difficulty and maintenance costs are also low governance difficulty and maintenance operation costs are relatively low. It is recommended that the PPP (Public-Private Partnership) model be adopted for the transformation of idle land in the Macau Peninsula to reduce the financial pressure on the government. Attract social capital participation, accelerate the construction process and improve the quality of the project [12,13].

5.2.3 Comprehensive Integration to Form a Systematic Management

One of the significant characteristics of idle land in the cities of the Macau Peninsula is that it is scattered and fragmented, and irregular. Corresponding management and transformation methods should be developed according to the characteristics of the type of idle land and its relationship with the surrounding parcels. At the same time, the utilization of idle land should not be developed separately from the actual development of the city. However, it should be integrated into the urban planning and development requirements to avoid inefficient use of the land to make it idle again.

5.2.4 Encouraging Public Participation in the Transformation of Unused Urban Land

Before the arrival of the "bottom-up" policy, some "bottom-up" uses of unused urban land often existed, and such informal uses often reflect the most genuine needs of users. Encouraging the public to participate in the renovation of unused land from users' perspective can ensure the utilization rate of the renovated land on the one hand and ensure fairness on the other. Involving the public in the renovation and use of unused land will promote the concern of urban residents for urban construction and will have a positive impact on the government's integrity and social harmony.

5.2.5 Improve the Evaluation System

A comprehensive evaluation system should be developed for completed idle land-use projects to judge whether they are sufficient to meet the design objectives. It should be considered at the level of three guidelines: ecological benefits, economic benefits, and social benefits, and should have different focuses for idle land use with different types of characteristics; for example, for idle land-use projects with larger areas, more attention should be paid to their ecological benefits, and for idle land use with smaller areas, more attention should be paid to their economic and social benefits. Only by improving the

evaluation system can we better guide the utilization of unused urban land to produce more significant benefits.

6. Conclusions

The lack of management policies is the main reason for the problem of idle land. The shift in population and industry, as well as the shift in investment brought about by reclamation projects, further exacerbates the idle land situation on the Macau Peninsula. Idle land in the city has a negative impact on streetscape, community quality, and even human health. Improving relevant policies is the first task to improve and prevent the problem of unused land in Macau, and also to encourage public participation in the renovation and construction of unused land to ensure the interests of all parties. Also, an assessment mechanism for the construction of unused land needs to be established.

Author Contributions

Ye Lin was responsible for the primary data collection and analysis in this study and was also the paper's principal author. Hanxi Li was responsible for proofreading this study.

Funding

This research received no external funding.

Conflict of Interest

The authors declare no conflict of interest.

References

[1] Macao Special Administrative Region Government Statistics and Census Bureau: Population and Households, 2020. https://www.dsec.gov.mo/zh-MO/. (Accessed 24 January 24 2021).

[2] Yi, X.X., Zhao, T.Y., Wu, Y.F., et al., 2020. "Crisis" or "opportunity"? --A study of international experience in addressing the problem of shrinking urban vacancy. Journal of Urban Planning. (02), 95-101. DOI: https://doi.org/10.16361/j.upf.202002012

[3] Liu, Z.F., 2019. Spatial distribution, formation mechanism and reuse of urban vacant land (Master's thesis, Tung Wah University of Science and Technology). https://kns.cnki.net/KCMS/detail/detail.aspx?dbname=CMFD202001&filename=1019627981.nh.

[4] Xie, L., Tang, Ch., 2015. On the modification and improvement of the public tender for land grant in Macao. Contemporary Hong Kong and Macau Studies. (03), 75-91. DOI: https://doi.org/10.13521/b.cnki.ddgayj.2015.0020

[5] Chen, J.J., Zhang, Zh.X., Long, Y., 2020. Strategies to promote public health-oriented street space quality from the perspective of spatial disorder. Urban Planning. (09), 35-47.

[6] Viewpoint Property Network: Savills: Macau Land Survey Research Summary,2020. https://www.savills.com.mo/. (Accessed 25 June 2021).

[7] Huang, G.C., 2020. Analysis of the current situation and evaluation of the potential utilization of the vacant land in Yueyang City (Master's thesis, Hunan Normal University). https://kns.cnki.net/KCMS/detail/detail.aspx?dbname=CMFD202101&filename=1020321754.nh

[8] Municipal Services Department: "Municipal Services Department makes good use of unused land to increase open space Taipa to build a car tire park to promote conservation and environmental protection". https://gb.iam.gov.mo/c/news/... /90b10d4e-a170-4c89-9b91-58ef10aa92a8gb.iam.gov.mo ' news ' detail. (Accessed 25 June 2021).

[9] Song, X.Q, Ma, Zh.H., Zhao, G.S., et al., 2018. Urban vacant land: Cold thoughts on the urbanization boom. Journal of Geography. (06), 1033-1048.

[10] Gong, C., Wu, C.Y., Hu, C.J., 2017. A Systematic Planning Approach for Transforming Urban Open Space into Green Infrastructure: The Case of Richmond, USA. China Gardening. (05), 74-79. DOI: https://doi.org/CNKI:SUN:ZGYL.0.2017-05-015

[11] Yang, S., 2019. The Development of "Transitional Use" and Related Research in China and Overseas - A New Perspective of Urban Research. International Urban Planning. (06), 49-55. DOI: https://doi.org/CNKI:SUN:GWCG.0.2019-06-009

[12] Galen, N., Lai, D.Y., Zhu, R., et al., 2018. Urban reengineering and resilience enhancement: An economic performance assessment of green infrastructure-oriented reuse of vacant land. Landscape Architecture. (06), 10-23. DOI: https://doi.org/CNKI:SUN:JGSJ.0.2018-06-003

[13] Chen, W.Zh., Liu, T., 2016. Potential and value of informal development landscape projects in urban renewal. China Gardening. (05), 32-36. DOI: https://doi.org/CNKI:SUN:ZGYL.0.2016-05-008

BILINGUAL PUBLISHING CO.
Pioneer of Global Academics Since 1984

Journal of Geographical Research
https://ojs.bilpublishing.com/index.php/jgr

ARTICLE

The Use of Airborne LiDAR in Assessing Coastal Erosion in the Southeastern USA

David F. Richards IV[1*] Adam M. Milewski[1] Brian Gregory [2]

1. Water Resources & Remote Sensing Lab (WRRS), Department of Geology, University of Georgia, Athens, GA 20602, USA
2. Southeast Coast Inventory & Monitoring Network (SECN), Main Office, Southeast Coast Network, Athens, GA 30605, USA

ARTICLE INFO

Article history
Received: 31 May 2022
Revised: 01 July 2022
Accepted: 11 July 2022
Published Online: 02 August 2022

Keywords:
Coastal
Erosion
LiDAR
Elevation
Volumetric change
Geomorphology
Sea level

ABSTRACT

Changes in sea level along the coastal southeastern United States (U.S.) influence the dynamic coastal response. In particular, the Southeast Coastal Network (SECN) of the National Park Service (NPS) has exhibited evidence of fluctuations in sea level which caused coastal erosion. Airborne LiDAR acquired from NOAA for Fort Matanzas National Monument, Fort Pulaski National Monument, Charles Pinckney National Historic Site, and Cape Lookout National Seashore were analyzed to identify changes in both elevation and the spatial volume of unconsolidated sedimentary material in the coastal southeast over time. Areas that exhibited an increase (deposited material) or decrease (eroded material) in elevation were mapped across the study area from 2006 to 2018. Results indicate a quasi-cyclic process where unconsolidated sediment distribution and the morphodynamic equilibrium changes with time. The coastal zones are steadily oscillating between the process of erosion and deposition affecting the coastal geomorphological dynamic. The use of LiDAR for evaluating coastal sustainability and resiliency due to this environmental phenomenon is clear.

1. Introduction

The coastal southeast United States (U.S.) is highly susceptible to geomorphological and hydrogeological changes in response to relative sea level rise. Climate change increases both the quantity and intensity of storms which results in subsequent sea level rise [1-3]. Many variables play a role in the geomorphological and hydrological response to this shift. These variables are intrinsically connected, defining the interaction and link of hydrologic and geomorphic processes in both temporal and spatial dimensions [4,5]. The Atlantic Coastal Plain is extremely sensitive to sea level rise, causing accelerated erosion

*Corresponding Author:
David F. Richards IV,
Water Resources & Remote Sensing Lab (WRRS), Department of Geology, University of Georgia, Athens, GA 20602, USA;
Email: milewski@uga.edu

DOI: https://doi.org/10.30564/jgr.v5i3.4762

rates and changes in the amount of sediment deposited in coastal areas [6-8]. As this is representative of the hydrogeological impact, the economic impacts are analogous to the direct damages of sea level rise [9-11].

Global mean sea level rise has risen about 21 centimeters ~ 24 centimeters (0.21 meters ~ 0.24 meters) since 1880, with about a third of that coming in just the last two and a half decades [12]. By 2100, research suggests that sea level rise could exceed 2 meters, given the climate regimes continue at their current rates [13]. Along the southeastern US coastline, approximately 43% (~2,000 km) of the area is projected to have an increase in coastal erosion vulnerability by the 2030s, with respect to its present vulnerability [14]. Studies have shown that the coastal sediment budget, representing the sediment supply, is extremely vulnerable [15-17]. Coastal erosion is continuously altering the environment and mitigating its effects has become increasingly important. To meet the increasing demand of coastal resource management, remote sensing techniques are being used to provide rapid data acquisition of large areas that would normally require extensive and lengthy field surveys. Furthermore, the ability to use light detection and ranging (LiDAR) in both natural resource management and economic sustainability, creates the opportunity to distinctively characterize the coastal dynamic response at high spatial resolutions.

Typically, LiDAR is used in forest management to understand biomass dynamics as it was historically believed to show the greatest promise over these areas, however, it's use in coastal applications has become a pivotal tool in coastal change detection [18,19]. The ability of LiDAR has garnered efficient, productive, and accurate measurements of topographical mapping [20-22]. LiDAR's application enables rapid elevation data collection through repeated measurements of the observed topographic region [23]. The high spatial resolution data retrieved produces digital elevation models (DEMs) indicative of current and historical coastal geomorphological changes. The results have become an asset in improving the knowledge of complex coastal geomorphological processes creating better preventative and mitigating initiatives [24-26].

In recognition of the changes occurring along the coastal southeast US, the sediment budget has displayed both aggraded and degraded material [27,28]. In this paper, we present the usefulness of LiDAR in characterizing the spatial and temporal changes of the coastal southeast US, and quantify these changes at select National Park sites. More specifically to identify the temporal changes in elevation, and quantify the spatial volumetric changes of unconsolidated sedimentary material in the Southeastern Coastal Network (SECN) of the National Park Service (NPS).

In the acquisition of temporal LiDAR of SECN NPS sites, land cover data is used to represent the topographic features of the coastal southeast US through ArcGIS and ENVI LiDAR. The final outputs are presented in a GIS framework, providing a volumetric spatial change analysis detailing the specific areas where erosional activity occurred (net loss) and where unconsolidated material was returned in the environment (net gain). This high-resolution LiDAR data not only exhibits the advantages of LiDAR to improve coastal water resources and the understanding of the coastal geomorphologic dynamic, but also its applicability in providing sustainability and resiliency of environmental change.

2. Study Area

The SECN of the NPS monitors seventeen national parks extending along the Atlantic coast from the North Carolina-Virginia border to Cape Canaveral, Florida providing natural resource management. The areas used in this study are Fort Matanzas National Monument (NM) in St. Augustine, Florida, Fort Pulaski National Monument (NM) in Savannah, Georgia, Charles Pinckney National Historic Site (NHS) in Sullivan's Island, South Carolina, and Cape Lookout National Seashore (NS) in Harkers Island, North Carolina. The areas used for Fort Matanzas NM and Cape Lookout NS are within the SECN site boundaries, while the areas used for Fort Pulaski NM and Charles Pinckney NHS are in the vicinity of the SECN site boundary. These sites were selected as each is representative of the states in a longitudinal context along the southeastern US coastline covering 959 km (959,000 m). The distance between each site location is as follows: Fort Matanzas NM to Fort Pulaski NM is 312 km (312,000 m), Fort Pulaski NM to Charles Pinckney NHS is 189 km (189,000 m) and Charles Pinckney NHS to Cape Lookout NS is 468 km (468,000 m). The climate within this region can be categorized as humid subtropical where a wide range of extreme weather and climate events persist [29,30]. The El Niño Southern Oscillation (ENSO) is key in understanding the interannual variations of the climate of the SECN. El Niño will usually have lower temperatures in winter and spring, increased winter precipitation, and fewer tropical systems [30]. Mean annual precipitation in the SECN is mostly consistent, however, precipitation increases towards the Atlantic coast. In each of the SECN NPS sites the mean annual precipitation is between 1,001-1,400 millimeters (mm)/year [30]. Along the Atlantic coastline precipitation is more present during the summer months. Temperatures in the SECN vary largely as a function of latitude and proximity to the coast. Mean annual temperatures are between 14.1 °C to 24 °C [30]. The

temperatures are higher towards the southern states and lower in the northern states. Winter temperatures show a strong latitudinal gradient, while summer temperatures are moderate along the coast but warmer inland. Although the proximity of oceans generally moderates extreme temperature conditions with average summertime maximum temperatures around 30 °C, daytime temperatures can occasionally reach 40 °C [30].

Each of the sites are in the Atlantic Coastal Plain geological province, where geomorphologic changes have occurred [31]. Fort Matanzas NM is located on the Southeastern Coastal Plain geologic province, specifically in the east central Floridan aquifer system (Figure 1). Within the site are saltwater marshes and freshwater wetlands underlain by a surficial aquifer, confining unit and the upper Floridan aquifer [32,33]. The surficial aquifer varies seasonally while containing sands, marl, peats, muds, and alluvium [33,34]. The upper Floridan aquifer contains materials from the Eocene to Miocene, where the Hawthorn, Suwanee limestone and Ocala limestone formations are present [33]. Separating the surficial aquifer from the upper Floridan aquifer unit is an unconformity where the Hawthorne formation is above the Suwannee limestone [35]. The Hawthorn formation contains interbedded sand, phosphatic clay, dolomite, and limestone [33]. Within the Suwannee limestone, silt and clay are present [33]. The Ocala limestone is separated by an upper and lower lithological unit. The upper member is a marine limestone with coquina and chert, where the lower member is a marine limestone with dolomite [33].

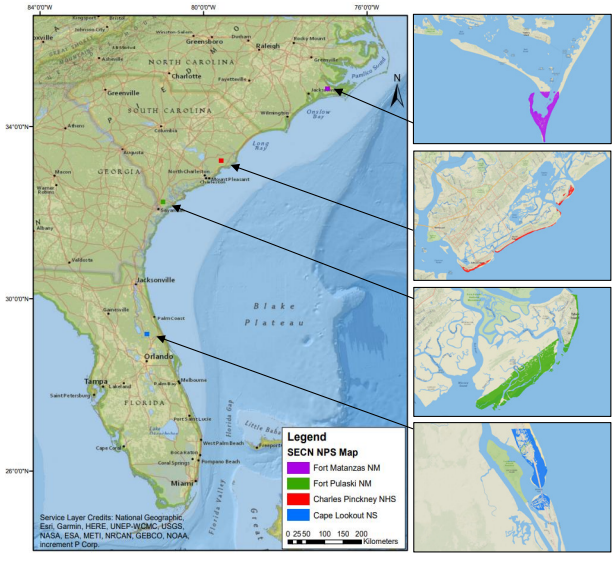

Figure 1. GIS-derived map of Fort Matanzas NM, Fort Pulaski NM, Charles Pinckney NHS, and Cape Lookout NS locations.

Fort Pulaski NM is located within the Atlantic Coastal Plain geologic province lying at the bottom most region of the Savannah River, which consist of salt marshes and hummocks (Figures 1 and 2). This site is composed of sand, peat, alluvium, unconsolidated material, clay, and beach sand [36]. Most of the material is of carbonates, while the younger rocks are clastic with limestone present near the surface and traces of glauconite underneath the limestone [36]. These materials are of the Late Cretaceous to Holocene with rocks of early Eocene to Oligocene [36]. The sands are of the Satilla, Coosawhatchie, and Marks Head formations [37]. The Satilla Formation immediately underlies the land surface where it is composed of sand, clay, and silt deposited in shallow marine environments [38,39]. The Coosawhatchie Formation is mostly comprised of silty clay, clay diatomite and phosphate sands [37,40]. These materials persist heavily, thus, they are divided into individual sedimentary units. The five-unit members are Tybee Phosphorite, Meigs, Berryville Clay (upper) Berryville Clay (lower) and Ebenezer formations [39]. In the Marks Head formation is predominantly of medium to coarse phosphate-calcareous sands [39,41]. These formations are in the Upper and Lower Floridan carbonate aquifer system where the layers are of limestone and dolomite [37]. The Upper and Lower Brunswick aquifers are present in this region [36]. The upper Brunswick aquifer is home to the Marks Head and members of Coosawhatchie formations. The confining unit with the surficial aquifer above contains other members of the Coosawhatchie formation except for the Ebenezer formation [37].

Charles Pinckney NHS is in the Atlantic Coastal Plain geologic province of South Carolina (Figure 1). In this region there are layers of surficial aquifer systems that are separated by an unconfined upper surficial aquifer composed of artificial till and a partially to fully confined lower surficial aquifer composed of sands [42]. Specifically, this site is underlain by confining units, Black Creek, Middendorf, and Cape Fear aquifer systems [43]. The confining unit between the Black Creek aquifer and Middendorf aquifer consists of sandy clay material [44]. This lithology is similar in the confining unit between the Middendorf and Cape Fear aquifer. Black Creek's aquifer unit is composed of fine to medium sand where the aquifer's thickness remains constant [45]. The Middendorf aquifer consist of thin, laminated layers of fine to medium sand and clayey material [44]. The layers of clayey material persist in Cape Fear's aquifer unit, but it is separated by sand, silt, and gravel [44].

Cape Lookout NS is a member of the North Carolina Outer Banks, a barrier island within the Atlantic Coastal Plain geologic province (Figure 1). This site is underlain by surficial aquifers with confining units. Yorktown,

Castle Hayne, Beaufort, Peedee, Black Creek, Upper and Lower Cape Dear aquifer systems are composed of marine sediments [46]. The upper confined aquifer is part of the early Pliocene Yorktown Formation which is comprised of sand, partially consolidated shell beds and sandy limestone. Some of these sand and shell beds near the surface of the aquifer is of the Quaternary age [47]. The lower confined aquifer, Castle Hayne, is composed of medium to coarse grained limestone [47]. This aquifer is confined by the Pungo River formation of early and middle Miocene age, where layers of clay, silty clay, and clayey sand persist [46]. The Pungo River Formation is the highest yielding aquifer in the North Carolina coastal plain [48].

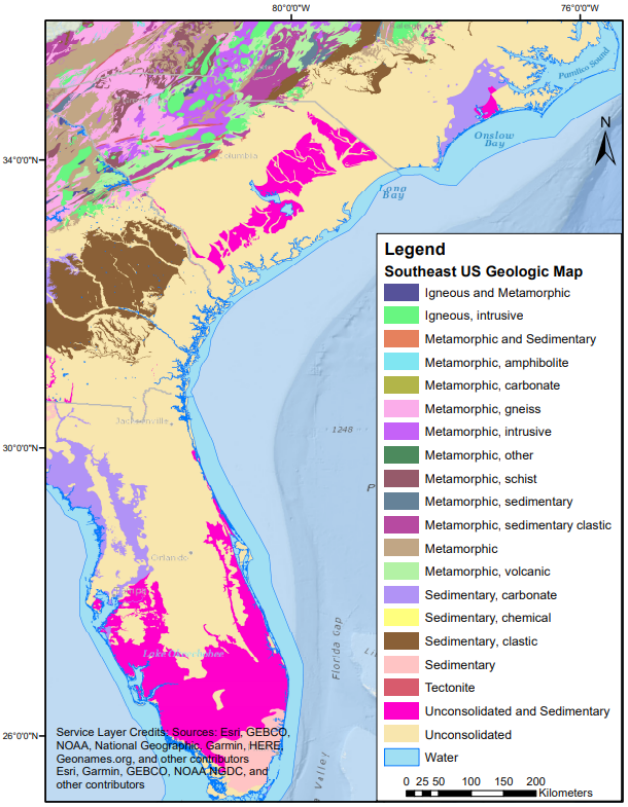

Figure 2. Geologic map of southeast US. Data retrieved from the USGS State Geologic Map Compilation geodatabase of the conterminous United States.

3. Methodology

The methodology implemented in this study incorporates a series of steps designed to synthesize volumetric, spatial, and temporal changes using LiDAR (Figure 3). The LiDAR data acquired were retrieved from the National Oceanic and Atmospheric Administration (NOAA), (https://coast.noaa.gov/dataviewer/#/lidar/search/), in LAS format. The data were collected, categorized, and processed individually for each of the four respective SECN NPS sites. The processed data was used to create a change analysis both spatially and temporally. Using ENVI LiDAR 5.5, each acquired LiDAR dataset generated point clouds, orthophotos and DEMs (horizontal accuracy: 1-meter, vertical accuracy: 0.196 meters) to produce the base maps. From the production of the temporal LiDAR base maps detailing changes in elevation, the data were then used to provide a volumetric spatial change analysis. The volumetric spatial change analysis was used to detail specific areas where erosional activity occurred (net loss) and where unconsolidated material was returned to the environment (net gain). Using the spatial analyst tool, raster calculator calculated the difference from each year to generate a difference map. The difference maps were then edited by the Cut Fill tool to display the volumetric changes that were quantified and measured to visually represent the net gain/net loss of unconsolidated material.

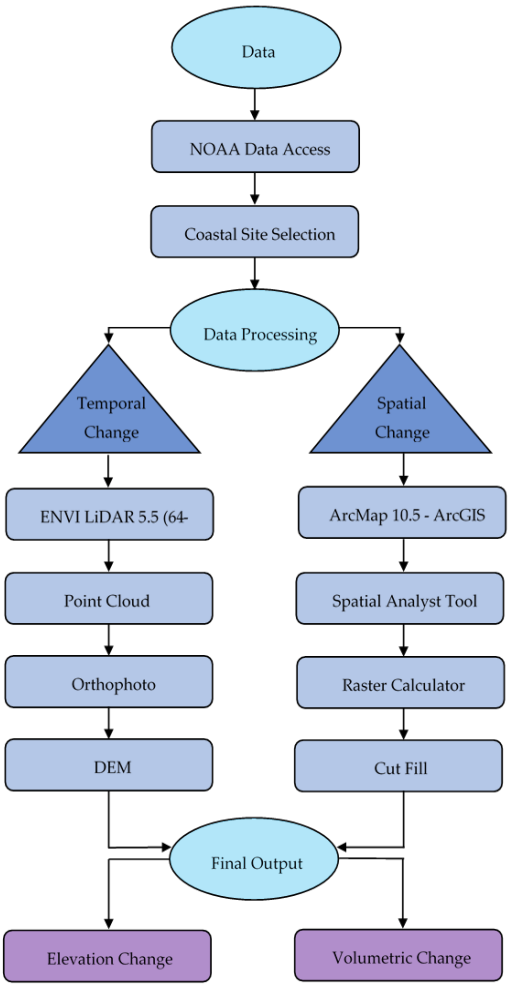

Figure 3. Processing flow chart representing data acquisition, processing procedure, and final output of the LiDAR dataset. Each step in this series was used to display the temporal changes over the specified period and the spatio-temporal volumetric changes.

3.1 Data Acquisition

Prior to the LiDAR acquisition, the LiDAR system underwent calibration to verify the operational accuracy and misalignment angles. Boresight calibrations were performed for the LiDAR system at the beginning and end of each flight mission. LiDAR data was processed immediately after the acquisition to verify the coverage had no voids. The GPS/Inertia Measurement Unit (IMU) data was post processed using differential and Kalman filter algorithms to produce the best estimates of unknown variables [49].

The vertical and horizontal accuracy was performed using a standard method to compute the root mean square error (RMSE) based on comparing ground control points and filtered LiDAR data points. Each compiled vertical and horizontal accuracy value met the 95th percentile confidence level requirements recommended by the American Society for Photogrammetry and Remote Sensing (ASPRS) when analyzing elevation generated by LiDAR. The horizontal accuracy quantitative value is 1 meter, and the vertical accuracy quantitative value is 0.196 meters (19.6 cm). The ASPRS guidelines follow the National Digital Elevation Program sections on vertical accuracy testing that follows the Federal Geographic Data Committee and the National Standard for Spatial Data Accuracy [49]. The filtered LiDAR data represented the bare earth elevations from 2006 to 2018 for each NPS site (Table 1). The bare earth elevations collected multiple return x, y, and z data as well as intensity data. This data was then compressed in a LAS binary file format containing the information specific to the LiDAR data (number of returns, intensity value, x, y, z, etc.). The LAS data was projected to input datum NAD83, the projection system was geographic longitude/latitude, and the input units were converted to meters [49]. As a result, the data acquired from NOAA are as follows:

3.2 LiDAR-based DEM Temporal Changes

In the acquisition of temporal LiDAR at each of the SECN NPS sites, land cover data was used to represent the topographic features of the coastal southeast US using ArcGIS and ENVI LiDAR. The topographic features detailed the elevation changes that have occurred at each of the sites.

ENVI LiDAR was used to process the geo-referenced LiDAR point cloud data into geographical information system layers that were then produced in output formats for a 3D visual database. ENVI LiDAR created Digital Elevation Models (DEMs) from the Digital Terrain Models (DTMs) to characterize the elevation of the site's topography. Geospatial measurements of the point cloud data were used to provide accuracy of the existing topographic cover. Each point is classified by a value of elevation height to determine its class feature.

ENVI LiDAR used the DTM to create the DEM by including vector data of the natural terrain and linear features. The vector data are composed of regular spaced raw points and natural features of the observed area. The linear features used are representative of the shape of the bare-earth terrain. The regular spaced raw points, vector data and linear features are used to augment a DEM providing its distinctive terrain features. To ensure DEM extraction from LiDAR data based on DTMs was accurate, a density map was generated to check the raw point density and coverage of the LiDAR data. Each of the LiDAR datasets had more than the recommended minimum of 5 to 6 points per square meter by L3 Harris Geospatial. Due to the dense raw dataset, ENVI LiDAR identified features for extraction and avoided false readings including overestimations of topographical features. Usage of Variable Sensitivity Algorithm for low density datasets was not performed.

ArcGIS was used to provide the final output of the processed LiDAR point cloud data in a GIS produced map. The base maps were used to create the different maps, which display the differences in elevation over a specified year. These maps detailed the elevation values of the processed LiDAR points acquired from NOAA. The maps provide a geographical representation of the temporal changes that have occurred over time.

Table 1. LiDAR data details for each NPS site.

Sites											
Fort Matanzas NM			Fort Pulaski NM			Charles Pinckney NHS			Cape Lookout NS		
Value	**Season**	**Year**	**Value**	**Season**	**Year**	**Value**	**Season**	**Year**	**Value**	**Season**	**Year**
0.30 m	Fall	2006	0.30 m	Winter	2006	0.20 m	Winter	2007	0.30 m	Fall	2012
0.20 m	Fall	2010	0.24 m	Winter	2009	0.20 m	Fall	2010	0.10 m	Fall	2014
0.22 m	Winter	2013	0.20 m	Fall	2010	0.23 m	Winter	2016	0.23 m	Winter	2017
0.20 m	Fall	2016	0.23 m	Winter	2016	0.20 m	Fall	2018	0.20 m	Fall	2018
0.20 m	Fall	2017	0.10 m	Winter	2017	N/A	N/A	N/A	N/A	N/A	N/A

3.3 Spatial Change Analysis

The temporal LiDAR base maps provided a volumetric spatial change analysis detailing erosional activity (net loss) and deposition (net gain). To identify the changes occurring spatially, the ArcGIS Cut Fill tool was applied. This tool analyzed topographic features at two different periods of time to identify the volumetric change by (1) identifying regions of erosional activity and deposition, (2) calculating the volume of sedimentary material, and (3) identifying inundated regions.

The Cut Fill tool displays regions of net loss and net gain from the attribute table of the output raster. Each raster represents a regions volume, which is calculated for each individual cell, and the area, calculated by the number of cells in each region by the cell size. The volume is greater than zero in regions where the unconsolidated sedimentary material was cut, and less than zero where it was filled. This repeated spatial change analysis identified the erosional and depositional activity that has occurred.

4. Results

Each site analyzed in this study displays the temporal changes in elevation and the quantification of spatial volumetric changes of unconsolidated sedimentary material presented in a GIS framework. The LiDAR-based DEM temporal changes display the highest and lowest elevation for each year at each site. Of the temporal change analysis, the spatial changes occurring were displayed volumetrically to identify the deposited material and erosional activity occurring during specific years at each site.

Fort Matanzas NM, Fort Pulaski NM, Charles Pinckney NHS, and Cape Lookout NS are all depicted to display how each site individually changed temporally and spatially during the specified period of time (Figures 4-11, Tables 2-5). Tables 2-5 present the net loss and net gain of the given total area for each output raster's attribute table of the specified year. These tables detail the percentages of erosional and depositional activity that occurred spatially. The temporal changes were characterized by the acquisition of LiDAR derived DEMs for each location (Figures 4, 6, 8, 10). The earliest acquired DEM was selected as the base map to display how elevation changed from the base map's year to each specified year. The spatial change maps were derived from the temporal change maps to represent the volumetric distribution of erosional activity and deposited unconsolidated sedimentary material (Figures 5, 7, 9, 11). These maps display the extent and location of where changes have occurred over the study period. Results show instances of elevation and volumetric changes of sediment though no consistent trend was found.

4.1 Fort Matanzas National Monument

LiDAR derived DEMs of Fort Matanzas NM displays the elevation changes that have occurred from 2006 to 2017. During 2006 to 2010 the elevation dropped a meter and there was a majority net loss of material occurring (Table 2) (Figure 4).

Table 2. Fort Matanzas NM spatial change extent of sedimentary material deposited (net gain) and areas where erosional activity occurred (net loss).

FORT MATANZAS NATIONAL MONUMENT SPATIAL CHANGE ANALYSIS		
2010		
Total Area (m^2)	59,729	100%
Net Loss	48,497	81%
Net Gain	11,231	19%
2013		
Total Area (m^2)	104,255	100%
Net Loss	91,590	88%
Net Gain	12,664	12%
2016		
Total Area (m^2)	102,385	100%
Net Loss	90,863	89%
Net Gain	11,521	11%
2017		
Total Area (m^2)	100,803	100%
Net Loss	90,279	90%
Net Gain	10,523	10%

From 2006 to 2017, the elevation drops considerably within the middle of Fort Matanzas NM (Figure 4). During 2010 to 2017, the areas of the highest elevations, labeled in red, include the areas around the coastline and some of the inner portions of this coastal environment (Figure 4). As depicted from the images, the coastline is continuously altered as the elevation changes from year to year. From 2010 to 2013 the coastline is at its highest elevation, while from 2016 to 2017 the coastline continues to decrease. Near the Matanzas Inlet you see a consistent decline in elevation form 2010 to 2017. The eastern coastline displays higher elevation values in comparison to the inlet near Rattlesnake Island.

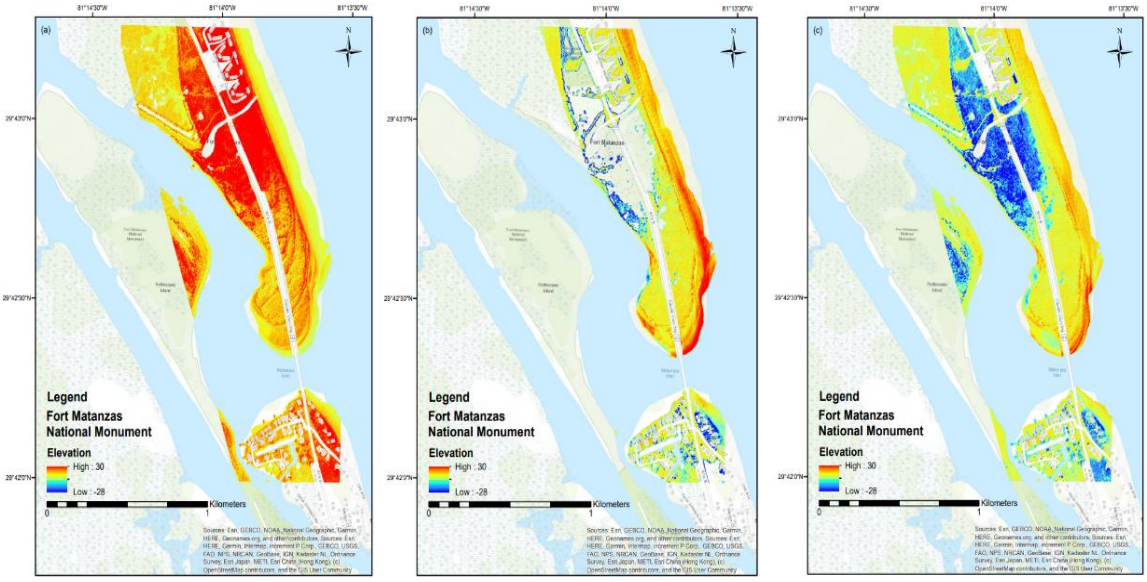

Figure 4. LiDAR derived DEM difference maps generating three-dimensional elevation changes of Fort Matanzas NM from 2006 to 2017. Each panel corresponds to the specified year: (a) 2006, (b) 2010, (c) 2013, (d) 2016, and (e) 2017.

The volumetric change of unconsolidated sedimentary material at Fort Matanzas NM displays a net loss from 2010 to 2017. During this time period, the spatial extent of where erosional activity occurred has increased (Table 2). In 2010, there was a net loss of 81%, while in 2017, the net loss increased to 90% over the given area. Though much of the material displayed is a net loss, there is also a net gain. Outlined by the red color on the volumetric change maps, the eastern coastline shows where much of the sedimentary material was deposited back into the environment representing a net gain (Figure 5). Additionally, there is a net gain of material where tidal inlets are present. According to the spatial change analysis, from 2010 to 2017, there is a decrease of sedimentary material being deposited back into this environment (Table 2).

4.2 Fort Pulaski National Monument

During 2006 to 2017, the area near Fort Pulaski NM exhibited varied changes in elevation. The LiDAR derived DEMs of this coastal environment display how the elevation is fluctuating over a given period of time. From 2009 to 2010, elevation values display an increase towards to southern most region of the site and towards the northeast. In 2016, there is a decrease in elevation in pockets near the southern most region and along the eastern coastline. In 2017, the elevation remains constant (Figure 6). The northernmost and southernmost regions exhibited the highest elevation values in Tybee Island and Little Tybee Island, while the center most regions recorded the lowest elevation values (Figure 6).

The volumetric change maps of this area show an overall net loss of unconsolidated sedimentary material from 2009 to 2017 (Table 3). In 2009, there was a net loss of 85% but the erosional activity that occurred from 2009 to 2010 decreased to 75% over the given area (Figure 6). In 2016 and 2017, there is an increase of unconsolidated sedimentary material with a net loss of 84% (Figure 7). The locations of where there is a net gain are similar during this temporal data collection. Material has been deposited back into this environment along the eastern coastline displaying a net gain of material in the tidal inlet between Little Tybee and Tybee Island. The most southern region along the coastline displays regions of a net gain where the majority of the unconsolidated sedimentary material is a net loss. The southern region displays a large portion of material being deposited back into this region (Figure 7).

4.3 Charles Pinckney National Historic Site

Areas near Charles Pinckney NHS experienced fluctuating elevations from 2007 to 2016. From 2010 to 2016, the elevation increased along the coastline and within the intercoastal waterway, while from 2016 to 2018 the elevation decreased along the coastline (Figure 8). Along this coastline the elevation changes that occurred were in many of the same areas. From 2010 to 2018 the areas representing the highest elevation remained constant as well as the areas with the lowest elevation. Though much of the area remained constant, the data represent areas that both decreased and increased in elevation along the coastline (Figure 8).

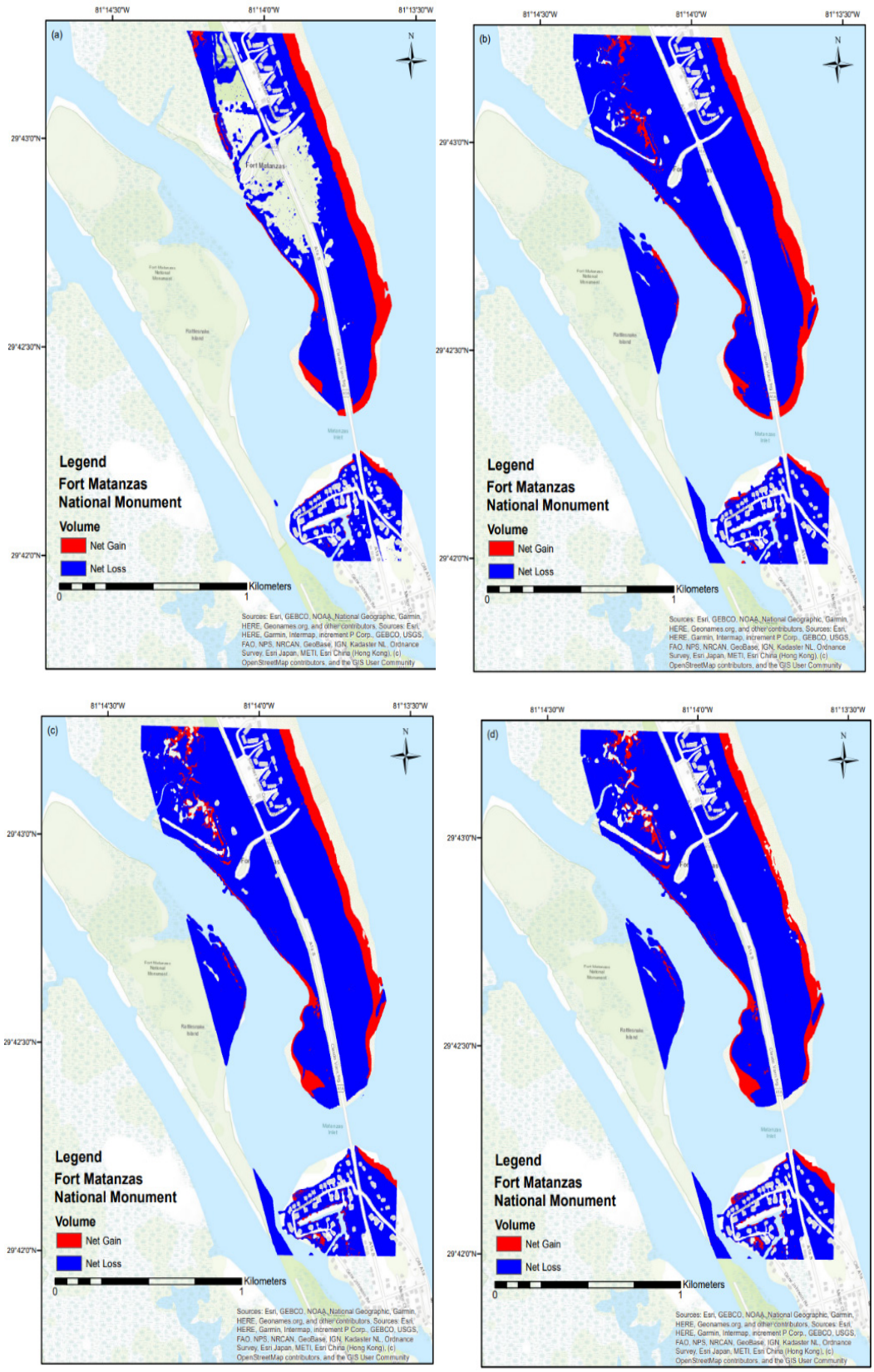

Figure 5. Spatial change maps detailing the volumetric distribution changes of both deposited (net gain) and erosional activity (net loss) of unconsolidated sedimentary material at Fort Matanzas NM from 2010 to 2017. Each panel corresponds to the specified year: (a) 2010, (b) 2013, (c) 2016, and (d) 2017.

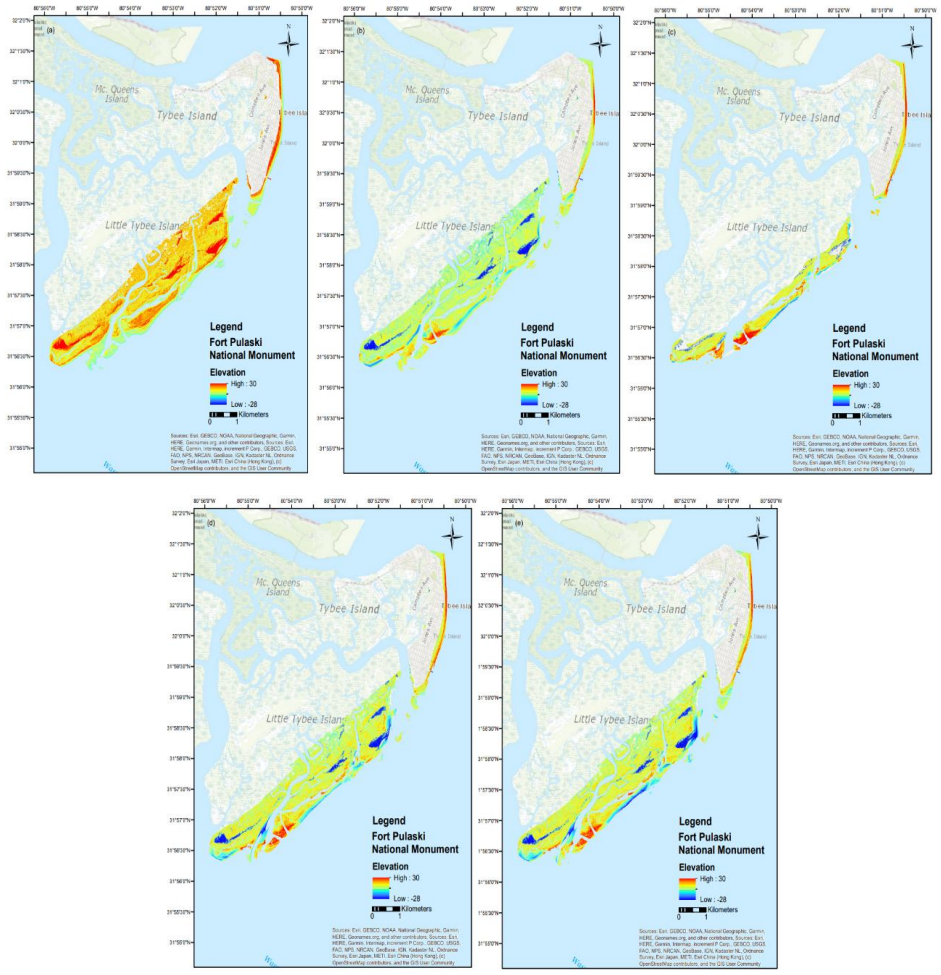

Figure 6. LiDAR derived DEM difference maps generating three-dimensional elevation changes of the area near Fort Pulaski NM from 2006 to 2017. Each panel corresponds to the specified year: (a) 2006, (b) 2009, (c) 2010, (d) 2016, and (e) 2017.

Table 3. Spatial change extent of sedimentary material deposited (net gain) and areas where erosional activity occurred (net loss).

SAVANNAH COAST SPATIAL CHANGE ANALYSIS		
2009		
Total Area (m^2)	1,018,432	100%
Net Loss	870,192	85%
Net Gain	148240	15%
2010		
Total Area (m^2)	377,555	100%
Net Loss	284,050	75%
Net Gain	93,504	25%
2016		
Total Area (m^2)	931,287	100%
Net Loss	785,213	84%
Net Gain	146,074	16%
2017		
Total Area (m^2)	964,442	100%
Net Loss	812,018	84%
Net Gain	152,423	16%

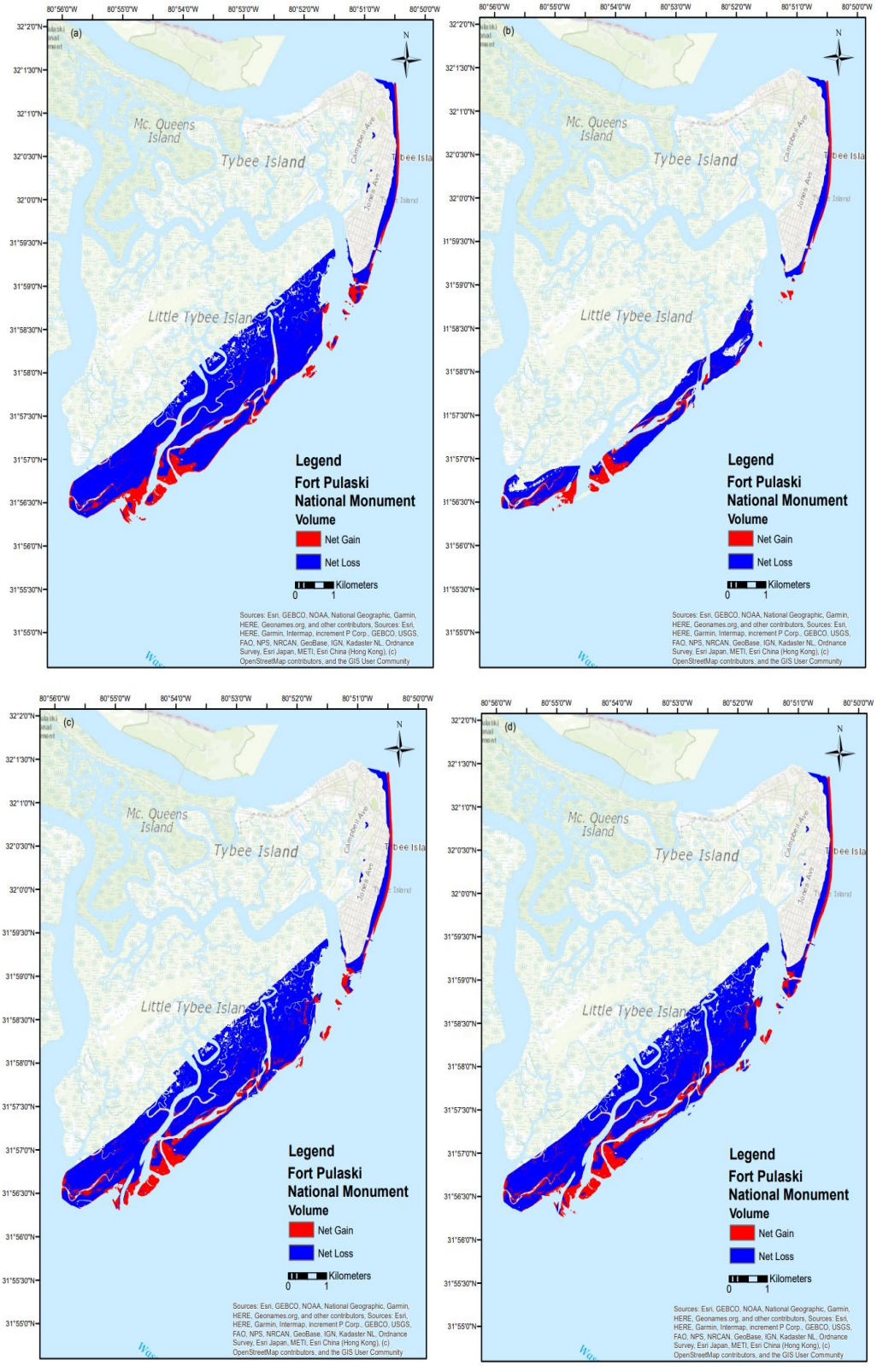

Figure 7. Spatial change maps detailing the volumetric distribution changes of both deposited (net gain) and erosional activity (net loss) of unconsolidated sedimentary material at Fort Pulaski NM from 2009 to 2017. Each panel corresponds to the specified year: (a) 2009, (b) 2010, (c) 2016, and (d) 2017.

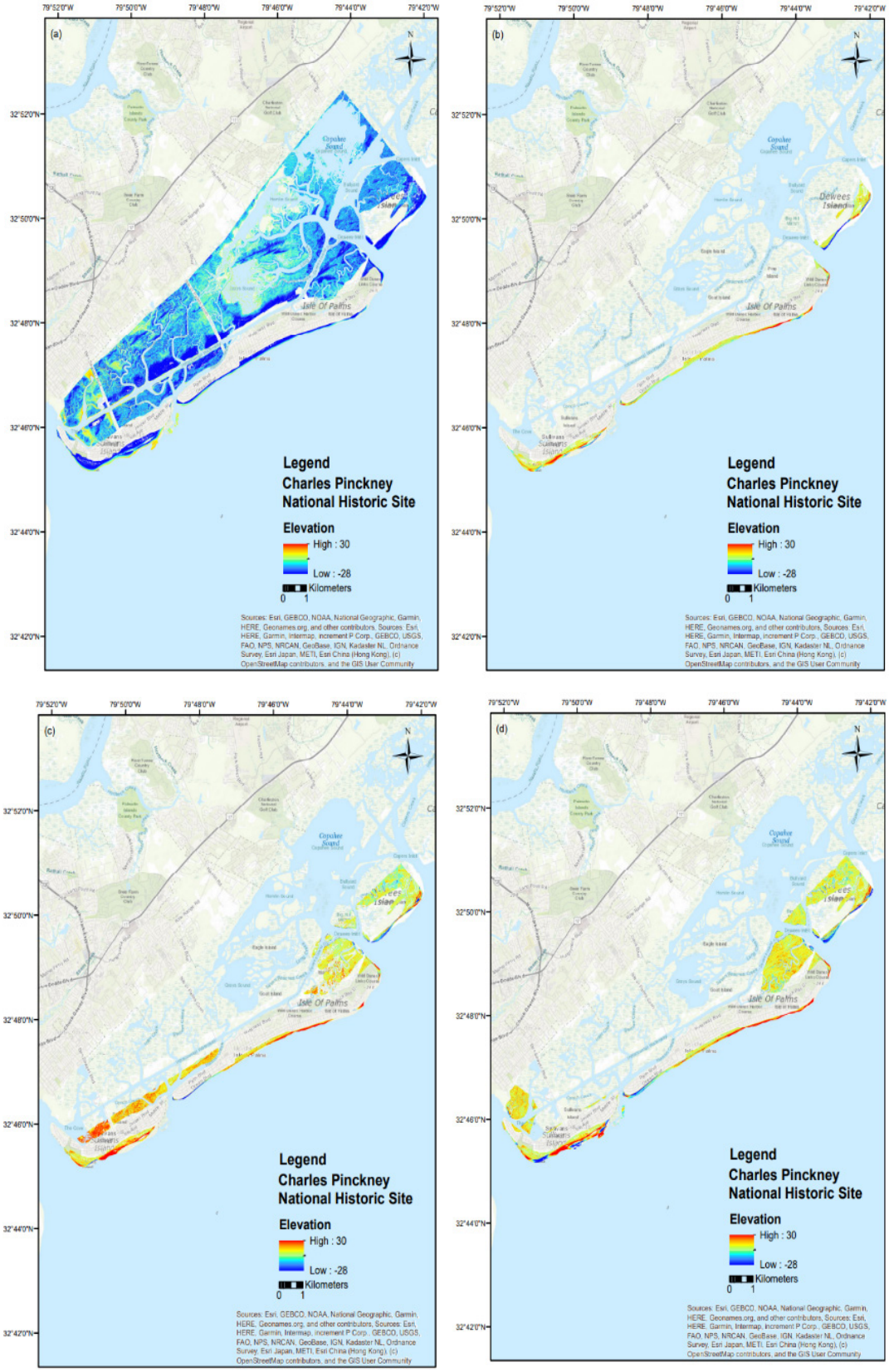

Figure 8. LiDAR derived DEM difference maps generating three-dimensional elevation changes of the area near Charles Pinckney NHS from 2007 to 2018. Each panel corresponds to the specified year: (a) 2007, (b) 2010, (c) 2016, and (d) 2018.

The volumetric change maps inform us that even though there is an overall net loss of unconsolidated sedimentary material, the volume has fluctuated between 2010 to 2018 (Table 4). In 2010, erosional activity occurred at approximately 89%, decreased to 87% in 2016, and then increased to 89% in 2018. This suggests the unconsolidated sedimentary material fluctuated between a net gain and loss (Figure 9). The net gain is mostly in the southernmost region, while also visible in the tidal inlets near the Isle of Palms (Figure 9).

4.4 Cape Lookout National Seashore

The LiDAR derived DEMs of Cape Lookout NS depict a coastal environment that has continuously changed from 2012 to 2018. Elevation decreased from 2012 to 2014, increased from 2014 to 2016, and decreased from 2016 to 2018 (Figure 10). The difference maps also display areas along the coastline where the lowest elevation (western coastline) values remain constant along with the areas of higher elevation (eastern coastline) (Figure 10). The center of this coastal environment displayed topography that remained nearly consistent.

The volumetric change maps of Cape Lookout NS display a majority net loss of unconsolidated sedimentary material. The spatial change analysis shows how erosional activity decreased during 2014 to 2016, but then increased in 2018 (Table 5). This coastal environment displays that most of the erosional activity occurring is around the coastline, while the unconsolidated sedimentary material being deposited back into this environment is more inland (Figure 11). Noticeably, there is a drastic change from 2014 to 2016, where the inland portions of this region shift from a net loss to a net gain (Figure 11). This depiction indicates how coastal environments can change over time. The volumetric distribution along the coastline shows a net gain, while the majority is a net loss. Identification of differences in the unconsolidated sedimentary material of this coastline is evident from 2014 to 2018. The inland portions of this region experienced the most change spatially. From 2014 to 2016, there was an increase of 47% of unconsolidated sedimentary material deposited back into this region, but in 2018 the volumetric distribution changed, resulting in a net loss of 60% (Table 5).

Table 4. Spatial change extent of sedimentary material deposited (net gain) and areas where erosional activity occurred (net loss).

SULLIVAN'S ISLAND COAST SPATIAL CHANGE ANALYSIS		
	2010	
Total Area (m^2)	242,790	100%
Net Loss	217,203	89%
Net Gain	25,587	11%
	2016	
Total Area (m^2)	672,972	100%
Net Loss	587,863	87%
Net Gain	85,109	13%
	2018	
Total Area (m^2)	846,323	100%
Net Loss	755,791	89%
Net Gain	90,532	11%

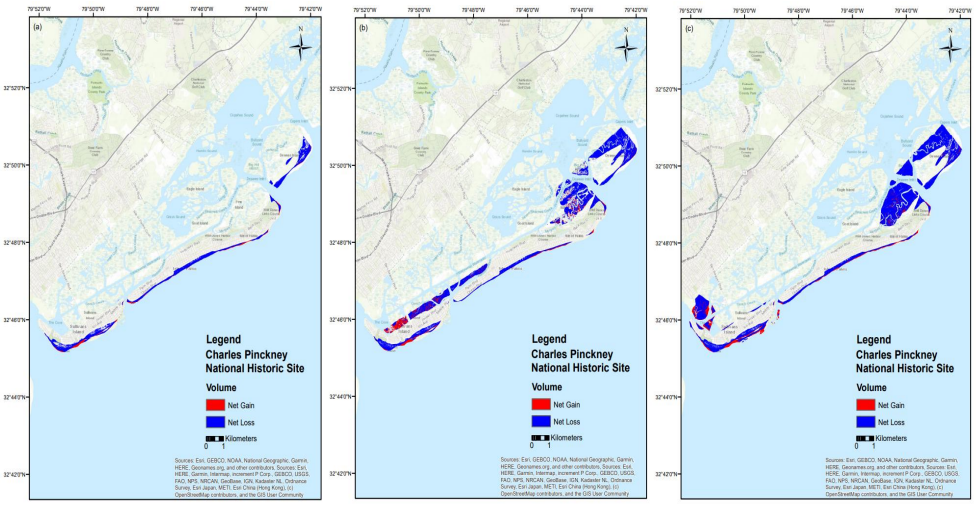

Figure 9. Spatial change maps detailing the volumetric distribution changes of both deposited (net gain) and erosional activity (net loss) of unconsolidated sedimentary material at Charles Pinckney NHS from 2010 to 2018. Each panel corresponds to the specified year: (a) 2010, (b) 2016, and (c) 2018.

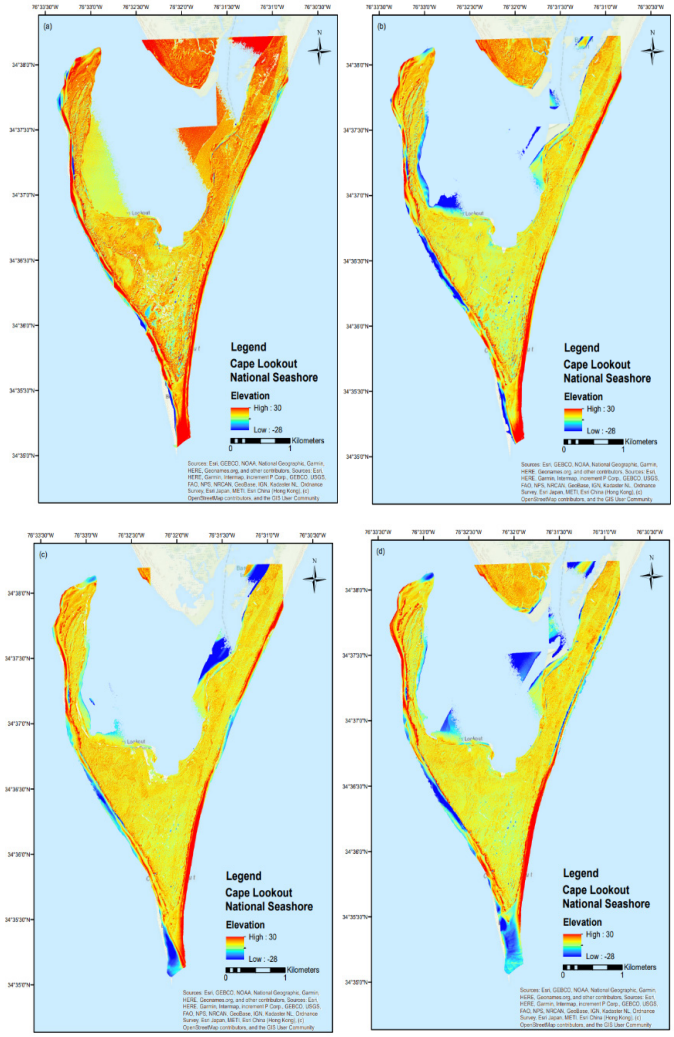

Figure 10. LiDAR derived DEM difference maps generating three-dimensional elevation changes of Cape Lookout NS from 2012 to 2018. Each panel corresponds to the specified year: (a) 2012, (b) 2014, (c) 2016, and (d) 2018.

Table 5. Cape Lookout NS spatial change extent of sedimentary material deposited (net gain) and areas where erosional activity occurred (net loss).

CAPE LOOKOUT NATIONAL SEASHORE SPATIAL CHANGE ANALYSIS		
2014		
Total Area (m^2)	594,181	100%
Net Loss	449,294	76%
Net Gain	144,886	24%
2016		
Total Area (m^2)	638,251	100%
Net Loss	337,810	53%
Net Gain	300,440	47%
2018		
Total Area (m^2)	605,340	100%
Net Loss	363,235	60%
Net Gain	242,105	40%

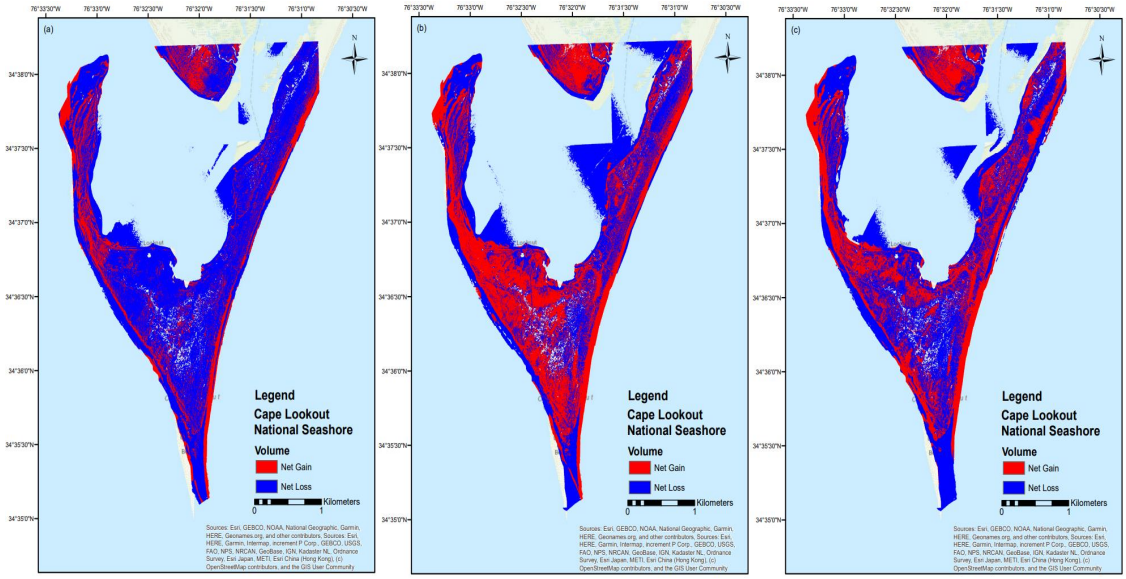

Figure 11. Spatial change maps detailing the volumetric distribution changes of both deposited (net gain) and erosional activity (net loss) of unconsolidated sedimentary material at Cape Lookout NS from 2014 to 2018. Each panel corresponds to the specified year: (a) 2014, (b) 2016, and (c) 2018.

5. Discussion

The coastal southeastern US has experienced the effects of sea level rise, storm frequency, and changes in climatic regimes that have caused this coastal region to be unstable. The steadily climbing sea level and increases in storm activity and intensity, threaten these coastal zones by making them susceptible to extreme flooding events, inundation, and erosion. These changes were demonstrated in this study using LiDAR at selected SECN NPS sites along the southeastern USA (Figures 4-11). Results indicated that though erosional activity was present, there was a net gain of sedimentary material returned within the sites (Figures 5, 7, 9, 11). Temporal erosion and longshore transport of sediment are results of the ever-changing climate producing storm surges and relative sea level rise.

Spatially distributed erosion occurred from 2006-2018 at each of the sites. In the data presented, Fort Matanzas NM displayed a steady decline in net gain of unconsolidated sedimentary material, while the areas near Fort Pulaski NM, Charles Pinckney NHS and Cape Lookout NS display how the geomorphology is steadily oscillating between erosional and depositional processes (Tables 2-5). It is clear the sediment budget of each of these coastal sites can

change in response to fluctuations of coastal depositional and erosional processes. The erosion that is occurring is in response to relative sea level and changes in climatic regimes, but what is most important is that these causes represent the quasi-cyclic phenomena [50,51]. This phenomenon represents how the unconsolidated sediment distribution and morphodynamic equilibrium changes from the influence of fluctuating climatic regimes. These processes are not just exclusive to the coastal southeastern US but are found in other regions as well [52,53]. As the variability and frequency of these events continue, the impact of longshore transport on these coastal zones is unforeseen.

Throughout the study period, unconsolidated sedimentary material was either eroded or deposited at these SECN NPS sites, however there was an overall net gain. This is most notable along the coastlines (Figures 5, 7, 9, 11) where eroded areas had new material deposited causing the overall net gain. There are multiple processes that can cause these coastal morphodynamics, however, longshore sediment transport is evident. Longshore sediment transport depends on many factors, but the direction and speed of the longshore current primarily depends on the direction and height of the wave energy. Though these are highly variably, and the wave energy is dependent on the transport gradient under varying wave conditions, the sites indicate this process is plausible (Figures 5, 7, 9). For example, Cape Lookout NS shows longshore currents have caused repeated oscillation of eroded and deposited sediments under various conditions [54]. Previous studies at Cape Lookout NS have shown evidence of longshore sediment transport just as the findings of this study [55].

Along the coastal southeastern US, storm surges pose an imminent threat to coastal geomorphology. In 2016 a Category 5 hurricane, Hurricane Matthew, occurred in the coastal southeastern US causing inundation from precipitation in a geologically unstable coastal zone [56]. Post-Hurricane Matthew LiDAR datasets from this study show the impact of such hurricanes (Figures 5, 9, 11). The amplitude of the storm surge created the abnormal rise of sea level by wind energy. The wind energy produced strong tides and currents causing coastal erosion to increase. Erosional activity and longshore sediment transport events changed the volumetric distribution of unconsolidated sedimentary material of the coastal zone.

These elevational changes demonstrate how change in the land surface can impact the coastal hydrogeologic framework. Coastal recharge and discharge drainage networks can be altered with changes in sedimentary material [56]. Within this coastal zone there are both shallow and deep aquifers, thus, each respond differently [33,36,37,42,44-47,57]. The shallow aquifers are more responsive to the immediate climatic regimes, while the deeper aquifers have a delayed reaction. However, each aquifer is important as they each contribute to the coastal groundwater system of the coastal southeastern US.

5.1. Efficacy of Airborne LiDAR

LiDAR serves as a critical tool in understanding temporal and spatial topographic changes in the coastal southeastern US. LiDAR offers capabilities that allow researchers the opportunity to acquire large-scale elevation and derived topographic data for interpretation. The performance of the 3D laser scanners has advanced the speed and accuracy of assessing geomorphological changes within these coastal zones (Figures 4-11). The 3D lasers can take millions of precise measurements by examining earth's topographical features through volume and elevation [21,58]. This ability highlights the success and scientific merit in observing the elevation and volumetric changes occurring in this study. The high accuracy and relative surface reflectance to define the topographic features is key in understanding erosional activity and where unconsolidated sediment is being deposited.

The defined topographic features are in part due to LiDAR's capabilities, while also using an appropriate ground truth validation technique to identify coastal changes. Through ENVI LiDAR, point cloud classification was applied to identify each class feature determined by the value of elevation height. These class features provide the capability to extract the necessary data related to various features on the surface. Point cloud classification displays the ability of being an appropriate approach to ground truth validation for the extraction of ground features representative of the earth's surface. This capability removed all roads, bridges, and buildings to accurately represent each region's surface. This technique will assist in providing accurate resource management to future studies on coastal environments [20-23,26,57,58].

Although more investigations are needed to understand the geomorphological changes that are occurring temporally and spatially, the remote sensing techniques used are advantageous. (1) Observations and investigations were performed remotely using available public domain datasets. (2) Surface data represented high sample density while not being affected by extreme weather conditions. (3) Data were acquired in accessible areas with no geometric distortions. (4) The vast datasets provide the opportunity to identify relationships and new insights to better understand these coastal zones. The remote sensing techniques used through the acquisition of temporal LiDAR provided an appropriate representation of the geomorphological changes occurring [20-26].

5.2 Limitations and Applicability

This study provides sound results in distinctively describing the geomorphology of the coastal southeast US, along with some limitations that provide opportunity for further research. First, the temporal LiDAR datasets aren't collected at the same time. This is important because the time in which the climatic regimes persist per unit area must be accounted for to characterize and understand which processes are occurring in an entire coastal zone. Second, under certain conditions elevation errors can occur while on water surfaces. This can produce a return value that is unreliable due to the height of the water depth affecting the reflection of the pulses. These errors are corrected by vertical and horizontal accuracy when using a standard method to compute the root mean square error (RMSE). Vertical accuracy is assessed by the fundamental accuracy value calculated at the 95th percentile confidence level as a function of the RMSE. The 95th percentile indicates that 95 percent of the errors in the dataset have absolute values of equal or lesser value, while 5 percent of the errors will be of larger value. Thus, there is approximately a 5 percent error. In suspected inundated areas where there was no return signal, no interpolation was applied. ENVI will interpolate the elevation data for missing data, however, this interpolation can result in false readings. Lastly, access to LiDAR data is limited. The temporal LiDAR data acquired for Fort Matanzas NM and Cape Lookout NS were in the SECN site boundaries, however, data acquired for Fort Pulaski NM and Charles Pinckney NHS were not in the SECN site boundary. The LiDAR data presented represented an area in the vicinity of the Fort Pulaski NM and Charles Pinckney NHS SECN site boundaries. The quality of this study is not only relevant to the advancement of understanding the coastal dynamic response, but it also presents efficient results with limited LiDAR derived datasets over the selected sites [21,57,58].

6. Conclusions

The southeast of the US is composed of numerous SECN NPS sites where each has experienced coastal changes. Outlined in this paper, Fort Matanzas NM, area near Fort Pulaski NM, area near Charles Pinckney NHS, and Cape Lookout NS, were analyzed to understand the geomorphologic changes occurring through the acquisition of temporal LiDAR derived datasets. These sites represented a portion of the coastal southeastern US to display the usefulness and versatility of processed LiDAR. Identifying the temporal changes in elevation and quantifying the spatial volumetric changes of unconsolidated sedimentary material allows for further understanding of the coastal dynamic response of the coastal southeast. This temporal and spatial change analysis displayed the vulnerability of these coastal zones due to elevation changes. In some cases, the elevation changes occur rapidly, but in other cases they occur over extended periods of time. Fort Matanzas NM displayed a 1-meter decrease in elevation from 2006 to 2017. Also, these elevation changes fluctuate causing these coastal zones to be unstable, presenting the opportunity for continuous change. Fort Matanzas NM elevation increased during 2010 to 2013 but decreased from 2016 to 2017 along the coastline. Fort Pulaski NM elevation increased from 2009 to 2010 and decreased in 2016. Charles Pinckney NHS elevation increased by 1-meter from 2010 to 2016 and decreased by 1-meter between 2016 to 2018. Cape Lookout NS elevation increased from 2012 to 2014, decreased from 2014 to 2016 and decreased from 2016 to 2018 on a magnitude of 2-3 meters. In respect to the coastal sediment budget, the volumetric spatial change of sedimentary material responded in conjunction to the elevation changes, however, the changes were not consistent. Areas in which there was a net gain/net loss of returned sedimentary material, the elevation increased and areas where there was a net loss/net gain displaying erosional activity, the elevation decreased. Fort Matanzas NM displayed a 7% increase of erosional activity from 2010 to 2013, 1% increase from 2013 to 2016, and a 1% increase from 2016 to 2017. From 2009 to 2010 erosional activity in Fort Pulaski NM decreased by 10% but increased by 9% in 2016. Charles Pinckney NHS erosional activity decreased by 2% from 2010 to 2016 but increased in 2018 by 2%. Cape Lookout NS erosional activity decreased by 23% during 2014 to 2016 but increased in 2018 to 60%. These volumetric changes infer the climatic regimes that are persisting in the southeast US expose these coastal zones to instability. The quasi-cyclic phenomena that are occurring are due to these coastal zones being exposed to fluctuating climate regimes. As a result, there are different erosional processes and longshore sediment transport affecting the coastal hydrogeological and geomorphological dynamic.

The use of processed LiDAR derived data has furthered the understanding of coastal environments. The ability to use remote sensing techniques has offered the opportunity to identify the changes in geomorphology and its relationship with the climatic regime effects. As technology advances, new tools emerge, and more datasets are produced, the high-resolution data will improve coastal water resources and its applicability in providing sustainability and resiliency of coastal geomorphological change.

Author Contributions

David F. Richards, IV is the principal author of this manuscript and was responsible for the design, processing, interpretation, and writing of the manuscript. Adam M. Milewski made significant contributions to the design, processing, interpretation, writing, and review of the manuscript. Brian Gregory helped with the design, interpretation, and the review of the manuscript.

Conflict of Interest

The authors declare no conflict of interest.

Funding

This work was funded by the National Park Service under cooperative agreement award: P17AC01646. Also, partially supported by the SEGS 2019 Student Research/ Field Work Grant and the NSF/GSA Graduate Student Geoscience Grant # 13005-20, which is funded by NSF Award # 1949901.

References

[1] Gornitz, V.M., Daniels, R.C., White, T.W., et al., 1994. The development of a coastal risk assessment database: vulnerability to sea level rise in the U.S. Southwest. Journal of Coastal Research Special Issue. 12, 327-338. http://www.jstor.org/stable/25735608.

[2] Wu, S.Y., Yarnal, B., Fisher, A., 2002. Vulnerability of coastal communities to sea-level rise: A case study of Cape May county, New Jersey, USA. Climate Research. 22(3), 255-270.

[3] Church, J.A., Hunter, J.R., McInnes, K.L., et al., 2006. Sea-level rise around the Australian coastline and the changing frequency of extreme sea-level events. Australian Meteorological Magazine. 55(4), 253-260.

[4] Leatherman, S.P., 1984. Coastal geomorphic response to sea level rise: Galveston Bay, Texas. Barth and Titus (eds). Coastal Zone. 151-178.

[5] Nicholls, R.J., Wong, P.P., Burkett, V., et al., 2007. Coastal systems and low-lying areas. https://ro.uow.edu.au/scipapers/. 164, 315-356.

[6] Markewich, H.W., Pavich, M.J., Buell, G.R., 1990. Contrasting soils and landscapes of the Piedmont and Coastal Plain, eastern United States. Geomorphology. 3(3-4), 417-447.
DOI: https://doi.org/10.1016/0169-555X(90)90015-I

[7] Leece, S.A., Pease, P.P., Gares, P.A., et al., 2006. Seasonal controls on sediment delivery in a small coastal plain watershed, North Carolina, USA. Geomorphology. 73 (3-4), 246-260.
DOI: https://doi.org/10.1016/j.geomorph.2005.05.017

[8] Philips, J.D., Wyrick, M., Robbins, J.G., et al., 1993. Accelerated erosion on the North Carolina coastal plain. Physical Geography. 14(2), 114-130.
DOI: https://doi.org/10.1080/02723646.1993.10642471

[9] Hauer, M.E., Evans, J.M., Mishra, D.R., 2016. Millions projected to be at risk from sea-level rise in the continental United States. Nature Climate Change. 6(7), 691-695.
DOI: https://doi.org/10.1038/nclimate2961

[10] Desmet, K., Kopp, R.E., Kulp, S.A., et al., 2018. Evaluating the economic cost of coastal flooding (No. w24918). National Bureau of Economic Research.
DOI: https://doi.org/10.3386/w24918

[11] Klein, R.J.T., Nicholls, R.J., 1999. Assessment of coastal vulnerability to climate change. Ambio. pp. 182-187. https://www.jstor.org/stable/4314873.

[12] Lindsey, R., 2019. Climate Change: Global Sea Level. National oceanic and atmospheric administration (NOAA), National Ocean Service, Silver Spring. https://www.climate.gov/news-features/understanding-climate/climate-change-global-sea-level (Accessed on 18 January 2020).

[13] Bamber, J.L., Oppenheimer, M., Kopp, R.E., et al., 2019. Ice sheet contributions to future sea-level rise from structured expert judgment. Proceedings of the National Academy of Sciences. 116(23), 11195-11200.
DOI: https://doi.org/10.1073/pnas.1817205116

[14] Von Holle, B., Irish, J.L., Spivy, A., et al., 2019. Effects of future sea level rise on coastal habitat. Journal of Wildlife Management. 83(3), 694-704.
DOI: https://doi.org/10.1002/jwmg.21633

[15] Morton, R.A., 2003. An overview of coastal land loss: With emphasis on the southeastern United States. United States (p. 28). US Geological Survey, Center for Coastal and Watershed Studies. https://citeseerx.ist.psu.edu/viewdoc/download?-doi=10.1.1.730.5008&rep=rep1&type=pdf.

[16] Morton, R.A., Miller, T.L., 2005. National assessment of shoreline change: Part 2, Historical shoreline change and associated land loss along the U.S. Southeast Atlantic coast. U.S. Geological Survey. Open-File Report. 1401, 1-40.
DOI: https://doi.org/10.3133/ofr20051401

[17] Gutierrez, B.T., Plant, N.G., Thieler, E.R., 2011. A Bayesian network to predict coastal vulnerability to sea level rise. Journal of Geophysical Research: Earth Surface. 116(F2).
DOI: https://doi.org/10.1029/2010JF001891

[18] Brock, J.C., Purkis, S.J., 2009. The emerging role of lidar remote sensing in coastal research and resource management. Journal of Coastal Research. (10053), 1-5.
DOI: https://doi.org/10.2112/SI53-001.1

[19] Carson, W.W., Anderson, H.E., Reutebuch, S.E., et al., 2004. May. LiDAR applications in forestry – An overview. Proceedings of the American Society of Photogrammetry and Remote Sensing Annual Conference (pp. 1-9) 04-1-2-02_04_1_2_02_deliverable_06.pdf (firescience.gov).

[20] Sallenger, A.H., Jr., Krabill, W.B., Swift, R.N., et al., 2003. Evaluation of airborne topographic lidar for quantifying beach changes. Journal of Coastal Research. 125-133. https://www.jstor.org/stable/4299152.

[21] Woolard, J.W., Colby, J.D., 2002. Spatial characterization, resolution, and volumetric change of coastal dunes using airborne LIDAR: Cape Hatteras, North Carolina. Geomorphology. 48(1-3), 269-287.
DOI: https://doi.org/10.1016/S0169-555X(02)00185-X

[22] Young, A.P., Ashford, S.A., 2006. Application of airborne lidar for seacliff volumetric change and beach-sediment budget contributions. Journal of Coastal Research. 22(2), 307-318.
DOI: https://doi.org/10.2112/05-0548.1

[23] O'Dea, A., Brodie, K.L., Hartzell, P., 2019. Continuous coastal monitoring with an automated terrestrial lidar scanner. Journal of Marine Science and Engineering. 7(2), 37.
DOI: https://doi.org/10.3390/jmse7020037

[24] Gesch, D.B., 2009. Analysis of lidar elevation data for improved identification and delineation of lands vulnerable to sea-level rise. Journal of Coastal Research. 53, 49-58.
DOI: https://doi.org/10.2112/SI53-006.1

[25] Elaksher, A., 2008. Fusion of hyperspectral images and lidar-based dems for coastal mapping. Optics and Lasers in Engineering. 46(7), 493-498.
DOI: https://doi.org/10.1016/j.optlaseng.2008.01.012

[26] Titus, J.G., Richmond, C., 2001. Maps of lands vulnerable to sea level rise: modeled elevations along the US Atlantic and Gulf coasts. Climate Research. 18(3), 1-24.
DOI: https://doi.org/10.3354/cr018205

[27] Barnhardt, W., Denny, J., Baldwin, W., et al., 2007. Geologic framework of the Long Bay inner shelf: implications for coastal evolution in South Carolina. Coastal Sediments. 2151-2160.
DOI: https://doi.org/10.1061/40926(239)169

[28] Warner, J.C., Armstrong, B., Sylvester, C.S., et al., 2012. Storm-induced inner-continental shelf circulation and sediment transport: Long Bay, South Carolina. Continental Shelf Research. 42, 51-63.
DOI: https://doi.org/10.1016/j.csr.2012.05.001

[29] Ingram, K., Dow, K., Carter, L., et al., 2013. Climate of the southeast United States: Variability, change, impacts, and vulnerability. Washington DC; Island Press/Center for Resource Economics.

[30] Davey, C.A., Redmond, K.T., Simeral, D.B., 2007. Weather and Climate Inventory, National Park Service, Southeast Coast Network. Natural Resource Technical Report NPS/SECN/NRTR- 2007/010. National Park Service, Fort Collins, Colorado.

[31] Phillips, J.D., 1997. A short history of a flat place, three centuries of geomorphic change in the Croatan. Annals of the Association of American Geographers. 87(2), 197-216.
DOI: https://doi.org/10.1111/0004-5608.872050

[32] Campbell, K.M., Rupert, F.R., Arthur, J.D., et al., 2001. Geologic map of the state of Florida. Tallahassee, FL: Florida Geological Survey.

[33] Faulkner, G.L., 1970. Geohydrology of the Cross-Florida Barge Canal area with special reference to the Ocala vicinity. Diane Publishing.

[34] Graham, J., 2009. Geologic resources inventory scoping summary Fort Matanzas National Monument, Florida. Geologic resources Division National Park Service U.S. Department of the Interior. 1-9.

[35] Tibbals, C.H., 1990. Hydrology of the Floridan aquifer system in east-central Florida. U.S. Geological Survey Professional Paper; (USA).

[36] Clarke, J.S., Hacke, C.M., Peck, M.F., 1990. Geology and ground water resources of the coastal area of Georgia. Bulletin (USA).

[37] Weems, R.E., Edwards, L.E., 2001. Geology of Oligocene, Miocene and Younger deposits in the coastal area of Georgia (Vol. 131). Department of Natural Resources, Environmental Protection Division, Georgia Geologic Survey.

[38] Veatch, O., Stephenson, L.W., 1911. Preliminary report on the geology of the Coastal Plain of Georgia (No. 26). Foote & Davies Company.

[39] Huddleston, P.F., 1988. A revision of the lithostratigraphic units of the Coastal Plain of Georgia: The Miocene through Holocene. Georgia Geological Survey, Bulletin. 105, 1-152. B-104.pdf (georgia.gov).

[40] Heron, S.D., Robinson, G.D., Johnson, H.S., Jr., 1965. Clays and opal-bearing claystones of the South Carolina Coastal Plain (No. 31). State Department Board.

[41] Sloan, E., 1979. Catalogue of the mineral localities of

South Carolina. South Carolina Geological Survey.

[42] Campbell, B.G., 1996. Geology, hydrogeology, and potential of intrinsic bioremediation at the National Park Service Dockside II site and adjacent areas, Charleston, South Carolina, 1993-94 (Vol. 96, No. 4170). US Geological Survey.

[43] Aucott, W.R., Davis, M.E., Speiran, G.K., 1987. Geohydrologic framework for the Coastal Plain aquifers of South Carolina (No. 85-4271).

[44] Aucott, W.R., 1996. Hydrology of the Southeastern Coastal Plain aquifer system in South Carolina and parts of Georgia and North Carolina (No. 1410-E). U.S. Geological Survey.
DOI: https://doi.org/10.3133/pp1410E

[45] Aucott, W.R., 1988. The predevelopment groundwater flow system and hydrologic characteristics of the Coastal Plain aquifers of South Carolina (Vol. 86, No. 4347). US Department of the Interior, U.S. Geological Survey.

[46] Lautier, J.C., 2001. Hydrogeologic framework and groundwater conditions in the North Carolina Central Coastal Plain. North Carolina Department of Environment and Natural Resources Division of Water Resources.

[47] Winner, M.D., 1978. Ground-water resources of the Cape Lookout National Seashore, North Carolina (No. 78-52) U.S. Geological Survey, Raleigh, North Carolina. 78-52, 1-59.

[48] Lautier, J.C., 2009. Hydrogeologic framework and groundwater conditions in the North Carolina East Central Coastal Plain. North Carolina Department of Environment and Natural Resources Division of Water Resources.

[49] NOAA: Data Access Viewer. n.d. National Oceanic and Atmospheric Administration (NOAA), NOAA Office of Coastal Management. https://coast.noaa.gov/dataviewer/#/lidar/search/ (Accessed on 3 May 2018).

[50] Ranasinghe, R., 2016. Assessing climate change impacts on open sandy coasts: A review. Earth Science Reviews.160, 320-332.
DOI: https://doi.org/10.1016/j.earscirev.2016.07.011

[51] Clarke, D.J., Eliot, I.G., 1987. Groundwater level changes in a coastal dune, sea-level fluctuations and shoreline movement on a sandy beach. Marine Geology. 77(3-4), 319-326.
DOI: https://doi.org/10.1016/0025-3227(87)90120-4

[52] Aubrey, D.G., 1983. Beach changes on costs with different wave climates. Sandy beaches as ecosystems. pp. 63-85.

[53] Vousdoukas, M.I., Ranasinghe, R., Mentaschi, L., et al., 2020. Sandy coastlines under threat of erosion. Nature Climate Change. 10(3), 260-263.
DOI: https://doi.org/10.1038/s41558-020-0697-0

[54] Park, J.Y., Wells, J.T., 2005. Longshore transport at Cape Lookout, North Carolina: shoal evolution and the regional sediment budget. Journal of Coastal Research. 21(1), 1-17.
DOI: https://doi.org/10.2112/02051.1

[55] Park, J.Y., Wells, J.T., 2005. Longshore transport at Cape Lookout, North Carolina: shoal evolution and the regional sediment budget. Journal of Coastal Research. 21(1), 1-17.
DOI: https://doi.org/10.2112/02051.1

[56] Leung, L.R., Prasad, R. 2019. Potential impacts of accelerated climate change: Third Annual Report of Work (No. PNNL-27452-Rev. 1). Paciffic Northwest National Lab. (PNNL), Richland, WA United States.
DOI: https://doi.org/10.2172/1524249

[57] Hoover, D.J., Odigie, K.O., Swarzenski, P.W., et al., 2017. Sea-level rise and coastal groundwater inundation and shoaling at select sites in California, USA. Journal of Hydrology: Regional Studies. 11, 234-249.
DOI: https://doi.org/10.1016/j.ejrh.2015.12.055

[58] Deronde, B., Houthuys, R., Henriet, J.P., et al., 2008. Monitoring of the sediment dynamics along a sandy shoreline by means of airborne hyperspectral remote sensing and LiDAR: a case study in Belgium. Earth Surface Processes and Landforms: The Journal of the British Geomorphological Research Group. 33(2), 280-294.
DOI: https://doi.org/10.1002/esp.1545

BILINGUAL PUBLISHING CO.
Pioneer of Global Academics Since 1984

Journal of Geographical Research
https://ojs.bilpublishing.com/index.php/jgr

ARTICLE

Analysis of Chinese Citizens' Perception and Its Differences of City Spirit: A Case Study of Hefei City

Zhiguo Yao[1] Fei Liu[2] Min Xiang[3*]

1. School of Economics and Management of Shanghai Polytechnic University, Shanghai, 201209, China
2. Department of International Cooperation and Exchange of Tianjin Foreign Studies University, Tianjin, 300071, China
3. Faculty of Tourism, Shanghai Nanhu Vocational Technical College, Shanghai, 200439, China

ARTICLE INFO

Article history
Received: 13 June 2022
Revised: 23 July 2022
Accepted: 29 July 2022
Published Online: 31 July 2022

Keywords:
City spirit
Hefei City
Perception

ABSTRACT

City spirit is the soul of the city. The spread of city spirit not only could establish a civilized specimen for citizens, but also create a good cultural atmosphere for the city. Hefei residents' perception of city spirit is extensive, and most of Hefei citizens consider the expression words of city spirit are very appropriate, which is enlightened, open-minded, actual and innovate. Great majority of Hefei citizens willing to support the propaganda and promotion of the city spirit, and they think the promotion of the city spirit plays a key role in the way of city's development. In addition, significant differences in the perception of urban spirituality emerge among residents with different economic and social characteristics. There are four aspects about how to enhance the public perception of city spirit, which including increasing dissemination channels and means, strengthening guidance according to the difference of residents, encouraging participation of community residents, and building good atmosphere depending on the city's advantages.

1. Introduction

The city spirit is a comprehensive response to the city's historical tradition, cultural accumulation, social atmosphere and civilization, which represent the city's image, highlighting the city's appearance and leading the future development of the city. The city spirit is also a comprehensive reflection of citizens' views on legal system, public morality, folk customs and aesthetics, and play an important role in shaping the tourism image of a city. According to Liu (2011), urban spirit is the core element of urban civilization, the concentrated embodiment of urban soft power and inexhaustible resource of core competitive-

*Corresponding Author:
Min Xiang,
Faculty of Tourism, Shanghai Nanhu Vocational Technical College, Shanghai, 200439, China;
Email: yzgzszz@163.com

DOI: https://doi.org/10.30564/jgr.v5i3.4788

ness, and the main content of urban cultural personality [1]. Chen and Wei (2005) argue that urban aesthetics provides the theoretical basis for the shaping of Shanghai's urban spirit, while the process of shaping Shanghai's urban spirit also promotes the maturation and development of urban aesthetics [2]. Shi and Wei (2003) studied the historical and cultural characteristics of Hangzhou and their relationship with the new humanistic spirit and proposed that the humanistic spirit of Hangzhou originated from the historical and cultural traditions, and this humanistic spirit is the exquisite harmony and atmospheric openness, which has been the driving force of Hangzhou's social development for thousands of years [3]. Shen (2007) believes that the competitiveness of all countries and cities ultimately depends on the cultural spirit of the people, and that true modernization should be implemented in the modernization of people, the modernization of the spirit of the nation and its citizens [4]. The perception of urban spirit by citizens as urban subjects directly affects the effectiveness of urban spirit dissemination, but there is little literature on the perception of urban spirit by citizens.

Foreign research results on city spirit perception are relatively few, and some of scholars mainly focus on the mental perception model of city image [5] and the differences between domestic and foreign tourists' perceptions to tourism city [6]. These research results are somewhat different from the relevant domestic studies, and also have something to learn from. Based on the systematic analysis of the concept, connotation and role of urban spirit, this paper focuses on urban residents' perception of urban spirit, including familiarity with the expressions, recognition, willingness to support, and significance of dissemination, etc., through questionnaire surveys and statistical analysis, and proposes initiatives to improve the perception of urban spirit citizens, and the research findings have certain theoretical and practical values for shaping and dissemination of city spirit.

2. Methodology and Technology of the Study

2.1 Case Study Area

As the capital of Anhui Province China, Hefei is the political, economic and cultural center of the province, which has obvious geographical advantages, great potential for economic development, unique historical and cultural charm, and a distinctive urban temperament. Based on the extensive collection of social opinions, the participation of citizens in voting, and the selection of experts, the expression of Hefei city spirit was officially determined as: "enlightened, open, seeking, innovative".

Hefei city spirit has its connotation, first of all, from the geographical point of view, Hefei in the middle of Anhui, east and west, even south and north, is the intersection of the Central Plains culture, Chu culture, Wu-Yue Culture, regional cultural characteristics for Hefei people to accept foreign things and compatible with all sides of the idea to provide the conditions, creating the Hefei open-minded city temperament, which emphasizes not being stubborn or conservative. Secondly, from the historical point of view, from the origin of the Hui merchants in the Ming Dynasty to Li Hongzhang, who implemented the "foreign affairs movement" in the Qing Dynasty, Hefei people have the notion of open-mindedness, openness is the temperament of the city of Hefei, Hefei is moving towards a regional megacity, the spirit of openness is more and more important. Again from the realm, "seeking" is the cultural cornerstone of the city's great development, construction and environment, Hefei choose to seek is the spirit of the city, it is from the reform and opening up, the development of the Yangtze River, the rise of the central practice of consensus. Finally, from the practical point of view, Hefei has always had the gene of innovation, Hefei has several Chinese or world firsts in the field of technological innovation, and still has rich scientific and educational resources, the essential of Huizhou business spirit is the spirit of thinking, change and innovation of Anhui people, innovation is the sinews and bones that support the prosperity of the city, and is the core of the city to leapfrog and catch up.

As a highly concentrated economic area and a place where human civilization is concentrated, the city is the center of regional politics, economy and culture. In recent years, as people pay more attention to cultural construction, more and more cities in China have started to cultivate "city spirit" as the cultural brand of the city, and to refine and publicize "city spirit" as an important city flag, which coalesces the ideological soul of a city, represents the overall image of a city, highlights the characteristics of a city, and leads the future development direction of a city culture. Urban construction should not focus only on the modern production of material space, but ignore the shaping of urban spirit. Cities need to make good use of every existing urban space to make it more culturally magnetic, shared and livable, and enhance citizens' sense of belonging, participation and happiness [7]. It is based on the recognition of the importance of city spirit that many cities in China have now developed a unique combination of urban spirit expressions (Table 1).

Table 1. The city spirit expressions of some Chinese cities

City	City spirit expressions	City	City spirit expressions
Beijing	Patriotic, innovative, tolerant and virtuous	**Nanjing**	Open-mindedness, honesty and integrity, entrepreneurship and innovation
Shanghai	Fairness, Inclusion, Integrity, Responsibility	**Haerbin**	Honest and dedicated, harmonious and progressive
Tianjin	Patriotic, honest, pragmatic and innovative	**Hangzhou**	Exquisite and harmonious, open atmosphere
Chongqin	Climbing to the top and carrying the weight forward	**Jinan**	Integrity, Innovation, Harmony
Huhehaote	Stallion spirit, grassland temperament	**Nanchang**	openness, integrity, keep strength
Changsha	Concerned about the world, dare to be the first	**Wuhan**	Civilized, tolerant, resilient, innovative
Yinchuan	Strong and everlasting	**Guangzhou**	Pragmatism, truth-seeking, tolerance, openness, and innovation
Hefei	Open-minded, inquisitive and innovative	**Lanzhou**	Innovation, harmony and progress
Changchun	Tolerance and self-improvement	**Chengdu**	Harmony, tolerance, and integrity
Zhengzhou	Profound, open, innovative and harmonious	**Guiyang**	Knowing and acting, working together to be the first
Taiyuan	Compatible and Harmonious, Integrity and Excellence	**Kunming**	Spring melts everything, harmoniously, dares to be the first, pursues excellence

2.2 Data Collection and Study Design

In this paper, random stratified sampling was used to obtain the research data, and the questionnaire was designed to include citizens' familiarity with city spirit, recognition of city spirit, willingness to support the city spirit, and significance of communication. The values of "very supportive", "supportive", "average", "opposed" and "very opposed" are 5, 4, 3, 2 and 1 respectively. A higher for score value, means the residents are more supportive to the city spirit. The statistical data were mainly from the centralized interviews from May 5th to July 10th, 2019. The research interviews were conducted twice, mainly for the citizens of Hefei, and the questionnaires were distributed in city parks and residential areas with more than 1000 people. The respondents were all identified after two face-to-face screening, and they were all sensitive to city spirit-related terms, and had a strong willingness to respond and express, and the total sample after excluding invalid data was 2897, with a valid sample rate of 94.8%, and the sample size and representativeness met the needs of the study.

After collecting the relevant data, SPSS19.0 statistical package was used to conduct the basic frequency analysis, chi-square test and other mathematical and statistical analyses of the relevant variables in order to study the descriptive statistical characteristics of the research subjects, the reliability and validity of the sample data, the citizens' perception of urban spirit, the differences in the perception of city spirit among citizens with different characteristics, and to gain insight into the correlation between the variables of citizens' economic and social attributes and the differences in the perception of city spirit. The main objectives of the study were to reveal the factors influencing city spirit perception, provide theoretical basis for improving city spirit perception, optimizing urban tourism image, and enhancing urban soft competitiveness.

3. Results

3.1 Citizens' Perception of Hefei City Spirit

The ultimate purpose of city spirit release, propaganda and promotion is to influence citizens' behavior implicitly and to promote city culture and civilization construction. A good city spirit expression depends on city residents' understanding, recognition and support of the city spirit slogan. Judgment is made. According to the sample data of the sample survey, the survey method of Likert scale was used, and each question was rated according to "strongly agree", "agree", and "disagree". Higher scores indicate that residents are also more supportive of city spirit. The statistical analysis of citizens' perception of Hefei city spirit is as follows (Table 2).

Table 2. Analysis of citizens' perception of Hefei city spirit

variables	Variable Description	Mean	Standard deviation	(%)
Familiarity of City Spirit	Very familiar with city spirit expressions	3.12	0.63	57.3
	Partial understanding of city spirit expression	4.58	0.37	89.4
	Have no idea of city spirit expression	2.14	0.65	46.7
Recognition of City Spirit	The city spirit is very expressed aptly	4.63	0.35	91.2
	City spirit expressions are partially similar	4.10	0.52	85.5
	The expression of city spirit is not very appropriate	2.15	0.62	35.8
Willingness to support the City Spirit	Very supportive of city spirit promotion	4.34	0.28	90.1
	Support city spirit promotion as long as it is available	3.67	0.43	78.5
	Reluctance to support city spirit promotion	1.58	0.49	27.6
Significance of City Spirit	Beneficial to improve the visibility of the city	4.39	0.31	89.5
	Beneficial to the improvement of urban civilization	4.20	0.42	90.3
	Beneficial to the promotion of social harmony	4.52	0.38	87.6
	Little impact on urban development	2.56	0.64	35.6

3.2.1 Familiarity of City Spirit

In the face of the government-led activities of collecting, releasing and promoting the city spirit expressions, many citizens and organizations are involved in them, and they are familiar with the city spirit expressions to some extent, the greater the degree of familiarity the citizens perceive, and the more familiar the citizens are with the city spirit, the more conducive to the proliferation and influence of the city spirit. On the whole, the citizens of Hefei are familiar with the city spirit, and the proportion of those who "know part of the expression of the city spirit" is the highest (mean and approval rate are 4.58 and 89.4%, respectively), followed by those who are "very familiar with the expression of the city spirit" (mean and approval rate are 3.5 and 78.6%, respectively). The proportion of those who are "not familiar with the expressions of city spirit" is smaller (mean and approval rate are 2.14 and 46.7%, respectively). Increasing familiarity with city spirit is a long-term task, and measures can be taken to increase dissemination channels and create cultural brands.

3.2.2 Recognition of City Spirit

The city spirit is the condensation of the mainstream consciousness of the city culture [8]. Most of the expressions of city spirit are formally released and publicized to the society after a long period of gestation, community-wide solicitation, and multi-faceted revision, therefore, a more satisfactory proposal is obtained. The public's approval of

the city spirit expressions is reflected in whether they think the expressions aptly summarize the city's history, culture, temperament, economy, and other elements. Hefei's city spirit expressions were recognized by most citizens, and the summary was relatively concise, with "the city spirit is very relevant" (mean value and approval rate were 4.63 and 91.2%, respectively) scoring much higher than "the city spirit is not very relevant" (The mean value and approval rate are 2.15 and 35.8% respectively), and the perceived consistency of the recognition of the city spirit is strong (the standard deviation of "very relevant" is 0.35), while some people think that some of the expressions are similar to other cities (mean value and approval rate are 4.10 and 85.5%), which needs to be improved and optimized.

3.2.3 Willingness to Support the City Spirit

The citizens are the ambassadors of the city, the citizens are the best disseminators of the city spirit, and the good words and actions of the citizens are the best interpretation of the city spirit. The higher the citizens' willingness to support the city spirit, the more they are willing to participate in shaping the city spirit, and the more conducive to expanding the influence of the city spirit. The mean value of "very supportive of city spirit" propaganda is 4.34, and the approval rate is 90.1%; the mean value of "supportive of city spirit propaganda as long as conditions allow" is 3.67, and the approval rate is 78.5%. On the other hand, the mean value of "unwilling to support city spirit propaganda" is 1.58, and the approval rate is 27.6%, both of which have lower scores. Creating conditions and strengthening community participation could make more citizens understand the meaning of city spirit are conducive to increase public support.

3.2.4 Significance of City Spirit

On the one hand, the propagation of city spirit itself can stimulate citizens to think about the connotation of city spirit, on the other hand, the propagation of city spirit also plays a role in promoting the construction of city civilization in reality, and effectively changes the spiritual and civilized appearance of the city. Hefei citizens have a positive perception of the significance of the dissemination of city spirit, and the scores of the three positive variables are all high, with the mean values of "conducive to improving the city's popularity", "conducive to improving the city's civilization", and "conducive to promoting social harmony" are 4.39, 4.20, and 4.52, and the approval rates are 89.5%, 90.3%, and 87.6%, respectively, while the mean value of "not significant for urban development" is 2.56, and the approval rate is 35.6%, all with lower scores.

3.2 Differences of Citizens' Perception to City Spirit

The chi-square test based on urban residents' perceptions of urban spirituality is not only useful for determining the influencing factors of urban spirituality perception differences, but also for understanding the distribution of perception differences among different types of urban residents, and then for formulating perception improvement strategies. The results showed that the significance level of the chi-square test of urban spirituality perception of residents with different economic and social characteristics was less than 0.05, so the original hypothesis of the chi-square test was rejected, and the economic and social variables such as gender (0.001), age (0.000), education level (0.001), income level (0.001), and occupation type (0.002) of urban residents were found to be significantly related to urban spirituality perception. These economic and social variables are all influential factors in the difference of city spirit perceptions. Urban management departments need to fully consider the influence of these variables and propose targeted countermeasures based on the analysis of the influence mechanism to improve the perception and support of city spirit among local residents.

The proportion of "high perception" urban residents is greater than that of "medium perception" and "low perception" urban residents. Taking the "high perception" option as an example, the perception of women (50.34%) is higher than that of men (43.25%), indicating that female residents have a higher potential to support city spirit. In terms of the difference in the perception of different age groups, "30-39 years old" (42.88%) have a higher perception of city spirit. (42.88%), followed by "20-29 years old" (38.12%) and "20 years old and below" (37.25%). Residents with higher education levels are more concerned about the spirit of the city, with "undergraduate" (46.90%), "college" (46.33%), and "graduate and above" (45.287%) ranking in the top three in terms of perception. residents with higher average monthly income Residents with higher average monthly income also have higher perceptions, residents with "monthly income of CNY 6,000-7,999" (40.34%) having the highest perception, followed by residents with "monthly income of CNY 5,000-5,999" (38.42%) and "monthly income of CNY 5,000-5,999" (38.42%) and "more than CNY 8,000" (37.32%); among the types of occupation, "civil servants" (42.11%), "others" (38.94%) have relatively higher perceptions of city spirit. In addition, residents with high scores on the "high perception" option have relatively low scores on the "medium perception" and "low perception" options, which means that the scores of the same category of residents on the perception variables are mutually coupled (Table 3).

Table 3. Residents' perception differences to the city spirit by their socio-economic characteristics

Demographic characteristics		n	Perception to city spirit			x^2	Sig.
			High perception	Medium perception	Low perception		
			Percentage (%)				
Gender	male	1326	43.25	30.33	26.42	5.238	0.001
	female	1571	50.34	33.18	16.48		
Age	≤20	271	37.25	36.53	26.22	4.164	0.000
	20—29	549	38.12	33.21	28.67		
	30—39	543	42.88	31.27	25.85		
	40—49	498	34.84	49.54	15.62		
	50—59	474	30.22	43.08	26.70		
	≥60	562	31.18	37.23	31.59		
Education level	Middle school or below	88	38.22	46.47	15.31	5.987	0.001
	High school	346	44.75	42.54	12.71		
	College	930	46.33	36.18	17.49		
	Undergraduate	775	46.90	34.62	18.48		
	Graduate	758	45.27	28.43	26.30		
Average monthly revenue (CNY)	≥8000	576	37.32	36.77	25.91	4.021	0.001
	6000—7999	859	40.34	29.66	30.00		
	5000—5999	904	38.42	32.15	29.43		
	3000—4999	427	36.54	35.43	28.03		
	2000—2999	116	31.54	44.76	23.70		
	≤1999	15	31.23	43.75	25.02		
Occupations	Civil Servant	302	42.11	32.40	25.49	2.365	0.002
	Enterprises	396	38.77	32.87	28.36		
	Servant industry	446	38.65	34.65	26.70		
	workers	275	37.62	35.77	26.61		
	Commercial staff	623	35.63	38.65	25.72		
	students	187	56.23	22.07	21.70		
	Retired	399	35.14	34.87	29.99		
	others	269	38.94	35.58	25.48		

Significance level $p < 0.05$.

4. Conclusions

4.1 The Differentiation of Residents' Perception to City Spirit

In China, provincial capitals pay much attention to the shaping and promotion of city image, especially city spirit is seen as an important part of city culture and city image. The spirit of the city is the soul of the city. Lewis Mumford pointed out that the city has the function of magnet first and then the function of container [9]. This magnet function in a certain sense refers to the cultural attractiveness and spiritual centripetal force of the city, and the perception of city spirit by city residents as the main body of the city directly determines the effect of city spirit dissemination.

This paper selects four perceptual variables, which including citizens' familiarity with city spirit, recognition of city spirit, willingness to support for city spirit, and significance of dissemination of city spirit. Hefei is a famous historical and cultural city in China, with high economic growth and rising living standards of the people in recent years, the citizens have a high perception of the city spirit, and the government has strongly promoted and publicized the city spirit, which has greatly stimulated the pride and spiritual motivation of the citizens.

According to the results of mathematical statistics, this paper shows that there are certain group differences

in urban residents' perceptions to city spirit. Female citizens, highly educated citizens, high-income groups, middle-aged and young residents, and government workers are the right types of citizens who have higher perceptions and satisfaction with city spirit. This means that the process of designing, publicizing and promoting the spirit of the city needs to take full account of the economic and social attributes of the residents. These findings have strong guiding significance for further targeted enhancement of citizens' perception of city spirit.

4.2 Measures to Enhance Citizen Perception of City Spirit

City spirit is a highly condensed version of a city's economy, society, culture and history. Only when the city spirit is known and recognized by more citizens, the information and concepts conveyed by the city spirit will be transformed into behavioral motivation and play a role in promoting social harmony and civilization progress. Combined with the above analysis of the characteristics of Hefei citizens' perception of city spirit, the main measures to enhance the perception of city spirit in Hefei are reflected in the following aspects. In order to improve the overall perception level of urban spirit and fully consider the factors influencing the difference of urban spirit perception, we can enhance the urban spirit perception of citizens with low perception from the perspectives of policy incentive, publicity and education, and community participation, and promote the transformation of citizens with low perception types to high perception types.

4.2.1 Enrich the Carrier and Increase the Channels

The main media include TV, radio, newspapers, outdoor media, internet, etc. Although the proportion of Hefei citizens who know about the city spirit is high and the proportion of people who "know nothing about the city spirit" is small (many of them are foreigners), it is necessary to continue to enrich the dissemination carriers and increase the publicity channels to expand the familiarity of the city spirit. From the perspective of the long-term dissemination strategy of the city spirit, it is necessary to continue to enrich the dissemination carriers, increase the publicity channels, expand the familiarity of the citizens with the city spirit, such as adding the expression of the city spirit slogans on the packaging of enterprise products, so that consumers can feel the city spirit while shopping, carrying out special publicity in the main buildings and public places of the city, regularly carrying out the exhibition of the results of the dissemination of the city spirit, and forming the impression that the city spirit is everywhere. We can strengthen the city culture, improve and optimize the city environment, and increase the citizens' sense of belonging to the city.

4.2.2 Focus on Differences and Strengthen Guidance

There are many reasons for the differences in the perception of urban spirituality among citizens with different demographic characteristics. For example, there are differences in thinking styles by gender, differences in cognitive abilities by education level, and differences in the ability to understand the city by occupation type and income level. In order to increase citizens' acceptance, appreciation and recognition of the city spirit, two aspects are very important: one is to "speak with one voice", to build the city spirit as a long-term project, to form perceptual inertia, and to strengthen citizens' psychological perception. The other is to pay attention to the variations of different groups of citizens. Strengthen the guidance, and take targeted publicity measures to improve the effect of spreading the city spirit, for example, civil servants and students have the most significant knowledge in the city spirit. We can improve people's cognition of city spirit through differentiated ideas and measures.

4.2.3 Community Engagement for Greater Impact

City spirit is the cultural symbol of a city, which come from history and are rooted in people's lives. The best city spirit penetrates into citizens' lives and becomes part of their cultural lives, and such city spirit is relevant to citizens' psychological distance. Therefore, enhancing the perception of city spirit requires strengthening community participation so that the city spirit melts into the subjective consciousness of citizens and influences their daily habits. Enriching and expanding community activities, arts and culture activities, and campus activities with the theme of city spirit will not only make the already formed city spirit known to citizens, but also loved and recognized by them. Citizens who implicitly feel the role of city spirit in participating activities are influenced by city spirit, and they are more willing to support the promotion of city spirit. For example, the greening and beautification of Hefei's Ring City Park provide a platform for the dissemination of the city spirit, and the special promotion of the city spirit in this civic park enables citizens to enhance their pride of the city, and everyone becomes an ambassador and propagandist of the city spirit.

4.2.4 Reinforcing Advantages and Creating an Atmosphere

The dissemination of city spirit has a very important

significance. The city spirit not only unites people and establishes an integrated city image, but also creates a good environment for the development of the city, it makes the city image more individual and leads the development direction of the city [10]. At the same time, it is also a systematic project of shaping and dissemination the city spirit, which requires maximizing the advantages of the city by using modern means [11,12]. It takes long-term efforts to truly cultivate a city spirit with regional characteristics through the formation of the city's cultural brand, for example, Hefei can take advantage of cultural resources such as universities and animation bases to collect and create a number of animation works, movies and plays reflecting the city spirit of Hefei, so as to turn the city spirit of Hefei into cultural products with thematic characteristics. In the process of construction of the city's spiritual civilization, the city spirit can be used as a highlight for urban marketing and image dissemination.

Conflict of Interest

There is no conflict of interest.

References

[1] Liu, J.X., 2011. Rumination on the spirit of Harbin city and its realistic efficacy. Journal of Harbin College. 32(10), 26-32. (in Chinese).

[2] Chen, W., Weng, X.L., 2005. Urban aesthetics and the spirit of Shanghai city. Journal of Shanghai Normal University (Philosophy and Social Science Edition). 34(1), 69-71. (in Chinese).

[3] Shi and Wei, 2003. The urban humanism of Hangzhou. Urban Issues. (2), 34-36. (in Chinese).

[4] Shen, W.S., 2007. Modernization of People and the Spirit of Capital City Culture. Urban Issues. (4), 50-53. (in Chinese).

[5] Escalas, J.E., 2004. Image yourself in the product: Mental simulation, narrative transportation, and persuasion. Journal of Advertising. 33(2), 37-48. DOI: https://doi.org/10.1080/00913367.2004.10639163

[6] Bonn, M.A., Joseph, S.M., Dai, M., 2005. International versus domestic visitors: An example of destination image perceptions. Journal of Travel Research. 43(3), 294-301.

[7] Lu, S.M., 2011. Strategies for shaping urban spirit based on spatial events. Urban Development Research. 18(8), 120-124. (in Chinese).

[8] Zhang, J.Q., 2008. Urban culture and urban spirit: Dialectical unity in planning. Planner. 24(11), 10-13. (in Chinese).

[9] Lewis, M., 2005. The history of urban development: origins, evolution and prospects. Beijing: China Construction Industry Press. (in Chinese).

[10] Wang, Q.,2009. On the spirit of the city and the improvement of urban competitiveness. Journal of Shenyang University of Architecture (Social Science Edition). 11(3), 360-362. (in Chinese).

[11] Wang, Z.J., 2020. Cultivating and carrying forward the spirit of Shenyang city. Shenyang Cadre Journal. 22(5), 63-64. (in Chinese).

[12] Zhang, L.,2021. Exploring the strategy of using new media in the dissemination of Liaoning city image. Media Forum. 4(2),36-37. (in Chinese).

BILINGUAL PUBLISHING CO.
Pioneer of Global Academics Since 1984

Journal of Geographical Research
https://ojs.bilpublishing.com/index.php/jgr

ARTICLE

Comparative Assessment of Heavy Metals Pollution in Surface Water in Ikoli River and Epie Creek in Yenagoa Metropolis Using Geographical Information System

Egai Ayibawari O.[1*] Edirin Akpofure[1] Digha Opaminola Nicholas[2]

1. Department of Geology, Niger Delta University, Bayelsa State, Nigeria
2. Department of Geography, Jasper Boro College of Education Sagbama, Nigeria

ARTICLE INFO

Article history
Received: 05 May 2022
Revised: 16 August 2022
Accepted: 22 August 2022
Published Online: 31 August 2022

Keywords:
Multivariate treatment
GIS
Pollution index
Anthropogenic
Geogenic
Ikoli river
Epie Creek

ABSTRACT

The article is the investigation of heavy metals pollution on surface water in Ikoli River and Epie creek in Yenagoa, metropolis, Bayelsa State. Pb, Cd, Ni, Cr, Fe, Zn was determined and evaluated using Geographical Information System. Zinc concentration was below the permissible limit of 3 mg/L in all the locations sampled. Iron is 77.78% below the limit of WHO 2011 of 0.3 mg/L while other heavy metals examined in Ikoli River and Epie creek are highly polluted. The pollution index for contamination index shows 11.11% sample are high and 88.89% are low while the evaluation of heavy metal index and the pollution index load of the heavy metals contain 22.11% of the sample are low and 77.78% are high which imply the Ikoli River and Epie creek is polluted. Multivariate treatment of the result revealed a good correlation between the PCA and HCA, which showed activities of natural processes and man influenced environmental sources of the heavy metals which were mainly products of automobiles exhaust, water tank leakages as well as dumping of radioactive wastes and burning. The study investigated successfully the potential use of GIS with the help of multiple criteria decision analysis to predict and characterize areas of high pollution, medium, and low pollution in the study area.

1. Introduction

Water pollution is situations whereby toxic materials from the environment are found in the water course, deter the quality of the given water body and also destroy the environment and health system of humanity [1]. Water is a vital resource that is widely acceptable for good number of purposes such as drinking and for so many industries uses [2]. Water has been a powerful substance for sustenance and balancing of human ecosystem system. These practices have been widely used globally. Being a solvent that is occurring universally, It is also one medium which introduces infection to the end user if not properly treat-

*Corresponding Author:
Egai Ayibawari O.,
Department of Geology, Niger Delta University, Bayelsa State, Nigeria;
Email: aegai19@yahoo.com

DOI: https://doi.org/10.30564/jgr.v5i3.4696

ed. The World Health Organization (WHO) reported that about, 80% of diseases in the environment are waterborne. Most water that are used for drinking in the various Countries in the world do not meet the standards of WHO [3]. About 3.1% of deaths globally occur as a result of unhealthy bad and untreated water systems [4]. The underground system is fundamentally a recycling process due to its esteemed self-filtration and purification processes that took place at the soil. The interaction of water with other earthly materials is enormous and its constant exposure to human activities ie anthropogenic effects causing various routes of pollution forming mainly accumulating toxic metals such as lead, cadmium, and zinc. Deterioration of water quality is as a result of introduction of pathogens and other solutes are a notable challenge facing developing countries and industries around the world. The careless discharge of wastes domestic and industrial waste etc. to large water bodies have greatly destroy both the quality of water and stampeding aquatic diversity, economic strangulation owing to increases of pollution pathways [5]. Rapid industrialization and non-availability clean freshwater resources and pollutants have become a worsen situation. Heavy metal pollution is mainly caused by the introduction of waste as effluents and domestic wastes, sullage, polluted river sedimentation, and atmospheric processes. Heavy metals can also enrich the environment; the microbes introduced into the natural environment cannot easily degrade. Finally, food chain is also another medium (bioaccumulation) in which heavy metals are introduced into human body system and directly or indirectly jeopardizes human health system [6].

Statistical approach with incorporation of Geographic Information System (GIS) as a method is fundamentally useful in realizing and determining groundwater quality as its assessment [7]. Hence Geographical Information System a fundamental tool for data analysis, data management, display of spatial data, and also gathering of non-spatial data system and also Geographic Information Systems (GIS) tools are reliable have proven integrity and could stand the test of time for data storage and management of data, spatial data display for water resources managements and assessments [8]. Today, GIS tools are also very productive and its method is increasing in the search for groundwater resource management. With emphasis and understanding the applications and the use of Geographical Information System for determining groundwater resources and water management. Similarly, its applications are aligning and this current study is deploying the inverse overlay method using the inverse weighted technique.

The results gotten from GIS applications have proven realistic in diverse fields of study for easy decision making and storage of data [9]. GIS knowledge transfer has been a model for environmental studies site assessment, resources of the earth and also assessment of underground water potentials. In research studies of groundwater, underground water mapping, inventory site mapping date, analysis of site suitability, vulnerability of groundwater site estimation with respect to degree of contamination, solute transport modeling, infiltrations, under-groundwaater flow mapping, and also assessment of groundwater quality index models [8,10,11]. Nitrate presence in water body suggests sewage pollution. Chloride concentration varies in aquatic system which is related to presence of mineral content. Usually seawater shows appreciable chloride concentrations and this can also be indicated from coastal aquifers. Effluents can also be a source of high chloride concentration especially from the dispose of their raw materials [12]. Lack of environmental enforcement protective laws by Nigerian government has worsened the disposal effluents municipal wastes and other kinds of wastes etc into the water system [13]. Unhealthy waste disposal practices and untreated effluents disposal have led to deteriorate of water quality. According to Tsai et al., (2003) heavy metals presence in surface water bodies indicates human impact on the environment and in most cases depicts anthropogenic interplay thus destroying the physical environment [14]. Heavy metal pollution index (HPI) and metal index (MI) has profusely and often used as creative tool for risk assessment of heavy metals global water system [15]. Therefore, there is need to assess the heavy metal concentration in the in the environment. The specific objective of the current study is to evaluate the concentration of heavy metal in Ikoli River and Epie Creek comparatively with the help of GIS as determinant tool to unravel spectral distribution.

2. Study Location

The study area is part of the sedimentary basin of Niger Delta, Southern Nigeria (Figure 1). It is at the Capital City of Bayelsa State. The area shows within Latitude 5°3’30”N - 4°68’30”N and Longitude 6°15’0”E - 6°21’0”E. Good road network links which makes easy accessibility of the study area accessible.

The study area is characterized by high rainfall during the rainy season and a short duration of dry season which is about four (4) months. The average annual rainfall is about 4000 mm [16] and this serves as the major source of groundwater recharge. There are two (2) major seasons which defined this region. They are the dry and wet seasons. The dry season lasts from November to early March and the rainy season begins from late March to October. A short break in the rainy season is observed around

mid-August. The mean monthly temperature varies between 25 °C and 32 °C. The annual mean temperature is constant within Bayelsa State. The organic debris which originates in these swamps, assist in the sedimentation of this region climate, vegetation root, types of trees, shrubs, of four ecological zones which supports luxuriant fast-growing swamp forest. These are fresh water swamp, mangrove forests, coastal barrier island forests and low-land rain forests. These types of vegetation are connected with the different soil units in the area, and they are part of the Niger Delta complex ecosystems. The region is characterized by low lands with topography or contour which is part of the surface and it shows the altitude nature of the terrain. Contour lines shown in Figure 2 with areas of equal elevation it was generated at 2 m intervals. The spot height indicates the direction in which water flows through. The areas are drained mainly by the creeks Epie creeks and tend to slope gently into Ikoli River which drains into the Atlantic Ocean. Due to the poor drainage of the area, it tends to flood during the rainy season.

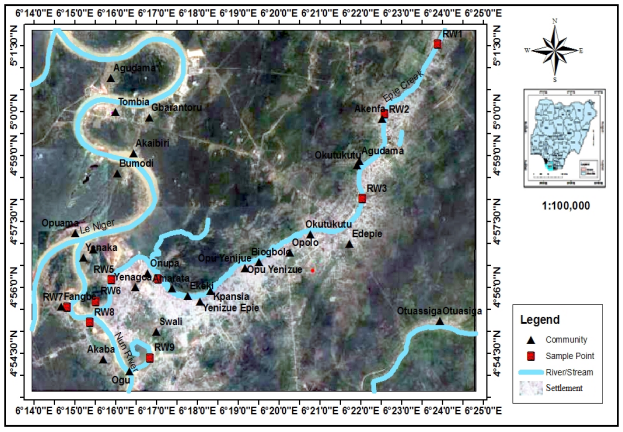

Figure 1. Google map showing sample point for surface water

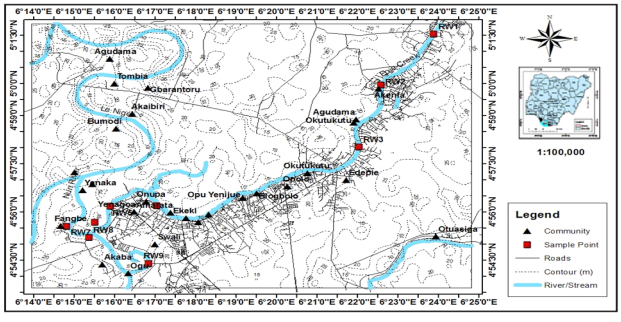

Figure 2. Contour map of the study area

The digital information showing on the topographic architecture in the current study area is pointing to low and high elevation showcasing the digital terrain of the area. The DEM of the current study ranges from 2.00 m to 22.60 m shown in Figure 3. It is used to determine area that is liable to flooding especially the rainy season [17]. The yellow colorations is indicating flood plain and this is also a reliable pointer to site suitability and for flood relief center and other similar projects and can also determine rice farming potentials for a peculiar terrain.

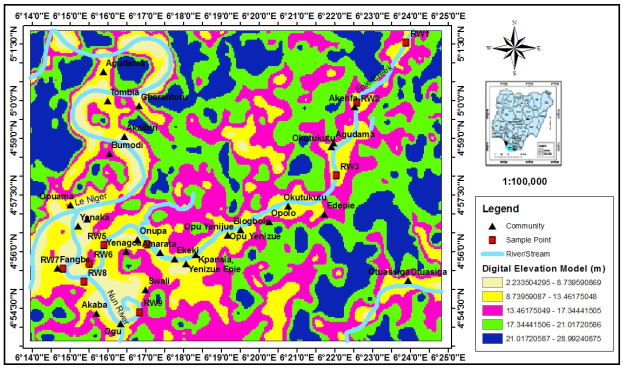

Figure 3. Digital Elevation map of study area

3. Geology of Study Area

Reyment (2018) geologically described the current study area is cutting across the South-Western side of the Niger Delta Region of Nigeria. The formation of the Niger Delta Basin was basically due to rifting of failed arm known as Aulacogen which was a manifestation of a basin that was pull -apart of South American plate from the African plate [18]. The initial rifting was initiated during the late Jurassic period and ended during Cretaceous. Faulting especially thrust faulting were predominant. According to Reijers (2011) the landmass of the Niger Delta basin is about 105,000 km^2 was recorded in the delta [19].

Notable structures of the delta are facies of the Agbada formation, facies of the pro-delta Akata Formation. The continental Benin Formation constitutes delta top facies with sand and aquiferous potentials. According to Reyment (2018) and Etu–Efeotor (1997) the Paleocene to Holocene Akata Formation is purely marine and is the basal lithostratigraphic unit found in the Niger Delta basin.

Its contains marine pro-delta mega facies and are thick shales, turbidite sands, and small amounts of silt and clay. High pressure, low density, and deep marine deposits containing of plant relics characterize the Akata formation and is overlying the Agbada formation [18,20]. Over 50 percent of planktonic foraminifera and the rich micro fauna and benthonic assemblage are found in the Agbada Formation [21]. This assemblage shows a depositional shallow marine shelf environment. Presumably the materials such as the sand streak and silt were deposited within the ambit of

high energy delta conditions which advanced into the sea. About 0-6000 meters is the approximate range of thickness. The formation is not visible at the shore and crops out and changes towards the sea at the outer delta area [20].

4. Materials and Method

4.1 Data Collection

A total of nine sampling points were identified for surface water sample collection in Ikoli River and Epie creek in the current study area. The prevailing creeks serve as refuse depositing channels for individuals, marketers and households residing around. Coordinates were also taken using Global Positioning System (GPS); the collection of the samples was within a distance of 10 cm to 15 cm depth using polypropylene decontaminated bottles. The acidification was done with concentrated nitric acid to a pH below 2.0 to reduce precipitation and adsorption on the walls of the container. The samples were then kept within 4 ºC in an ice-container and were taken to the laboratory for analysis. The samples were analyzed for Pb, Zn, Fe, Cd, Ni and Cr using atomic absorption spectrophotometer. Also Shuttle Radar Topographical Mission (SRTM) from USGS explore were determined before spatial locations of some Communities in the study area were also acquired by the use of Garmin72 GPS, and extracted using TCX, DNRGPS software including downloading of satellite image from google earth in 2020 with the aid of universal map downloader. An administrative map from where political boundaries and roads were digitized.

4.2 Data Analysis

Multivariate statistical analysis was performed using SPSS 21 for Windows 10. The PCA was used to reduce data and the data were extracted to analyze the relationship between the analyzed heavy metals in the water samples and the likely possible similarities of these metals in the water. The cluster analysis CA was used to classify the heavy metals on the basis of their similarities based on their chemical properties. While the hierarchical agglomerative cluster analysis was used to provides intuitive similarity relationship between the sample and the data set using the dendrogram which gives a visual of the clustering process. Finally, the correlation coefficient matrix was used to measure how the variance picture of each constituent can be explained by its relationship with each other. The multivariate technique was also used to predict the origin of the analyzed metallic ions in the analyzed surface water samples in addition to various assessment of water were analysis using heavy metals pollution indices such as Contamination index, heavy metal evaluation index and heavy metal pollution index.

4.3 GIS Data Processing

Arc GIS 10.6, TCX, DNRGPS, SPSS, Google Earth Pro and Microsoft Excel 2013 software for sample parameter spreadsheet preparation. The collection of the data were handheld with Global Positioning System (GPS) in degree, minute, second and imported into Microsoft Excel where the data was converted to degree decimal and transferred to Geographical Information System environment in Data Base in Arc GIS 10.6 using Arc map tools and add various layers such as road, Community, River to generate sample location map, Geologic map. Spatial analyst extension tools in Arc GIS 10.6 using hydrological tools to generate the height information from SRTM to produce Digital Elevation Model, Contour, drainage and watershed. Similarly, the spatial distribution maps for assessment of contamination for water quality of selected heavy metals produced using Arc GIS 10.6 software in Arc tool box to generate surfaces in spatial analysis tool using the inverse distance Weighted method IDW for heavy metals in water in other to generate various assessment of contamination in water such as Contamination index map, Heavy metal pollution map, Heavy metal evaluation index map. Thus, GIS provides the basis for us to look inward into the possible cause and outline the relationship using visual presentation.

5. Results and Discussion

The results from the analysis were collated for surface water presented in Table 1. The parameters analyzed are heavy metals which are chromium, Cobalt, lead, Zinc iron, nickel and cadmium. The results were compared with the World Health Organization (WHO) standard. Also, statistical treatments were carried out on the samples including basic descriptive statistics, correlation and cluster analysis with assessment of contamination which was incorporated in to the environment of geographical information systems using spatial analysis tool with Inverse Distance Weightage (IDW) method for environmental modeling for prediction of pollution zone base of pollution index on heavy metal, evaluation index and contamination index of heavy metal.

The descriptive statistics in Table 1 of the heavy metal in the water shows that the surface water in the study areas is the order of abundance in increasing order of the heavy metals is as follows: Cr<Ni<Pb<Cd<Zn<Fe and their Mean, Minimum, Maximum, values are show in the table above.

Table 1. Descriptive Statistics for surface water in the study area.

Long	Lat	SAMPLE Point	Pb	Cd	Ni	Cr	Fe	Zn
6.39825	5.02563	RW1 IGBOGENE	0.036	0.014	0.024	0.003	0.271	0.162
6.37654	4.99913	RW2 AKENFA	0.023	0.01	0.016	0	0.206	0.107
6.36729	4.96704	RW3 AGUDAMA	0.017	0.014	0.004	0.003	0.244	0.185
6.28393	4.93666	RW4 AMARATA	0.011	0.08	0.02	0	0.165	0.067
6.2651	4.9363	RW5 FMC	0.032	0.016	0.027	0.007	0.32	0.21
6.25865	4.9281	RW6 FAMGBE	0	0.001	0.01	0.001	0.126	0.055
6.24685	4.92577	RW7 OGBOGORO	0.001	0	0.001	0.001	0.164	0.048
6.25608	4.92012	RW8 SWALI	0.022	0.024	0.024	0.01	0.268	0.24
6.28062	4.90669	RW9 YENAGOA	0.032	0.016	0.027	0.007	0.32	0.21
		Min	0	0	0.001	0	0.126	0.048
		Max	0.036	0.08	0.027	0.01	0.32	0.24
		Mean	0.019	0.023	0.016	0.004	0.23	0.14
		WHO (2011)	0.003	0.01	0.07	0.05	0.3	3
		NSDWQ (2007)	0.003	0.01	0.07	0.05	0.3	3

The Pearson correlation coefficients surface of water samples. As shown in Table 2. Strong correlation among the heavy metals of Ni-Pb, Fe-Pb, Fe-Ni, Fe-Cr, Zn-Pb, Zn-Cr, and Zn-Fe while the rest are weak correlation and also the matrix is not positive definite.

Table 2. Pearson correlation coefficients between heavy metals concentrations in Surface water samples

	Pb	Cd	Ni	Cr	Fe	Zn
Pb	1					
Cd	0.008	1				
Ni	0.782*	0.331	1			
Cr	0.547	–0.106	0.592	1		
Fe	0.901**	–0.093	0.681*	0.782*	1	
Zn	0.775*	–0.08	0.603	0.892**	0.916**	1

* Correlation is significant at the 0.05 level (2-tailed).

** Correlation is significant at the 0.01 level (2-tailed).

The result of HCA in a dendrogram as shown in Figure 4 and Figure 5. The distance cluster expresses the degree of association between sampling sites. The lower the distance value of the cluster, the more significant association. Values of 0 and 25 were restricted between the total cluster distances in this study current comparing the HCA results and sampling locations Icicle diagram and R-mode Cluster actualize that there is a relation between geographical locations and total heavy metal concentrations with Cluster 1 (5 and 9) at Euclidean distance of 1, Cluster 2 (6 and 7) at Euclidean distance of 6, Cluster 3 (1 and 3) at Euclidean distance of 7, Cluster 8 (5, 9, 8, 1 and 3 also 6, 7, 2) at Euclidean of 25.

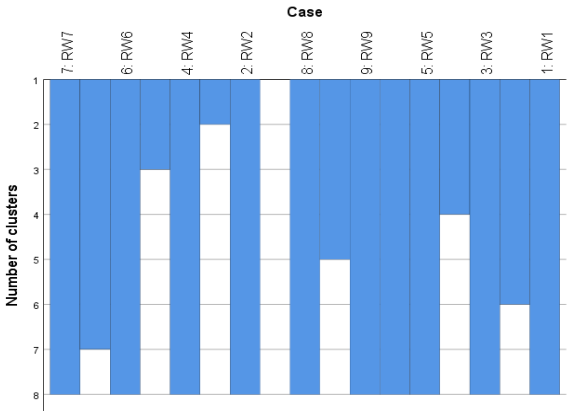

Figure 4. Icicle diagram for heavy metals in surface water Sample in the study area

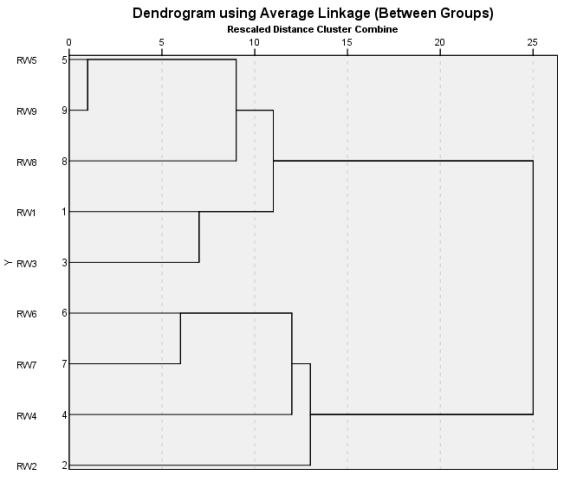

Figure 5. Dendrogram of sampling locations in terms of heavy metals concentrations in surface water (R-Mode)

The Principal Component Analysis output in Table 3, Figures 6 and 7 in surface water. Extraction of two principal components was identified, which explained 86.677% of the total variance. These results explain two main sources of heavy metals in the soil samples. The first principal component explained 66.718% of the total variance. This component was significantly loaded of Ni and Pb with loading values of, an almost similar pattern in Table 4. The second principal component explained 19.959% of the total variance, which was mainly loaded by Fe, Cd, Cr and Zn and from Table 4.

5.1 Iron (Fe) Content

Iron concentration in the surface water explicitly varies from 0.13 mg/L to 0.32 mg/L in Table 1 in the current study. Comparing with the tolerable limit for iron given by WHO (2011) standard for drinking water of 0.30 mg/L, the water is acceptable for drinking and also can be used for industrial purposes (e.g. in the bakery) except location RW 5 in FMC and RW 8 in Yenagoa in Figure 8. Higher concentration of iron may have some human health implications. The presence of iron can also manifest corroding in the water usually with an indication of offensive coloration with obvious smell and color in the water, making it unacceptable for drinking. The possible higher concentration of iron may be inferred to high refuse dumps of solid industrial and domestic wastes discharge to the Ikoli River which also is flowing into Epie creek. Significantly, the water from the creeks are good uses to humans in the surrounding in the study area because there is abrupt scarcity of clean water accessibility for household use in this area.

Table 3. Total Variance Explained for surface water sample of study area

Component	Initial Eigenvalues			Extraction Sums of Squared Loadings		
	Total	% of Variance	Cumulative %	Total	% of Variance	Cumulative %
1	4.003	66.718	66.718	4.003	66.718	66.718
2	1.198	19.959	86.677	1.198	19.959	86.677
3	0.494	8.241	94.918			
4	0.251	4.188	99.107			
5	0.046	0.762	99.869			
6	0.008	0.131	100.000			

Extraction Method: Principal Component Analysis.

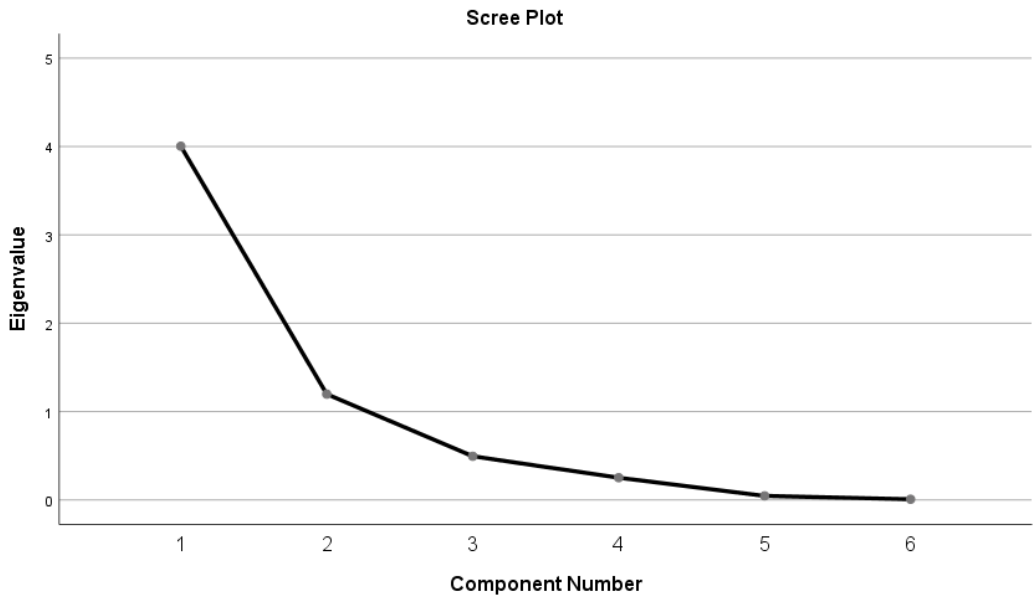

Figure 6. Eigenvalue vs Component Number in Surface water sample

Table 4. Component Transformation Matrix for surface water sample of study area

	Component	
	1	2
Pb	0.898	0.075
Cd	0.007	0.961
Ni	0.810	0.438
Cr	0.853	–0.191
Fe	0.962	–0.116
Zn	0.942	–0.163
Extraction Method: Principal Component Analysis.		
a. 2 components extracted.		

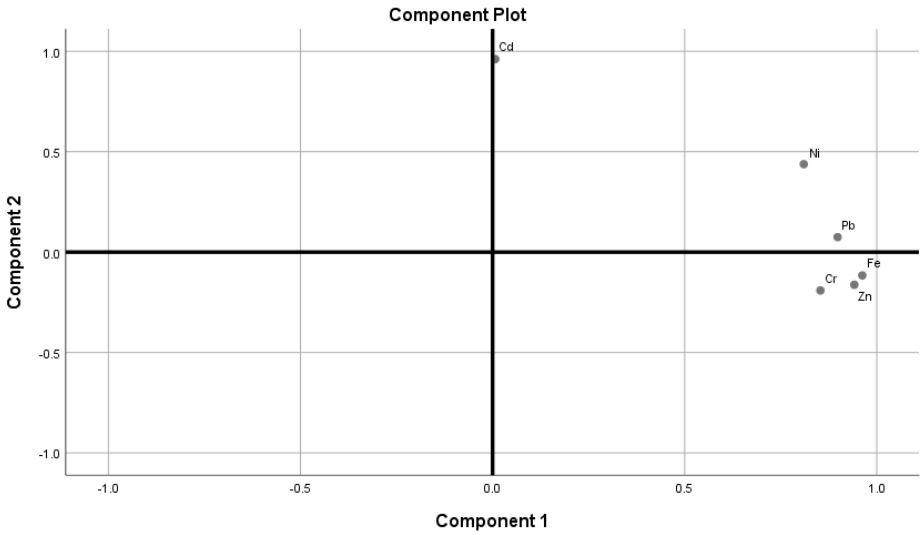

Figure 7. Loadings of principal components of heavy metals concentrations in surface water samples

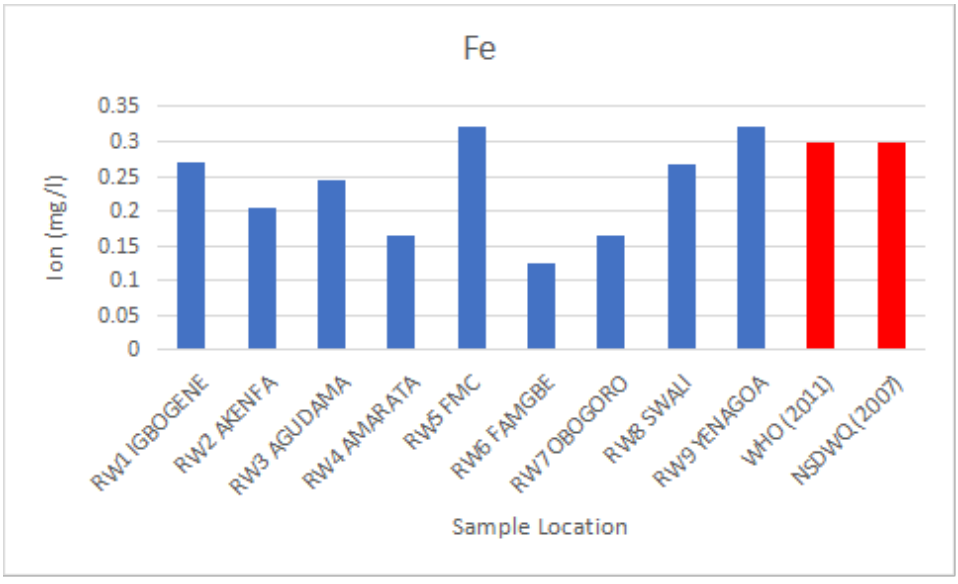

Figure 8. Concentration of Iron in surface water

5.2 Zinc

Zinc concentration in all the samples of the surface water sample varies from 0.05 mg/L to 0.24 mg/L (Figure 9) comparison with tolerable WHO limit of drinking water, the analyzed values were below the permissible limit given by WHO 2011 standard of 3.00 mg/L. which explicitly state that the water is safe for drinking. Zinc is a useful metal which can facilitate or boost female reproduction or excessive concentration of zinc to the environment is considered poisonous.

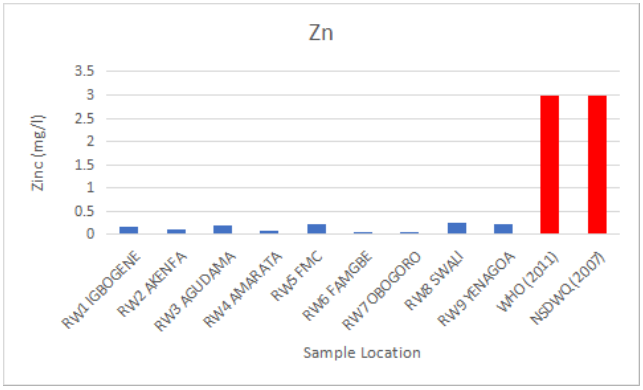

Figure 9. Concentration of Zinc in surface water

5.3 Chromium (Cr)

Chromium (Cr^{6+}) concentration in the surface water indicating from 0.00 mg/L to 0.01 mg/L (Figure 10) with 0.04 as mean value and when compared with the given limit of (WHO 2011 and NSDWQ 2007) of 0.05 mg/L, the analyzed values is lower than the standard thus indicating that the water is not affected by chromium toxicity. Excessive concentration of chromium is poisonous to the environment especially to aquatic environment.

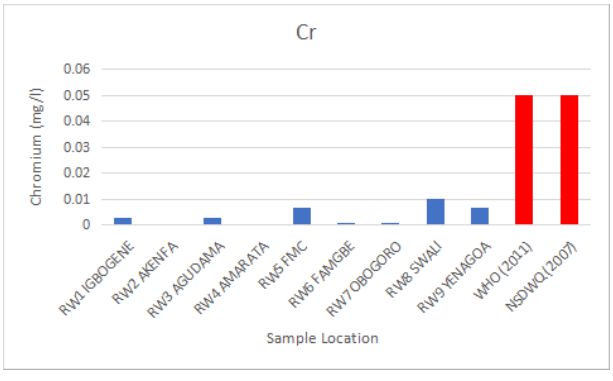

Figure 10. Concentration of Chromium in surface water

5.4 Nickel (Ni)

Nickel concentration in the samples of the surface water varies between 0.001 mg/L and 0.027 mg/L in Table 1. Looking forward the analyzed values of sampled location with the allowable limit of WHO standard for nickel concentration in the surface water samples make clear that the water samples concentrated values were below the given limit of WHO 2011 of 0.07 mg/L which clearly mark that nickel concentration of the water in the study area is minimal. The plotted values of nickel concentration against the regulatory bodies are shown below in Figure 11. Excessive concentration of nickel to the environment is injurious to human health.

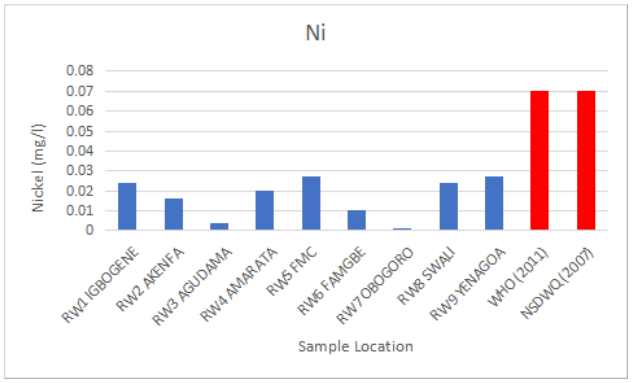

Figure 11. Concentration of Nickel in surface water

5.5 Cadmium (Cd)

Cadmium concentration varies from 0.00 mg/L to 0.08 mg/L in Table 1. The level of cadmium in surface water in sample location RW 6 in Famgbe, RW 2 and RW 7 at Ogbogoro is below the detection limit of WHO 2011 standard given as 0.01 mg/L while other samples location is above the stipulated limit. The occurrence of cadmium is mostly in association with zinc and percolates into water and also from the corrosion of zinc-coated materials. At higher concentrations, it is known to have potential toxic effect. Possible sources of cadmium into the environment are through industrial activities; the metal is widely used in making pigments electro plating, plastics, stabilizers and battery industries. Cadmium is highly toxic and can cause high blood pressure, and kidney failure at higher concentration, etc. Plot of cadmium against the regulatory bodies are shown below. Excessive concentration of Cadmium in the human body and environment can cause an illness called itaitai meaning brittle or fragmented bones.

5.6 Lead (Pb)

Concentration of lead in surface water samples varies from 0.00 mg/L to 0.04 mg/L (Figure 13) when compared with the given standard lead concentration was below the stipulated limit of 2.00 mg/L for drinking water given by

WHO 2011 standard in samples location RW6 in Famgbe and RW7 in Ogbogoro. While the rest samples were above the permissible limit given by WHO 2011 and is about 77.78% which imply that Ikoli River and the Epie Creek are highly polluted of lead toxicity. Plot of lead concentration against the regulatory are given below. Excessive concentration of lead in the environment and the human body affects IQ of infant babies and also attacks the peripheral nervous system of humans.

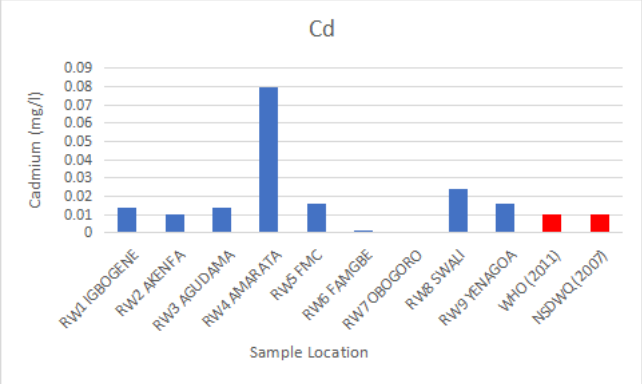

Figure 12. Concentration of Cadmium in surface water

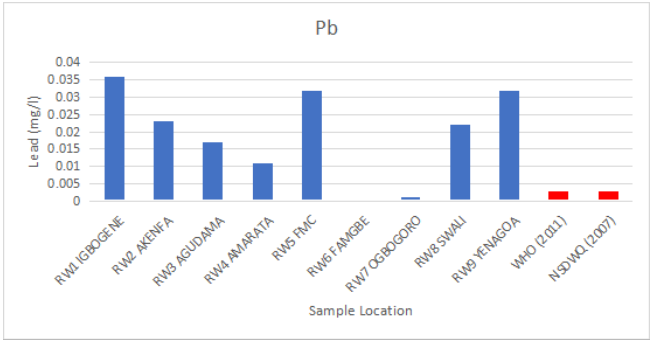

Figure 13. Concentration of Lead in surface water

5.7 Heavy Metals Pollution Assessment Indexes

The computed indexes for this research are presented in Table 5. Three quantitative methods were used in assessing the risk level of heavy metal concentration contamination in the samples: Contamination Index, Heavy Metal Pollution Index (HPI) and Heavy Metal Evaluation Index (HEI).

5.8 The Contamination Index

Contamination index which is also the degree of contamination for the study area was calculated using the concentration values of selected metals Fe, Zn, Pb, Cd, Ni and Cr with a minimum and maximum value shown in Table 7, the mean Cd value was found to be –1.62224 and only sample location RW4 in Amarata exceeds the critical pollution index value of 1 and the value of Cd average in the current research showed that the area have low contamination in terms of the Contamination index in Figure 13. In this current study the adoption after Backman et al., 1997 and Edet and Offiong 2012 was used for the grouping which indicated as thus, low (Cd < 1) medium (Cd 1-3) and high (Cd >3) [22,23].

Table 5. Groundwater quality classification based on adopted and modified pollution indices classes the table is referenced after Backman et al., 1997: Edet and Offiong 2012 and Kwala et al., 2017 [22-24]

Index Method used	Class source	Classes	Degree of Pollution
Cd	Adopted	<1 1-3 >3	Low Medium High
HEI	Modified	<5 5-20 >20	Low Medium High
HPI	Modified	<100 100-150 >150	Low Medium High

Table 6. Adopted Standard for computed indices

Heavy metal	Wi	S	I	MAC
Pb	100	0.003	0.003	0.003
Cd	333.33	0.01	0.01	0.01
Ni	14.29	0.07	0.07	0.07
Cr	20	0.05	0.05	0.05
Fe	3.33	0.3	0.3	0.3
Zn	0.33	3	3	3

MAC: maximum admissible concentration/upper permissible
Wi: Weightage (1/MAC)
S: Standard permissible
I: Highest permissible

Table 7. Assessment of Contamination results

Long	Lat	SAMPLE Point	Cd	HEI	HPI
6.39825	5.02563	RW1 IGBOGENE	–2.23981	14.76019	408.3911
6.37654	4.99913	RW2 AKENFA	–3.0491	9.617571	285.7462
6.36729	4.96704	RW3 AGUDAMA	–2.60786	8.05881	471.28
6.28393	4.93666	RW4 AMARATA	3.858048	12.52471	1910.695
6.2651	4.9363	RW5 FMC	–1.73762	13.92905	447.6419
6.25865	4.9281	RW6 FAMGBE	–4.29881	0.70119	24.39231
6.24685	4.92577	RW7 OGBOGORO	–4.40305	0.930286	2.63746
6.25608	4.92012	RW8 SWALI	–1.08381	11.24952	615.0358
6.28062	4.90669	RW9 YENAGOA	–1.73762	13.92905	447.6419
		Minimum	–4.40305	0.70119	2.63746
		Maximum	3.858048	14.76019	1910.695
		Mean	–1.62224	9.196524	593.3449

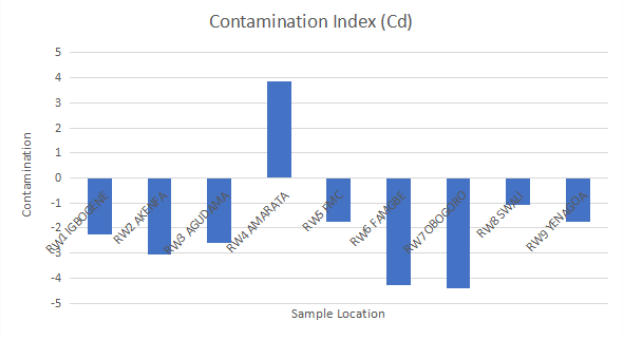

Figure 14. Concentration of Contamination Index in surface water

5.9 Heavy Metal Evaluation Index

Heavy metal evaluation computation indexes (HEI) of the current study areas give a mean value of 9.196524 with minimum and maximum values of 0.70 and 14.76 respectively. Adopting the procedure used after Edet and Offiong 2012 [23], the values of HEI computations were divided into 3 classes using a mean value multiplication. The three classes demarcated are HEI < 5 low, HEI 5-20 medium and HEI > 20 high. Based on these, 2 locations which represent 22.22% of all the locations had low HEI values, while 9 locations covering 77.78% of the sample water falls within the medium class in the study in Figure 15.

5.10 Heavy Metal Pollution Index

The pollution index for heavy metal in the study areas were done with a calculation using the concentration values of (Pb, Zn, Fe, Cd, Ni and Cr); the mean value of HPI was found to be 593.34 (Table 7) which extends the critical pollution index value of 100 exception of RW6 in Famgbe and RW7 in Ogbogoro which were below. This outline that the study areas (Ikoli River as well as Epie creek), is recorded with very high concentrations of heavy metals which were the critical pollution index. HPI values for all sampled location were observed to be greater than tolerable limit (HPI>100) with the highest value of (1910.69) recorded at RW4 in Amarata and the lowest value (2.64) observed at in (Figure 14 and Table 7). Although RW6 and RW 7 are characterized by non-industrial activities in the area but other adjourning areas may have been connected to possible dilution effect from discharge point towards the area of Epie creek due to solid waste disposal in the river. The HPI indicated that metal concentration decreases with respect to distance increasing away from the pollutant emission sources.

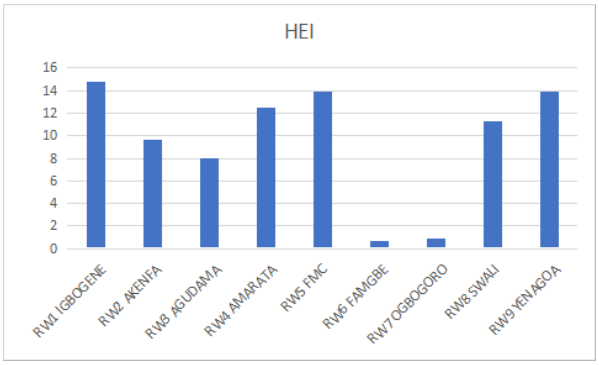

Figure 15. Concentration of Heavy Metal Evaluation Index in surface water

5.11 Interpolation of Water Contamination

The spatial distribution of contamination in surface water contamination surfaces created by using Inverse Distance Weighted (IDW) method and the techniques of GIS mapping were applied to produce distribution of spatial

maps of Contamination Index, Heavy Metal Evaluation Index and Heavy Metal Pollution Index surfaces created by using IDW method.

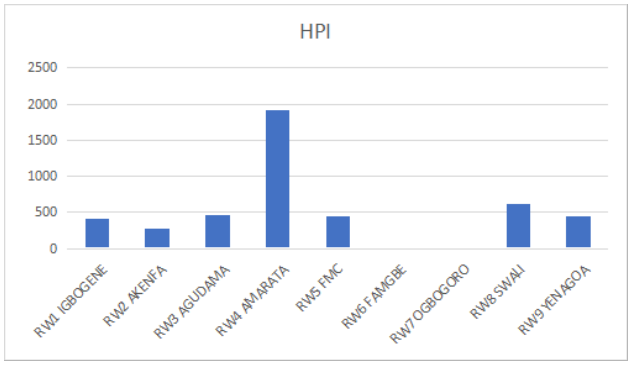

Figure 16. Concentration of Heavy Metal Pollution Index in surface water

5.12 Contamination Index Map

From Figure 17 the spatial distribution map of Contamination Index for surface water reveals that the area with blue colour has low contamination index, like wise area with yellow colour contain medium contamination index and area with red colour reflect high contamination index.

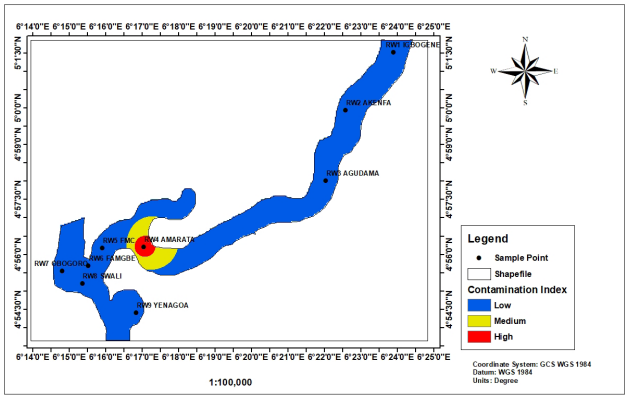

Figure 17. Contamination Index Map in surface water

5.13 Heavy Metal Evaluation Index

The distribution spatial map of evaluation of heavy metal index in Figure 18 reveals that blue colour contains low degree of pollution and red indicates medium degree of pollution when compared with Table 5.

5.14 Pollution Index of Heavy Metal

The spatial distribution map of pollution of heavy metal index for surface in Figure 19 reveals that area with blue colour indicate low Degree of pollution likewise area with yellow contain medium Degree of pollution and area with red colour is High Degree pollution when compared with Table 5.

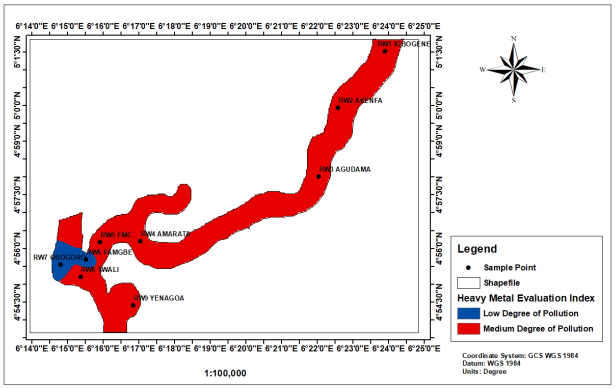

Figure 18. Heavy Metal Evaluation Index Map in surface water

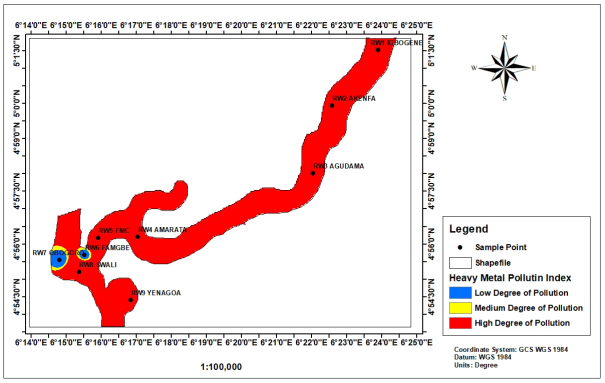

Figure 19. Heavy Metal Pollution Index Map in surface water

5.15 Analysis of GIS Using Weighted Overlay Method

The final prediction of the pollution zones, the evaluating criteria were needed to give a better understanding. GIS applications were assessed using the weighted Overlay method which gives a set of map classes referencing each input. The maps were given values of different scores and provisions of different weights. Limiting the criteria compromises the accuracy of the proposed approach the multiple criteria decision analysis (MCDA) methods for the importance weighting of various environmental criteria will increase the accuracy of ranking potential pollution indices. This method was accurate and resolved multi-criteria problems in many fields of study by integrating

GIS and MCDA to help tackle the real-world problem [25].

The pollution indices are used to denote heavy metal evaluation index, Contamination index, and heavy metal pollution index. The scores given for the three pollution index for each map classes was assigned along with the map weightings entered as attribute data and also the percentage of influence the on weightage of the spatial maps based on the class provided below.

Table 8. Multiple criteria decision analysis for ranking of pollution in study area

S/N	Pollution	% of Influence	Rank
1	Contamination index	20	2
2	Heavy metal evaluation index	40	5
3	Heavy metal pollution index	40	5

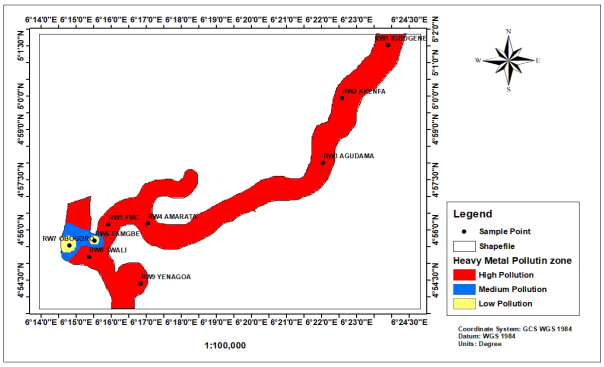

Figure 20. Heavy Metal Pollution Map in surface water.

The heavy metal pollution Map using Multiple criteria decision analysis reveals that Ikoli River, Epie creek is polluted which is due to careless dumping of industrial wastes domestic wastes and, also attributed to leakages from marine dumping wastes, water tanks, radioactive waste, and atmospheric deposition are some of the known causes of water pollution. Heavy metals that are disposed of industrial waste can accumulate in lakes and rivers, proving harmful substances to the ecosystem. These harmful toxins released into the environment especially effluents aggravate and suppress human immune system, causes reproductive failure, and acute poisoning. Some diseases causing infections such as cholera, typhoid fever [26], and other diseases gastroenteritis, diarrhea, vomiting, skin, and kidney problem are spreading through polluted water [27]. Human health systems are directly damaged due to poor environmental management. Water pollutants are degrading the marine environmental plants and animals such as seaweeds, mollusks, marine birds, fishes, crustaceans, and other sea organisms that serve as food for humans. Poor usage of insecticides such as DDT releases harmful concentration to the environment which is deteriorating food chain.

6. Conclusions

The evaluation for the Heavy metal concentration and pollution statue, out of all the metals detected and evaluated, Zinc concentration was below the required and permissible limit of 3 mg/L in all the locations samples of 9, and iron is 77.78% below the stipulated limit by WHO 2011 of 0.3 mg/L while other heavy metal in Table 1 reveals Ikoli River and Epie creek to be highly polluted. The calculated pollution index for contamination index gives 11.11% sample are high and 88.89% are low while both heavy metal evaluation index and heavy metal pollution index contain 22.11% of the sample are low and 77.78% are high which imply the Ikoli River and Epie creek is polluted. Also, multivariate treatment of the result revealed a good correlation between the PCA, and HCA, which showed geogenic and anthropogenic sources of the Heavy metals to be the products of automobiles exhaust, leakage from water tanks, marine dumping, radioactive waste, and burning. From Figure 17 this study investigated successfully the use of the application of GIS weighted overlay method with the help of Multiple Criteria Decision Analysis to predict and characterize areas of high pollution, medium and low pollution in Ikoli River, and Epie creek in Yenagoa. Consequently, recommendations such as sustainable development of waste water resources and public law and awareness campaign should be emphasized. Environmental law and public awareness should be placed high. The study contributed to knowledge by using geographical Information System and Remote Sensing technology have the potentiality to store, analyze, monitor, and use for mapping of pollution in water resource management for better visualizing the environmental policy.

Conflict of Interest

There is no conflict of interest.

References

[1] Briggs, D., 2003. Environmental pollution and the global burden of disease. British Medical Bulletin. 68, 1-24.
DOI: https://doi.org/10.1093/bmb/ldg019

[2] Bibi, S., Khan, R.L., Nazir, R., 2016. Heavy metals in drinking water of Lakki Marwat District, KPK, Pakistan. World Applied Sciences Journal. 34(1), 15-19.
DOI: https://doi.org/10.5829/idosi.wasj.2016.34.1.10252

[3] Khan, N., Hussain, S.T., Saboor, A., 2013. Physiochem-

ical investigation of the drinking water sources from Mardan, Khyber Pakhtunkhwa, Pakistan. International Journal of Physical Sciences. 8(33), 1661-1671. DOI: https://doi.org/10.5897/IJPS2013.3999

[4] Pawari, M.J., Gawande, S., 2015. Ground water pollution & its consequence. International Journal of Engineering Research and General Science. 3 (4), 773-776.

[5] Das, J., Acharya, B.C. 2003. Hydrology and Assessment of Lotic Water Quality in Cuttack City, India. Water, Air and Soil Pollution. 150, 163-175. DOI: https://doi.org/10.1023/A:1026193514875

[6] Zhang, X.J., Xu, Z.M., Song, X.Y., 2013. Application and study of several water quality evaluation method in rivers flowing into Qinghai Lake. Environmental Engineering. 31, 117-121.

[7] Arulbalaji, P., Padmalal, D., Sreelash, K., 2019. GIS and AHP techniques based delineation of groundwater potential zones: A case study from Southern Western Ghats, India. Scientific Reports. 9(1), 2082. DOI: https://doi.org/10.1038/s41598-019-38567-x

[8] Oyinkuro, O.A., Rowland, E.D., 2018. Spatial Groundwater Quality Assessment by WQI and GIS in Ogbia LGA of Bayelsa State, Nigeria. Asian Journal of Physical and Chemical Sciences. 4(4), 1-12. DOI: https://doi.org/10.9734/AJOPACS/2017/39055

[9] Lu, Y.L., Song, S., Wang, R., 2015. Impacts of soil and water pollution on food safety and health risks in China. Environment International. 77, 5-15.

[10] Burrough, P.A., McDonnell, R.A., Lloyd, C.D., 2015. Principles of Geographical information systems oxford: Oxford University Press. 352.

[11] Mukate, S., Wagh, V., Panaskar, D., et al., 2019. Development of new integrated water quality index (IWQI) model to evaluate the drinking suitability of water. Ecological Indicators. 101, 348-354. DOI: https://doi.org/10.1016/j.ecolind.2019.01.034

[12] Udom, G.J., Esu, E.O., Etu Efeotor, J.O., 1998. Hydrochemical Evaluation in parts of Port-Harcourt and Tai-Eleme Local Government Areas of Rivers State. Global Journal of Pure and Applied Sciences. 5(5), 545-552.

[13] Oludayo, G.A., 2012. Environmental Pollution and Challenges of Environmental Governance in Nigeria. British Journal of Arts & Social Sciences. 10(1), 26-30.

[14] Tsai, L.J., Yu, K.C., Chen, S.F., et al., 2003. Effect of Temperature on Removal of Heavy Metals from Contaminated River Sediments via Bioleaching. Water Research. 37(10), 2449-2457. DOI: https://doi.org/10.1016/S0043-1354(02)00634-6

[15] Ojekunle, O.Z., Ojekunle, O.V., Adeyemi, A.A., 2016. Evaluation of surface water quality indices and ecological risk assessment for heavy metals in scrap yard neighbourhood. SpringerPlus. 5, 560. DOI: https://doi.org/10.1186/s40064-016-2158-9

[16] Okiongbo, K.S., Douglas, R., 2013. Hydrochemical analysis and evaluation of groundwater quality in Yenagoa City and environs, Southern Nigeria. Ife Journal of Science. 14(2), 209-222.

[17] Desmond, E., Egobueze, F.E., Omonefe, F., 2019. Determination of Flood Hazard Zones Using Geographical Information Systems and Remote Sensing Techniques: A Case Study in Part Yenagoa Metropolis. Journal of Geography Environment and Earth Science International. 21(1), 1-9. DOI: https://doi.org/10.9734/jgeesi/2019/v21i130116

[18] Reyment, R.A., 2018. Richard A. Reyment (1926–2016) – Ammonitologist sensu latissimo and founder of Cretaceous Research. Cretaceous Research. 88, 5-35. DOI: https://doi.org/10.1016/j.cretres.2017.11.025

[19] Reijers, T.J.A., 2011. Stratigraphy and Sedimentology of the Niger Delta. Geologic, The Netherlands. 17(3), 133-163.

[20] Etu–Efeotor, J.O., 1997. Fundamentals of petroleum geology. Paragraphic publications, Port Harcourt, Nigeria, Press. pp. 135.

[21] Chukwu, G.A., 1991. The Niger delta complex basin: Stratigraphy, structure and hydrocarbon potential. Journal of Petroleum Geology. pp. 14211-14220. DOI: https://doi.org/10.1111/j.1747-5457.1991.tb00363.x

[22] Backman, B., Bodis, D., Lahermo, P., et al., 1997. Application of a Groundwater Contamination index in Finland and Slovakia. Environmental Geology. 36(1), 55-64. DOI: https://doi.org/10.1007/s002540050320

[23] Edet, A.E., Offiong, O.E., 2002. Evaluation of Water Quality Pollution Indices for Heavy Metal Contamination Monitoring. A Study Case From Akpabuyo-Odukpani Area, Lower Cross River Basin (Southeastern Nigeria). Geo-microbiology Journal. 57, 295-304. DOI: https://doi.org/10.1023/B:GEJO.0000007250.92458.de

[24] Kwaya, M.Y., Hamidu, H., Kachalla, M., et al., 2017. Geosciences. 7(4), 117-128.
DOI: https://doi.org/10.5923/j.geo.20170704.02

[25] Rowland, E.D., Omonefe, F., Erebi, J.L., 2021. Site suitability study for solid waste dumpsite selection using Remote Sensing and GIS-based multi-criteria analysis in Yenagoa, Bayelsa State. Annals of Geographical Studies. 4(1), 1-12.
DOI: https://doi.org/10.22259/2642-9136.0401001

[26] Juneja, T., Chauhdary, A., 2013. Assessment of water quality and its effect on the health of residents of Jhunjhunu district, Rajasthan: A cross sectional study. Journal of public health and epidemiology. 5(4), 186-191.
DOI: https://doi.org/10.5897/JPHE12.096

[27] Khan, M.A., Ghouri, A.M., 2011. Environmental Pollution: Its effects on life and its remedies. Journal of Arts, Science and Commerce. 2(2), 276-285.

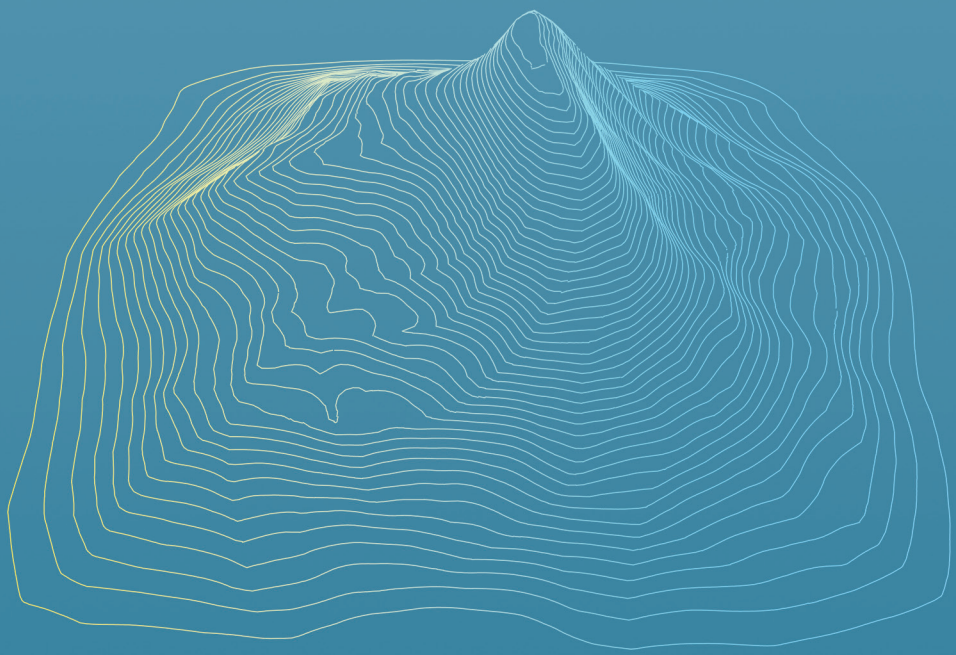

BILINGUAL
PUBLISHING CO.
Pioneer of Global Academics Since 1984

Tel.: +65 65881289
E-mail: contact@bilpublishing.com
Website: ojs.bilpublishing.com

2630-5070
03
9 772630 507228